Structure-Function Analysis of Membrane Proteins by Infrared Spectroscopy: Porin OmpF, Porin OmpG and Betaine Transporter BetP

Dissertation

zur Erlangung des Doktorgrades der Naturwissenschaften

vorgelegt beim Fachbereich Physik

der Johann Wolfgang Goethe-Universität

in Frankfurt am Main

von

Filiz Korkmaz

aus Amsterdam, The Netherlands

Frankfurt am Main, January 2009
(D30)

vom Fachbereich der Physik der

Johann Wolfgang Goethe-Universität als Dissertation angenommen.

Dekan: Prof. Dr. D. Rischke

Gutachter: Prof. Dr. W. Mäntele

Prof. Dr. B. Ludwig

Prof. Dr. Reinhard Krämer

Datum der Disputation:……

1. INTRODUCTION

1.1 Protein Structure

Proteins are involved in every process within living cells. Proteins perform a large variety of functions such as providing protecting functions, participating in transport processes, catalysis of all biochemical reactions within the cell and are basic substances of antibodies and certain hormones. Proteins constitute more than half of the dry weight of a cell. They are organic compounds formed by a linear chain of amino acids (Fig. 1.1). 20 different amino acids are used in different combinations to produce proteins in organisms. The sequence, in which the amino acids are connected via peptide bonds to each other, is determined by the gene sequence. Correct functionality of a protein depends on its structure and correct conformation. Therefore understanding the structure, function of proteins and conditions for functionality has been the focus of many scientific researches. Finding a cure for the illnesses, like cancer, caused by nonfunctional or malfunctioning proteins depends solely on such studies.

All amino acids share some common features like they have a α-carbon to which a carboxyl, an amino and a variable side chain group (R group) are attached. The structure of an amino acid and the linkage of two amino acids are seen in Figure 1.1. A chain of amino acids therefore has a free carboxyl group on one end, called C-terminal, and has a free amino group on the other end of the chain, called N-terminal. The repeated carbon-nitrogen-oxygen pattern is called the main chain or protein backbone. Amino acids attain different chemical characteristics depending on the side chain group attached to the α-carbon. The side chain group is represented by “R” in the figure. The amino acid is then classified as charged/uncharged, neutral, polar and hydrophobic/hydrophilic depending on the chemical property of the side chain.

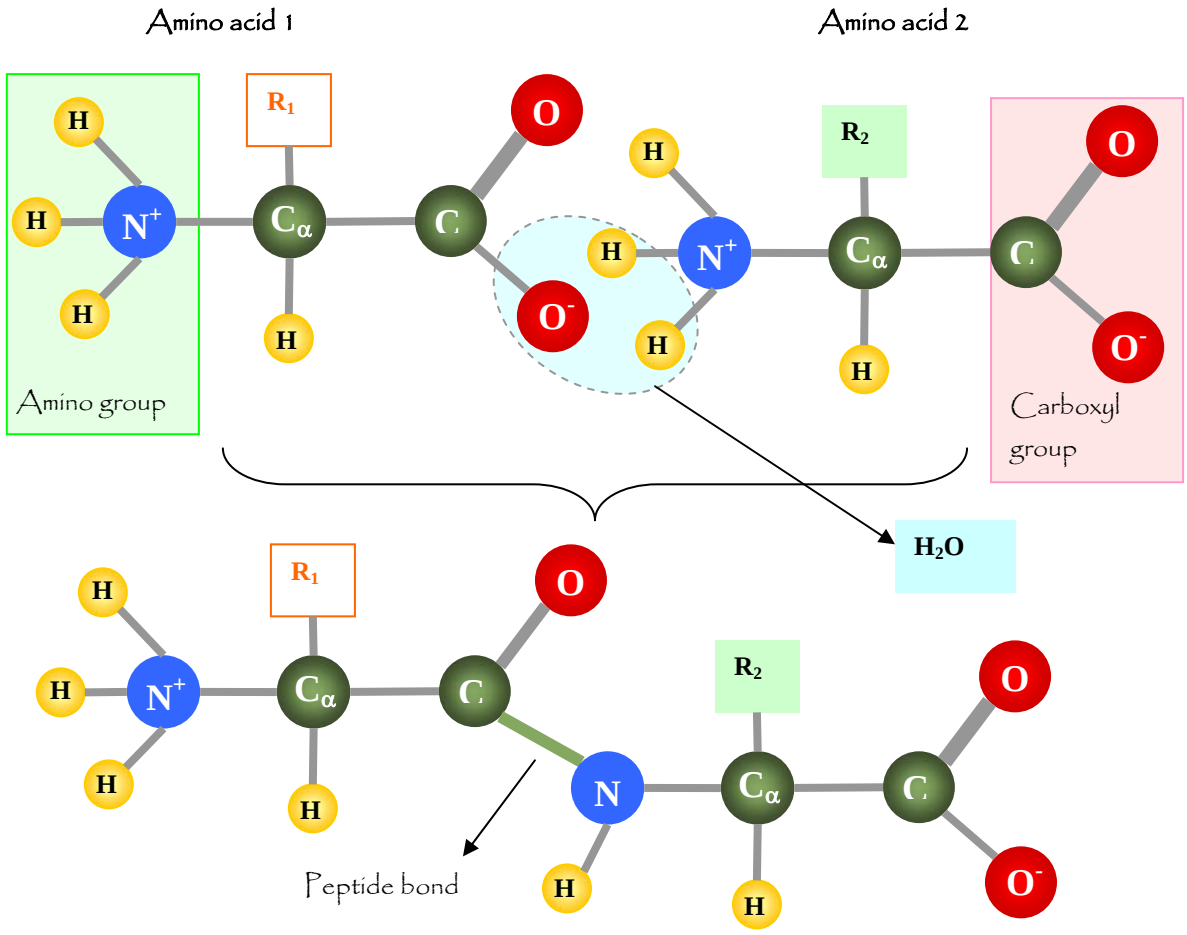

Figure 1. 1 The structure of two amino acids with different R groups are shown at the top. The peptide bond formation between the C- and N-atoms from the two amino acids is shown at the bottom. The amino group remaining on the left is called the N-terminus and the carboxyl group on the right is called the C-terminus of the main chain.

Hydrophobic side chains prefer to be buried in the lipid bilayer and the hydrophilic side chains prefer to be exposed to the solvent, depending on the polarity of the solvent. Leucine (Leu), isoleucine (Ile), phenylalaline (Phe), and valine (Val) are hydrophobic, along with tyrosine (Tyr), alanine (Ala) and tryptophane (Trp), to a lesser extent. The charges of the side chains are crucial for the structure and stability, in terms of ion binding capabilities, and also for the hydrophilicity. Lysine (Lys), histidine (His) and arginine (Arg) are positively charged. Glutamic (Glu) and aspartic (Asp) acid are negatively charged. The rest have generally smaller hydrophilic side chains. Additionally, serine (Ser) and threonine (Thr) have hydroxyl groups, and asparagine (Asn), glutamine (Gln) have amide groups. Cysteine (Cys) can form

covalent disulphide bonds, also called S-bridge, to other Cys, proline (Pro) and glycine (Gly) residues.

Tabel 1. 1 Structure and composition of amino acids.
[http://www.ionsource.com/Card/aatable/aatable.htm]

AA Codes		AA Residue Composition	Structure	AA Codes		AA Residue Composition	Structure
Gly	G	C_2H_3NO	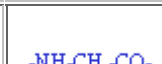	Asp	D	$C_4H_5NO_3$	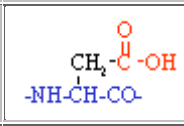
Ala	A	C_3H_5NO	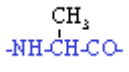	Gln	Q	$C_5H_8N_2O_2$	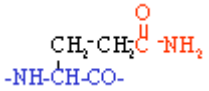
Ser	S	$C_3H_5NO_2$	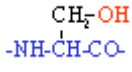	Lys	K	$C_6H_{12}N_2O$	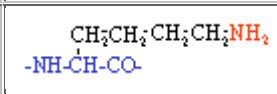
Pro	P	C_5H_7NO	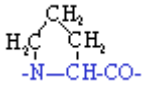	Glu	E	$C_5H_7NO_3$	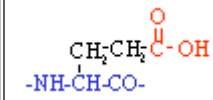
Val	V	C_5H_9NO	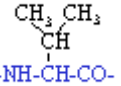	Met	M	C_5H_9NOS	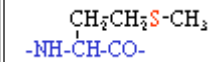
Thr	T	$C_4H_7NO_2$	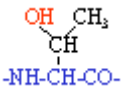	His	H	$C_6H_7N_3O$	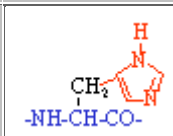
Cys	C	C_3H_5NOS	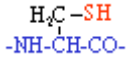	Phe	F	C_9H_9NO	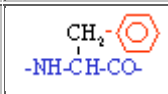
Leu	L	$C_6H_{11}NO$	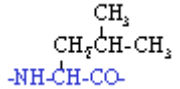	Arg	R	$C_6H_{12}N_4O$	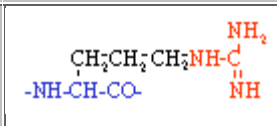
Ile	I	$C_6H_{11}NO$	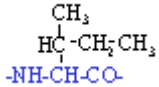	Tyr	Y	$C_9H_9NO_2$	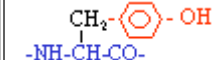
Asn	N	$C_4H_6N_2O_2$	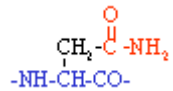	Trp	W	$C_{11}H_{10}N_2O$	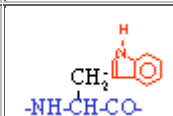

1.2 Protein Folding

As described in the previous section, a chain of amino acids has a certain chemical character due to the amino acid composition. Folding of this linear chain to a stable three-dimensional structure is called protein folding. A unique polypeptide may have more than one stable folded conformation, which could have a different biological activity, but usually, only one conformation is considered to be the active state. This state of the protein is called the native state. For most of the proteins correct folding is essential for functionality.

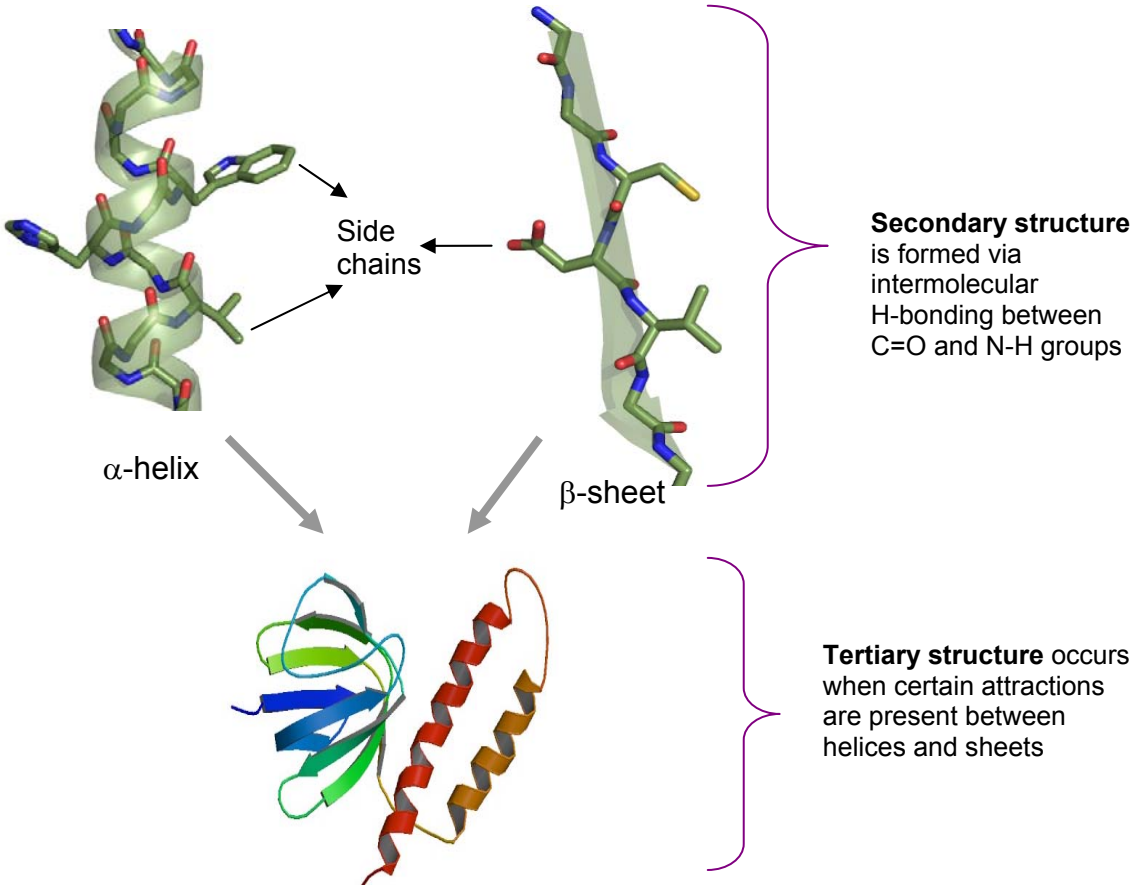

Figure 1. 2 Folding steps of a protein. Amino acid chain first attains a secondary structure by forming intermolecular H-bonds (top).In the figure, C-atoms are shown in green, N-atoms are in blue and O-atoms are in red. The tertiary structure is formed with the assembly of the secondary structure units. As an example to tertiary structure, ε–subunit of the F1-ATP-synthase[1] protein is shown at the bottom. The unstructured amino acid chain connecting the helices is a random coil structure and short connections among the β-sheets are the turn structures.

[1] PDB id: 1bsn. Picture generated by using PyMOL 0.99beta33.

A polypeptide chain is first folded into a two-dimensional structure. Depending on the order and characteristics of the repeating chain, the secondary structures are classified as α-helices, antiparallel/parallel β-sheet and turns. When the backbone is not in a regular, classified secondary structure form, then it is called to be a random coil (Fig. 1.2).

Tertiary structure is the three-dimensional spatial arrangement of a protein's secondary structure element. The formation of molten globules and tertiary structure are held together by structurally non-specific interactions. The specificity and stability of the tertiary structure is satisfied by the proper packing of the side chains, which results in the burial of hydrophobic residues; and the other interactions such as ionic interactions (i.e. salt bridges) and H-bonds. Tertiary structure encompasses all the noncovalent interactions that are not considered for the secondary structure, and it defines the overall fold of the protein. Therefore it is indispensable for the function of the protein.

Quaternary structure is the assembly of proteins or polypeptide chains' units to form functional complexes. Not all the proteins attain a quaternary structure. The individual chains are called the subunits. Complexes of two or more polypeptides (i.e. multiple subunits) are usually called multimers and named dimer, trimer, and tetramer if they contain two, three and four subunits, respectively. Those multimers composed of identical subunits referred to with a 'homo' prefix; and referred to with a 'hetero' prefix, if they are made up of different subunits. Therefore a homotrimer means the assembly of three identical subunits.

1.3 Membrane Proteins

Membrane proteins are buried in the membrane of a cell or organelle either totally or partially. They take part in many processes like substrate uptake and signal transduction. Structures of these proteins are stabilized by the membrane so that membrane-buried parts have hydrophobic character whereas the extracellular and intracellular parts have hydrophilic character. In the case of gram-negative bacteria, the outer membrane proteins generally have mainly β-sheet structure, such as porins (Fig. 1.3). On the other hand inner membrane proteins generally have mainly α-helical structure, like transporters.

1.3.1 Porins

Porins are found in the outer membrane of gram-negative bacteria. They are characterized by their β plated sheet structure, forming a diffusion channel through the membrane for the passage of many different molecules from ions to oligosaccharides. They exist as monomers or oligomers and are known to be extremely stable in terms of the structure (Sukumaran et al., 2004). Two examples to trimeric porins, OmpC and maltoporin sucrose complex are shown in Figure 1.3. Porins have aromatic amino acids arranged as two belts between the outer surface of the protein and the bilayer. These “aromatic girdles/belts” stabilize each monomeric porin unit in the membrane bilayer and the units are held together by folding one of the loops over the neighboring unit. Porins also have aromatic amino acids and one folded loop within the channel to restrict and control the transport gateway (Weiss et al., 1991; Yau et al., 1998). These series of amino acids are called “greasy slide” since they guide the ions through the channel and release them on the other side of the membrane. Depending on the chemical character of the amino acids forming the greasy slide, and depending on the channel size, most of the porins show specific preferences. OmpF and OmpC are known to prefer cations slightly over anions and PhoE prefers anions. Porins like LamB and ScrY are specific for sugar uptake. On the other hand, porins like OmpG shows preference based on the size of the molecule; having the size exclution limit of ~900 Da.

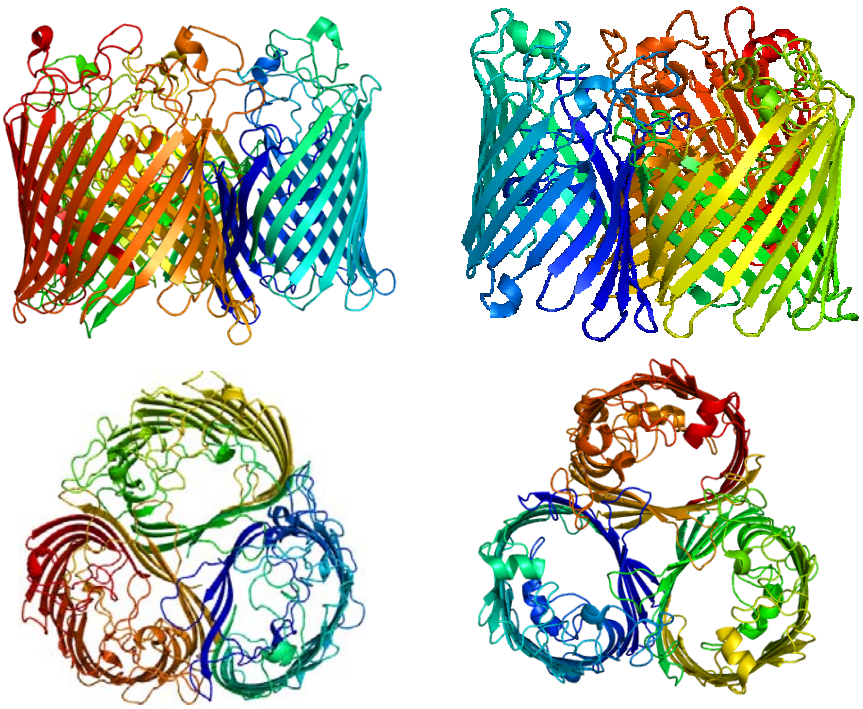

Figure 1. 3 Trimeric porin OmpC[2] on the left and maltoporin sucrose complex[3] on the right. Their top views are given below.

Porin from Paracoccus denitrificans

The structure of the *Paracoccus denitrificans* porin has been solved by Hirsch et. al. in 1997 by X-ray crystallography (Fig. 1.4). The size limit for the transport of hydrophilic molecules is below approximately 600 Da. The functional unit is a homotrimer and each monomer is composed of 16 stranded β-sheets and very few residues in α-helical conformation.

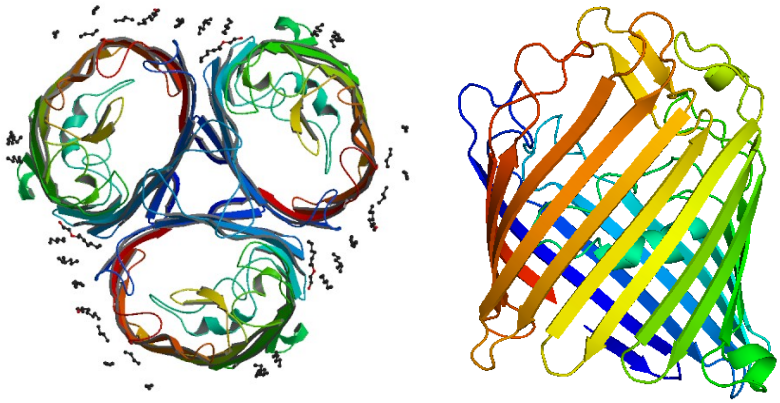

Figure 1. 4 Top view of homotrimeric porin from *Paracoccus denitrificans* on the left and side view of one monomer on the right.

[2] Osmoporin OmpC from *E. coli*. PDB id: 2j1n.
[3] Maltoporin. PDB id: 1af6.

Non-specific porins are known to be cation selective since negatively charged amino acids like Asp and Glu dominate the eyelet, except PhoE, which is an anion selective pore (Butz et al., 1993). Porin has a wide opening on both sides of the membrane; however, the eyelet is considerably restricted and the overall pore has the shape of an hourglass. The loop L3 is folded within the pore and carries 4 negatively charged amino acids. On the opposite wall, there are 5 arginine residues having positive charges. Due to the electrostatic interaction, these amino acids are maximally extended in pore lumen and by doing so further restrict the constriction zone. Mutations on these charged residues by neutralizing all of them led to increased cation selectivity (Phale et al., 2001). It appears that the cation selectivity can not solely been attributed to the eyelet residues and geometry. Interestingly, porin becomes anion selective at pH< 4 (Alcaraz et al., 2004). Also porin channel is asymmetric in solute diffusion. All these data lead to the conclusion that selectivity can be attributed to the electrostatic interactions between the diffusing ions and charged residues at the extracellular region and in the eyelet. Although this hypothesis seems to be in perfect agreement with the asymmetry of selectivity and response to pH changes, it is unable to explain the higher diffusion rate of K^+ ions over Na^+. Although *P. denitrificans* porin structure is now known for a decade, the mechanism of function still needs further research.

The structural integrity of porin and its position in the bilayer is satisfied by the aromatic amino acids in the aromatic girdle, which are 20-25 Å apart. In the case of *P. denitrificans* porin, this girdle contains 16 tyrosins, 2 tryptophans and 19 phenylalanins per monomer. Tyrosine OH groups and tryptophan indol groups point toward the lipid headgroups, while phenylalanins are located toward the lipid core. Altogether, they form the part of the protein interacting with the membrane by forming H-bonds in the bilayer-water interface. Porin structure is therefore very stable (Hirsch et al., 1997). A previous Fourier Transform Infrared (FTIR) spectroscopy study has shown that porin aggregates at ~95°C if reconstituted in liposomes (Sukumaran et al., 2004). Porin stability has also been tested under very acidic and basic conditions. Between pH 1 and 12 porin structure remains essentially unaffected (Sukumaran et al., 2006b).

OmpG from Eschericia coli

OmpG is another outer membrane protein. In contrast to *P. denitrificans* porin, OmpG from *E. coli* outer membrane is functional as monomer, as shown by functional and structural studies (Behlau et al., 2001; Fajardo et al., 1998). It has 14-stranded β-sheets and a channel width of approximately 0.1-0.15 nm allowing the passage of ions and molecules below 900 Da. OmpG is expressed in *Eschericia coli* if other sugar uptake porins like LamB can not be expressed due to a deletion in the gene sequence, which brings the *ompg* gene under the control of a promoter (Misra, 1989). The biological function of OmpG is still unknown but it could be shown that it enables the diffusion of maltodextrins across the outer membrane in the absence of the LamB maltoporin. A similar aromatic belt composed mainly of tyrosines exists which is also thought to keep the structural integrity in the hydrophobic core of the lipid bilayer.

The high resolution X-ray crystal structure of OmpG from 3D crystals revealed that OmpG retains a so-called closed form below pH 6 and an open form above pH 7.5, as shown in Figure 1.5 (Yildiz et al., 2006). This opening and closing of the protein is hypothesized to be controlled by the two histidines located at the centre of the pore at positions 231 and 261. At low pH they are protonated and hence repel each other causing the loop L6 to fold towards the channel entrance. This considerably restricts the channel permittivity at acidic pH. At high pH, histidines are deprotonated and form H-bond, which in turn causes the loop L6 to stand in upright position with respect to the channel entrance and leaves the channel completely open for passive diffusion.

The uptake of oligosaccharides is thought to be guided by a line of aromatic amino acids running parallel to the barrel axis similar to other sugar uptake proteins (Dutzler et al., 1996; Forst et al., 1998; Meyer et al., 1997). This “aromatic slide” is composed of mainly tyrosines and one phenylalanine residue.

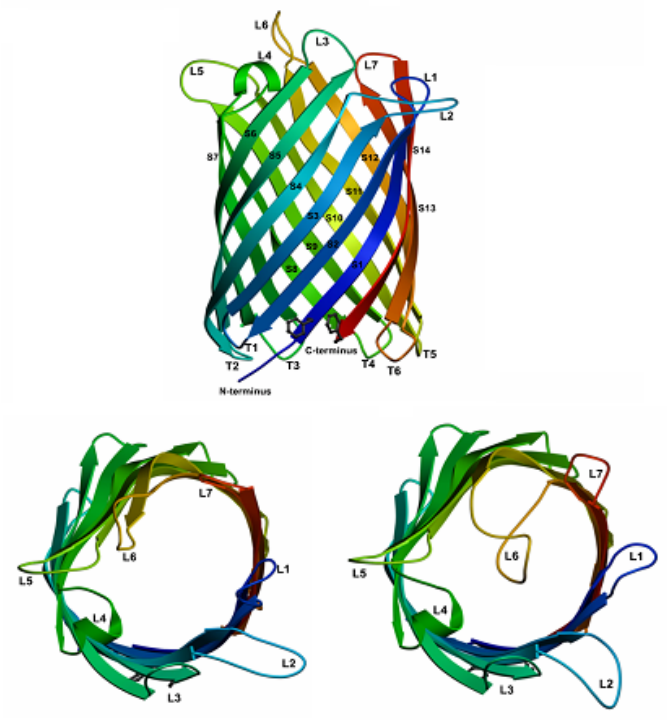

Figure 1. 5 Side view structure of OmpG[4] seen on top and top views of open and closed conformations seen on the right and left respectively (Yildiz et al., 2006).

1.3.2 Membrane Transport Proteins

A membrane transport protein is involved in the movement of ions, small molecules, or macromolecules. In order to transport substances, they span the membrane and hence are called integral membrane proteins. They usually have multiple helices spanning the membrane. The transportation of ions or molecules is achieved either by facilitated diffusion or by active transport. For the facilitated diffusion, the protein has specific amino acids lined across the membrane so that the molecule or ion to be transported moves down a concentration gradient. This process does not require free energy. The protein either has a channel so that the molecules pass through or it changes conformation to get the chemical from one side and release it to the other. A schematic representation of facilitated diffusion is seen in Figure 1.6.

[4] PDB id: 2iww (closed form) and 2iwv (open form).

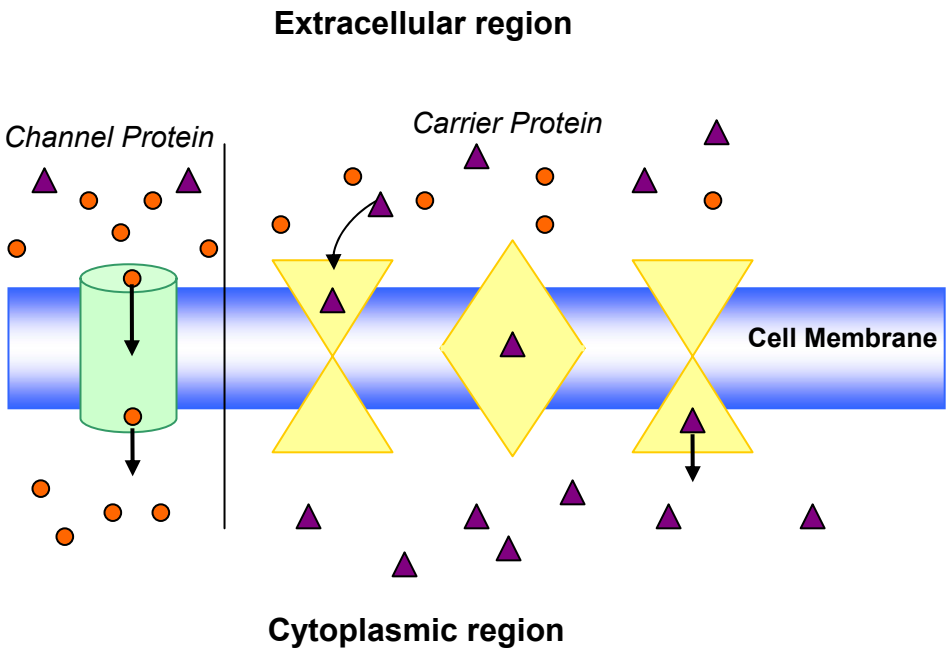

Figure 1. 6 Schematic representation of facilitated diffusion. Transport is through an existing channel in the protein on the left. Protein may also change its conformation during the transport as seen for a carrier protein model on the right.

In the case of active transport, the process requires free energy input. Prokaryotes typically use hydrogen ions as the driving force for chemiosmotic transport, while eukaryotes typically use sodium ions. If the transporter protein carries a chemical in the direction of the electrochemical gradient coupled with an ion, it is called a "symporter"/"coporter". An "antiporter" moves the target chemical in the opposite direction of the gradient in exchange of an ion like sodium or hydrogen. These proteins using the free energy produced by electrochemical ion gradient to transport small molecules are called secondary transporters. If the transport process involves the binding and hydrolysis of adenosine triphosphate (ATP), the protein is called a primary active transporter.

BetP from Corynebacterium glutamicum

Corynebacterium glutamicum is a gram-positive soil bacterium. In order to counteract hyperosmotic stress, it facilitates the uptake of solutes like glycine betaine, proline, ectoine or trehalose (Csonka, 1989; Wood, 1999) (Fig. 1.7) via secondary transporters like BetP, a member of the betaine-carnitine-choline (BCC) family of transporters. BetP acts as both an

osmosensor and osmoregulator by coupling the uptake of glycine betaine to the symport of two Na^+ ions.

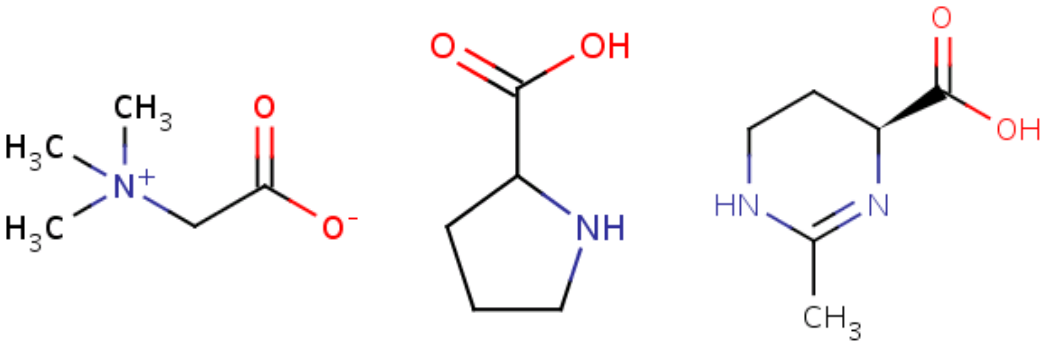

Figure 1. 7 Structures of glycine betaine, proline and ectoine, from left to right.

BetP is activated both on the level of expression and transport activity (Rübenhagen et al., 2001). It is predicted to have 12 transmembrane helices with a positively charged 50-residue long C-terminal and a negatively charged 57-residue long N-terminal, both facing the cytoplasm. The predicted secondary structure model of BetP is given Figure 1.8.

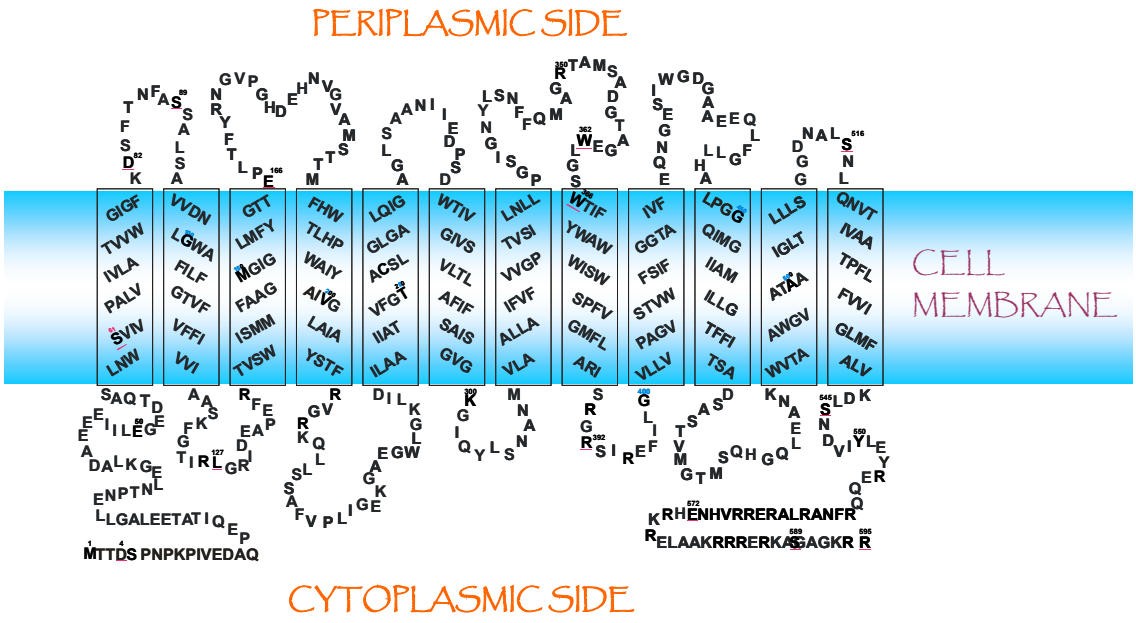

Figure 1. 8 Secondary structure model of BetP. It is characterized by 12 transmembrane helices shown by rectangules and long loops in the cytoplasmic and periplasmic side.

BetP is shown to have three different properties; catalytic activity by betaine transport; osmosensing via interactions of its C-terminal with the cytoplasmic side of the transporter

and the surrounding lipid bilayer; and osmoregulation via terminal interactions. The activity of BetP is regulated by the osmolarity changes induced by membrane impermeable solutes like NaCl, KCl or sorbitol. On the other hand, membrane permeable solutes like glycerol do not induce the activation. BetP is also activated by low temperatures. In the absence of any solutes, BetP is a fully active at 10 °C. However, the activation mechanism triggered by hyperosmotic shock and chill temperature requires the involvement of lipid molecules. Hence the membrane environment is considered to be the stimulus of activation. K^+ activation is observed for BetP in proteoliposomes. Thus, a certain interaction C-terminal domain with the headgroup of lipid molecules is suggested for the inactive state of the protein. The mechanism of activation due to high luminal K+ suggests that the C-terminus detaches from the lipid surface and interacts with either one or a group of cytoplasmic loops or with N-terminus (Fig. 1.9). The argument is based on the findings that although the N-terminus truncated protein can still be regulated, 23 or 32 a.a. deletions from the C-terminus results in down regulated protein. Therefore especially arginines in the C-terminus and the correct folding is crucial in the activation and regulation of BetP. It is one of the subjects of the present study to understand the mechanism of these properties.

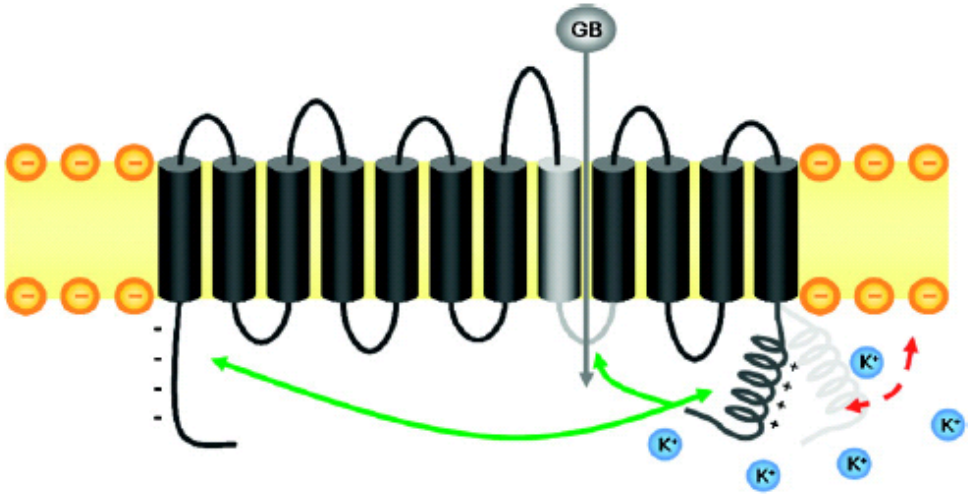

Figure 1.9 Working model of K^+ activation of BetP WT. Positively charged C-terminus is attached to the membrane surface in the inactive state. In the vicinity of excess K^+, C-terminus detaches and shifts either to loop 8 or to negatively charged N-terminus. Figure adapted from Ott et. al., 2008.

1.4 Protein Structure Determination

Protein structure determination is crucial in order to understand the function of a protein. Solved structures of proteins are published in journals and structure data is added to the *Protein Data Bank (PDB) (http://www.rcsb.org)*.

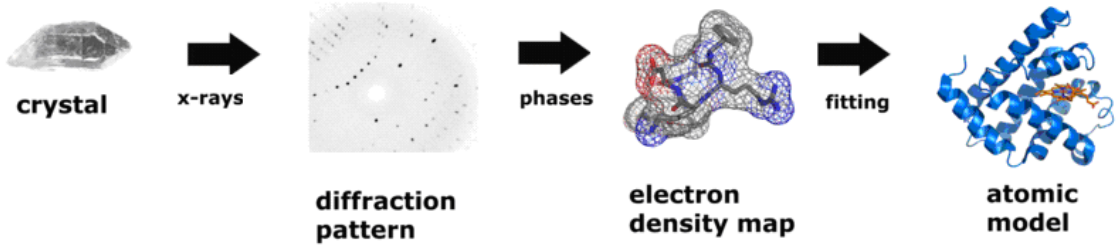

Figure 1. 10 Steps for solving the structure of a molecule by X-ray crystallography.

In determining the structure of proteins, X-ray crystallography is the most commonly used technique. Among the 50746 available protein structure coordinates in PDB by the end of the year 2008, ~44000 were resolved by X-ray crystallography, which corresponds to 86%. The technique is used to determine the arrangement of atoms in a protein crystal. The incident X-ray beam is directed onto the crystal and the beam is scattered in different directions depending on the spatial arrangement of atoms. Using the angles and intensities of these scattered beams, a three-dimensional picture of the electron density of the crystal is produced. Electron density map of a protein crystal enables to determine the mean positions of atoms and their chemical bonds. A schematic representation of the steps in solving a protein structure with X-ray crystallography is shown in Figure 1.10. Membrane protein crystallization is more difficult than soluble protein crystallization, since the membrane protein has to be surrounded by lipids or detergent molecules, which often interfere with crystallization.

Another technique utilized in protein structure determination is the Nuclear Magnetic Resonance (NMR) Spectroscopy. ~13% of the resolved structures have been determined using NMR. This technique allows one to work on proteins in solution. It is based on the principle of spin-magnetic field interaction. Nuclei having a net angular moment respond to external magnetic field applied during the NMR measurement. The chemical environment of

the nuclei determines the degree of this response and hence gives information about the molecule.

Electron crystallography, neutron Laue crystallography, cryo-electron microscopy, Circular Dichroism (CD) and Fourier Transform Infrared (FTIR) spectroscopy are also used as a means to obtain information about protein secondary structure.

1.4.1 FTIR Spectroscopy in Protein Research

Infrared (IR) spectroscopy, probing the vibrational modes of molecules, is based on the interaction of electromagnetic radiation with the electric dipole moment of the molecule. The energy transfer is possible for any orientation of the electric dipole except the perpendicular alignment of the dipole with respect to the electric field (Griffiths, 1986). Vibrations that do not affect the electric dipole moment are called IR-inactive and similarly molecules having no electric dipole, such as O_2 and N_2 having nonpolar bonds, are called IR-transparent in the mid-IR region.

IR spectroscopy is a non-invasive technique providing direct information on bond orders, electrostatic interactions, H-bonding, charge distributions, protonation states, redox states, dynamics and kinetics (Chirgadze and Nevskaya, 1976; Mantele, 1993; Siebert, 2008). If the emitted radiation frequency matches with the frequency of oscillation of the vibrating molecules, radiation is absorbed and the energy gained is used to excite the molecule among the vibrational energy levels. These transitions can be studied by IR and Raman spectroscopy. The IR region covers the range between 0.7-500 μm (14000 and 20 cm^{-1}) in electromagnetic spectrum. This region is divided into three groups as near-IR (0.8-2.5 μm or 12500-4000 cm^{-1}), mid-IR (2.5-25 μm or 4000-400 cm^{-1}) and far-IR (25-100 μm or 10-400 cm^{-1}).

An infrared spectrum is the plot of radiation absorption as a function of wavenumber ($\bar{\nu}$), frequency (ν) or wavelength (λ) ($\nu = c/\lambda$ and $\bar{\nu} = 1/\lambda$; where c is the speed of light). Excited molecular vibrations in a sample give unique absorption bands at almost exactly the same position in varying biological materials possessing the same group in their structure, so

called the group frequencies. Therefore, absorption spectra of the compounds are characterized by the functional group frequencies of the molecules. They are sensitive to any environmental changes or the changes in the structures and conformations of the molecules within. Those frequencies are also further characterized by the motions of the nuclei; which are mainly the twisting, bending, rotating and asymmetric/symmetric stretching modes. Some of the vibrational modes of a triatomic molecule are shown in Figure 1.11. Frequency values belonging to a specific mode of vibration are shown as ν_s for symmetric stretching, ν_{as} for antisymmetric stretching and δ for bending modes.

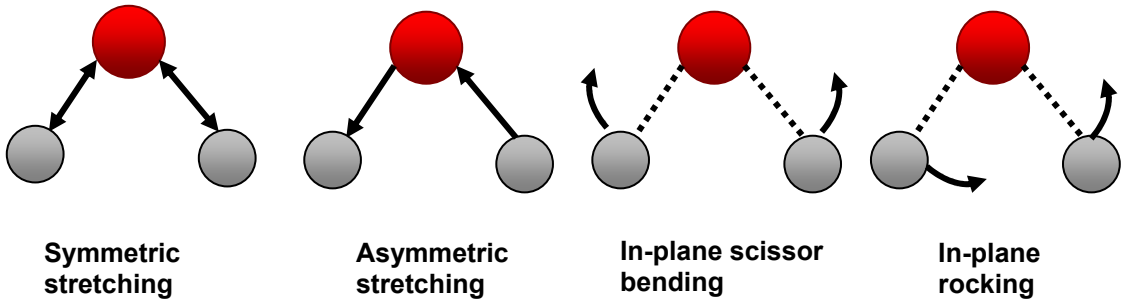

Figure 1. 11 Selected vibrational modes of a triatomic molecule. There are mainly two categories of vibration modes; stretching and bending. Bending modes has four types. In addition to the given two modes on the right in the figure, there are out-of-plane wagging and twisting modes.

Each of the vibrational modes of a molecule is associated with a characteristic frequency of the vibration. The energy levels of vibrational modes of a molecule are quantized and approximated by the energy expression for the quantum mechanical simple harmonic oscillator, simply to the behavior of a spring. The vibrational frequency, ν_{vib}, is given by the equation:

$$\nu_{vib} = \frac{1}{2\pi}\sqrt{\frac{\mu}{k}} \qquad (1)$$

where k is the force constant of the bond under question and μ is the reduced mass of the molecule possessing this bond, while the reduced mass is:

$$\mu = \frac{m_1 m_2}{m_1 + m_2} \quad (2)$$

where m_1 and m_2 are the atomic masses of two molecules connected through this bond.

Spectrometer

FTIR spectroscopy monitors the vibrational modes of a molecule. IR spectrum, thus, contains absorption bands originating from individual and coupled bonds of the protein together with the water and lipids and hence provides structural and functional information about proteins. It is a nonperturbing technique and requires small amount of sample (on the order of 2-5 μl). The instrument basically utilizes the principle of Michelson Interferometer. The classic Michelson Interferometer involves a Globar source (a silicon carbide rod heated to about 1000K), a beam splitter, two mirrors and a detector. The radiation emitted from the light source is split in two halves by a beam splitter. For the mid-infrared spectral range, the beam splitter is made up of a thin layer of Ge or Si, having high refractive index, deposited on KBr or CaF_2, having low refractive index. One half of the beam is transmitted to a moving mirror and the other half to a fixed mirror, from which they are reflected back to the beam splitter. Depending on the position of the moving mirror, a path difference between the two halves occurs when the beams recombine. The reflected light constructively and distructively interferes with the oncoming light. The beam then passes through the sample and reaches the detector. Two types of detectors are used; thermal and photon detector. In thermal detectors, IR radiation increases the surface temperature and changes the surface charge density of the substance. The detector monitors changes in intensity, and thus, the interferogram. Triglycine sulfate (TGS) and deuterated TGS (DTGS) are widely used substances for thermal detectors. Photon detectors operate at liquid N_2 temperature (77 K) in order to increase the sensitivity. IR radiation generates charge carriers in the material and thus, increases its conductivity. Measurement of the varying current with respect to the changing conductivity under constant voltage applied, enables monitoring the changing IR

radiation intensity. These detectors are made of a photoconducive film that is an alloy of mercury, cadmium and tellurium (MCT) deposited on an inert support.

Variation in the interference pattern intensity plotted against the mirror position, optical path difference is an interferogram as shown in Figure 1.12. It is then Fourier transformed by a computer to obtain the sample spectrum with the intensity as a function of wavelength. Fourier transformed interferogram is called a single beam spectrum. Fourier transform is performed to convert the signal from space domain to frequency domain as in equation 3.

$$S(\upsilon) = \int_{-\infty}^{\infty} I(\gamma)\mathrm{Cos}(2\pi\upsilon\gamma)\mathrm{d}\gamma \tag{3}$$

where S is the spectral intensity (amplitude), I is the intensity of the beam and γ is the path difference between the recombining beams.

Since the interferogram is a function of the moving mirror position, it is very crucial to precisely determine the mirror position. Therefore a monochromatic beam from a He-Ne laser of wavelength 632.8 nm is directed together and coaxial with the infrared beam in order to monitor the position of the mirror and also the digitization of the infrared interferogram, which is required for the mathematical process of Fourier tranformation.

Atmospheric water vapor and carbon dioxide have strong contributions to infrared spectrum. Therefore the sample chamber of the ineterferometer is continuously purged with dry air or N_2 and a background spectrum is recorded before the sample measurement. A single beam spectrum obtained without a sample is called a background spectrum. In order to eliminate the atmospheric or environmental contributions, the sample single beam spectrum is normalized against the background spectrum.

Consequently, the infrared absorbance of a sample is calculated as

$$A = \log \frac{I(\nu)}{I_0(\nu)} \tag{4}$$

where $I(\nu)$ and $I_0(\nu)$ are the single beam spectra of the sample and the background, respectively. Above equation is also called Beer-Lambert equation.

The resolution of an FTIR spectrometer is related to how precisely the moving mirror position is determined. While the mirror moves from the “+d” to “-d” position, a spectrum of approximately “1/d” resolution is obtained. The signal to noise ratio (S/N) of a spectrum is increased by collecting and averaging multiple interferometer scans of the sample before the Fourier transform. In this study, 250 scans were averaged for each spectrum with 2 cm^{-1} resolution.

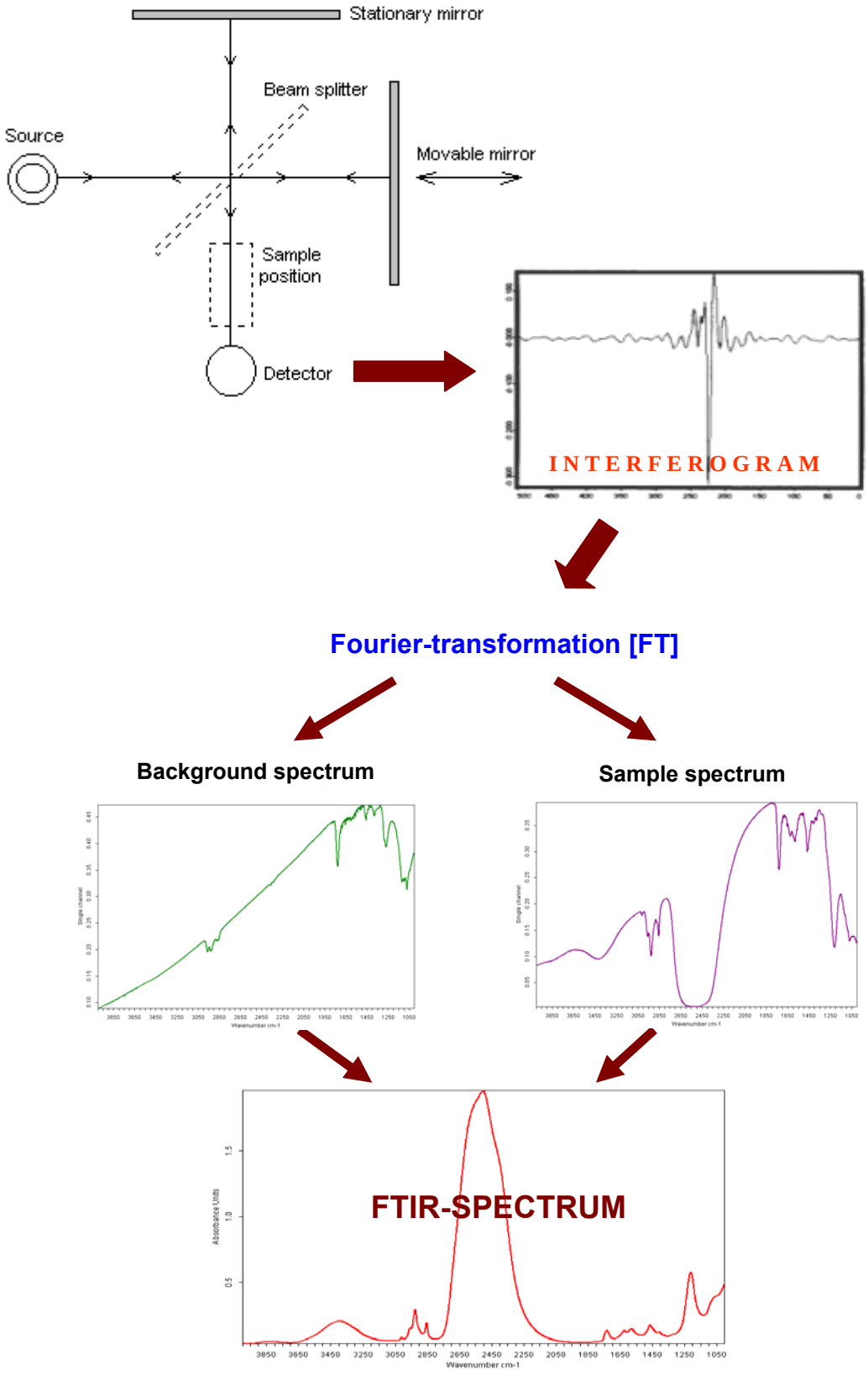

Figure 1. 12 Schematic diagram of Michelson Interferometer and how an FTIR spectrum is generated.
[Interferometer figure: http://teaching.shu.ac.uk/hwb/chemistry/tutorials/molspec/irspec3.htm]

FTIR Signatures of a Protein

The FTIR spectrum of a protein yields information about the structure of a protein through the protein backbone vibrations, which shows characteristic vibrational frequencies upon attaining different secondary structure profiles. The absorption signals from individual secondary structure elements originating from a specific vibration superpose in the amide modes, which are amide I-to-V and amide A.

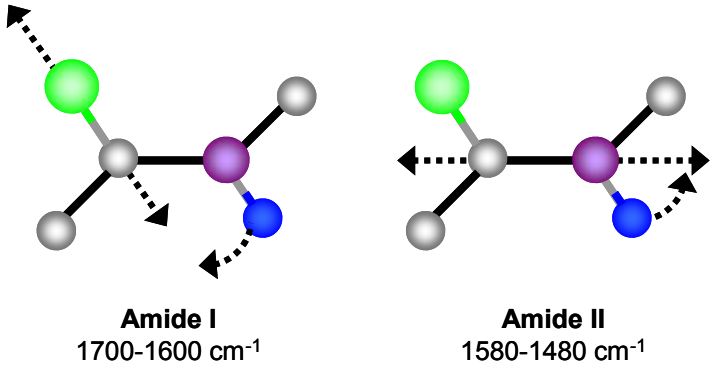

Figure 1. 13 The molecular motions of the amide I and II vibrations are shown. Carbon atoms are shown in grey, oxygens in green, nitrogen in purple and hydrogen in blue.

Amide I (1600-1700 cm^{-1}) is the most commonly used spectral region for the secondary structure analysis of proteins. It consists mainly of the C=O stretching vibrations of the protein backbone, having around 70-85 % contribution in the amide I range. It also has relatively small contributions from the out-of-phase C-N stretching modes (10-20 %) and from N-H in-plane bending (Fig. 1.13) (Bandekar, 1992; Krimm and Bandekar, 1986). Amide II (1480-1580 cm^{-1}) is mainly derived from the in-plane N-H bending (40-60 %), and the rest arises from both the C-N stretching vibrations (18-40 %) and the C-C stretching vibrations (roughly 10 %) (Fig. 1.13). Amide A (between 3225 and 3280 cm^{-1}) absorption is mainly, up to 95 %, due to the N-H stretching vibration and is sensitive to local environment of the protein. Amide III and V also bear structural information but are very complex blends of modes, therefore they are not preferred in protein structure analysis.

The amide I band is intrinsically rather broad and different secondary structural elements are not immediately evident. IR signatures of α-helix, unordered structure and β-sheet are shown

in Figure 1.13. Although the β-sheet has distinct features in the amide I region, α-helix and random coil structures overlap due to broad bands located at close wavenumbers in H_2O-buffer. There are, however, methods and analysis techniques developed to resolve this issue, which will be explained in the Materials and Methods section.

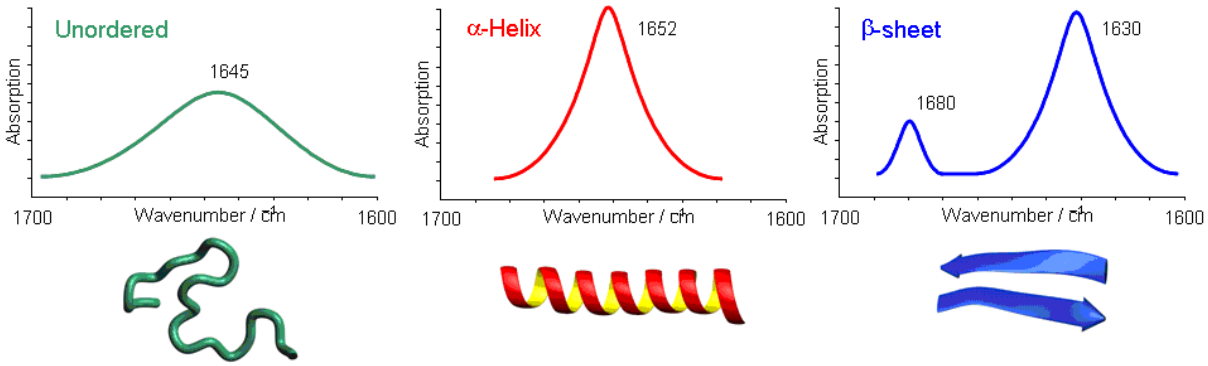

Figure 1. 14 Secondary structure motifs in the amide I region of IR spectrum (Figure is reproduced from Barth and Zscherp, 2002).

1.5 Objectives of This Study

This work will be focused on three membrane proteins, i.e., porin from *Paracoccus denitrificans*, OmpG from *Escherichia coli* and BetP from *Corynobacterium glutamicum*. The questions we address to porin are mainly focused on protein-lipid interaction at different oligomeric states of the protein and whether there are differences in these interactions at different states. OmpG is examined as a control sample in this respect, since the functional unit is a monomer.

OmpG porin structure-function relation will be addressed next. The pH dependent opening and closing mechanism for the channel has been proposed previously (Yildiz et al., 2006). The structural differences between the open and closed state and the mechanism that governs opening/closure of the channel will be investigated in this study. In this respect, we aim to study the secondary structure composition of OmpG in open and closed conformation; the thermal stability of OmpG wild type and mutants and compare the stability differences at different pH conditions; pH dependent conformational changes of the wild type protein and

the mutants; solvent accessibility differences among different states of wild type protein and mutants.

The glycine betaine transporter protein BetP from *C. glutamicum* will be the subject of studies. The structure of the protein is not known yet, however there are proposed mechanisms of activation as summarized in introduction. Therefore we aim to extend our work by doing structural analysis of BetP wild type protein and mutants in active and inactive state conditions. Among the three activating conditions, we only study the conformational changes with K^+ activation. The critical K^+ concentration will be determined in order to activate the protein in detergent solution and in 2D crystals and investigate the role of lipids in the conformational transition from inactive to active state. Comparing the thermal stability and solvent accessibility of the wild type protein and the mutants, we aim to get more information about the structure-function relation in active and inactive states of the protein.

2. MATERIALS AND METHODS

2.1 Materials

2.1.1 Chemicals

Agar-Agar	AppliChem
Ampicillin	AppliChem
Benzonase	Sigma
Biobeads SM-2	Bio-rad
$CaCl_2$	Merck
Deuteriumoxide	Aldrich
Ethylendiamin-tetraacid (EDTA)	Sigma
Isopropyl β-D-1-thiogalactopyranoside (IPTG)	Peqlab, MBI Fermantas
K_2HPO_4	Sigma
KCl	Roth
KH_2PO_4	Sigma
L-α-Phosphatidylcholine	Sigma
$MgCl_2$	Merck
N,N-Dimethyl-dodecyl-amine-N-oxid (LDAO)	Fluka
NaCl	Merck
n-Dodecyl-b-D-Maltosid (DDM)	Fluka
Octylglucoside (OG)	Fluka
Q sepharose fast flow	Amersham Pharmacia
Tris(hydroxymethyl)aminomethane	Merck
Triton X-100	Sigma
Tryptone	AppliChem
Urea	Roth
Yeast extract	AppliChem

2.1.2 Plasmid

The plasmid pJC40 with the recombinant PorG gene of *Paracoccus denitrificans* was provided by Prof. Dr. Bernd Ludwig and Dr. Krishna Saxena, Institute for Biochemistry, Goethe-University, Frankfurt am Main, Germany.

2.1.3 PDB Structure

The PDB structure of *P. denitrificans* porin was kindly provided by Prof. Dr. Wolfram Welte, Konstanz University, Konstanz, Germany.

2.1.4 Culture Medium

LB Medium

For 1000 mL of media: 10 g Tryptone, 5 g Yeast extract, 10 g NaCl

2.1.5 Buffers

TEN

100 mM Tris, 50 mM EDTA, 100 mM NaCl

TCM solution

10 mM Tris HCl, 100 mM $CaCl_2$, 10 mM $MgCl_2$. Final pH was adjusted to 7.

Potassium Phosphate Buffer

For 100 mM K-phosphate buffer, appropriate amounts acid and base salts (K_2HPO_4 and KH_2PO_4) were mixed for the desired pH as listed in Table 2.1. Final pH value was checked with pH meter or colored indicator sticks. Buffers in ^2H_2O were prepared acoording to the below table except that the desired p^2H is calculated by $p^2H = pH + 0.4$ (Glasoe and Long, 1960). Therefore, in order to have KPi buffer pD 6, calculations were made for pH 5.6.

Table 2. 1 Calculated amounts of 100 mM K-phosphate buffer components for 1ml volume.

pH	K_2HPO_4 (g)	KH_2PO_4 (g)
5.0	0.0135	0.00014
5.5	0.0130	0.0008
6.0	0.0121	0.0019
6.5	0.0089	0.0060
7.0	0.0056	0.0102
7.5	0.0017	0.0152
8.0	0.0005	0.0168

2.1.6 Antibiotics

Stock solution of ampicillin was prepared by dissolving 1g of ampicillin in 10ml distilled water. In order to sterilize, the solution was filtered through steril membrane filters of 0.22 µm diameter. Stock solution was stored at -20 °C. Final concentration of the ampicillin in culture media was set to 50 µg/ml.

2.2 Methods

2.2.1 Competent Cell Preparation and Transformation of *E. coli* cells

A single colony is grown in the shaker overnight in 5 ml LB medium at 37 °C. 25 µl of grown cells were used to seed 100 ml of LB medium. Cells were grown until the optical density at 546 nm (OD_{546}) is 0.3-0.4. The cells were then harvested in the centrifuge at 6000 RPM for 10 min at 4 °C (Sorvall GS3). The pellet was resuspended in 50 ml TCM medium and incubated on ice for 30 min. Cells were centrifuged again at 6000 RPM for 10 min at 4 °C and the pellet was suspended in 10 ml of 80% TCM- 10% glycerol. For long term storage, the mixture is divided into 100 µl aliquots, each frozen in liquid N_2 and kept at -80 °C until used.

Frozen competent cells were thawed for 5 min on ice. 2 µl of plasmid DNA was added, mixed gently by tapping and incubated on ice for 30 min. The cells were then heat-shocked by incubating at 42 °C for 45 seconds and left on ice again for 5 min. After adding 1000 µl of LB medium, the mixture was left in the shaker for 60 min at 37 °C. 100 µl of the mixture is used to plate LB plates with ampicillin. Plates were placed upside-down overnight at 37 °C in oven and later kept at +4 °C until used.

2.2.2 Biochemistry of Porin

Expression

A single colony from the plate was used to seed 10 ml of LB medium with 0.1% ampicillin (100mg/ml). The pre-innocula was incubated overnight in shaker at 37 °C. 1 l of LB medium is mixed with grown pre-culture and 0.1% ampicillin is added. Cells were grown for 4-5 hours in the shaker until OD_{600} was 0.6-0.7. Porin expression was started with 0.5 mM IPTG. Cells were incubated in the shaker for another 4-5 hours and then centrifuged at 5000 RPM (revolution per minute) for 30 min (Sorvall GS3). The pellet was suspended in TEN buffer and stored in sterilized tubes at -80 °C.

Purification

The purification of OmpF porin was done according to the protocol published by Saxena et. al (1997). Frozen harvested cells (from 1 l of culture) were thawed on ice and when half-thawed, benzonase was added for DNA digestion and incubated for 1 hour in the shaker at 37 °C. In order to break the cell walls, the solution was run twice through a narrow valve under 1000 atm pressure via French Press. It was then centrifuged at 5000 RPM for 40 min (Sorvall GS3)(pellet I & supernatant I in the SDS-PAGE in Fig. 2.1) and the pellet was suspended in 50 ml of TEN-2% (w/v) Triton X-100 buffer in order to solubilize the protein in the native state in detergent micelles and incubated overnight in shaker at 37 °C. The mixture is centrifuged at 5000 RPM for 30 min (Sorvall GS3) (pellet II & supernatant II in Fig. 2.1) and the pellet was suspended in 50 ml of TEN buffer. This washing step was repeated

and in between the washings the mixture solution was incubated for 2 hours in the shaker (pellet III & supernatant III in Fig. 2.1). The pellet was suspended in 8 M urea in buffer TEN and incubated for 2 hours at 37 °C and then centrifuged for 30 min at 35 kRPM (Sorvall ultracentrifuge, 60 Ti rotor)(pellet IV & supernatant IV). The pellet was then stored for SDS-PAGE analysis (Fig. 2.1) and the supernatant was mixed with TEN-LDAO (Lauryldimethyl aminoxide) 10% (w/v) buffer and loaded onto the Q sepharose fast flow column. The column was pre-washed with 2 bed volumes of 0.2% TEN-LDAO buffer before loading the mixture. The protein was eluted with a NaCl gradient of 0.1-1 M NaCl in 0.2% TEN-LDAO buffer. The gradient mixing, pumping the solutions through the column and U.V. screening at 280 nm was performed with automated liquid chromatography (ÄKTAprime, GE Healthcare, USA). The eluted protein was fractioned, loaded on to the SDS-PAGE for purity control of the protein and quantified as described in the following sections.

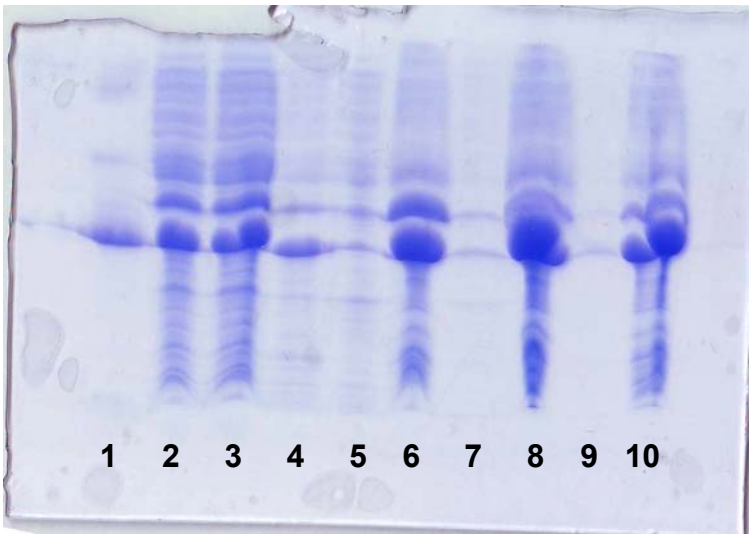

Figure 2. 1 SDS-PAGE of porin samples obtained at different steps of purification before loading on the Q-sepharose column. Lane 1: purified porin; 2: cells with benzonase ; 3: cell lysal after French press; 4: supernatant I; 5: supernatant II; 6: pellet II; 7: supernatant III; 8: pellet III; 9: supernatant IV; 10: pellet IV.

Protein Quantification

In order to quantify the protein, a Bio-rad protein assay kit was used according to the protocol available from the manufacturer.

Protein Quality Detection by SDS-PAGE

Sodium dodecyl sulfate polyacrylamide gel electrophoresis (SDS) was used according to Laemmli (1970). It separates proteins according to their mobility, which depends on the length of polypeptide chain or molecular weight and the order of the protein folding. SDS is an anionic detergent that denatures protein secondary and tertiary structure and gives a negative charge to the polypeptide. After loading the denatured protein in the gel, an electric current is applied across the gel so that the negatively charged proteins migrate towards the anode. Different proteins with similar molecular weights migrate along the gel due to different charge-to-mass ratios and hence, the distance of migration through the gel is related to the size of the protein. Shorter (lighter) polypeptides move through larger distances in the gel than the longer (heavier) polypeptides, allowing the user to distinguish proteins based on their molecular weights.

In this study, porin was analyzed using SDS-PAGE for its purity after purification and also during the purification steps in order to see whether there is loss of protein in washing+centrifuging cycles. Each sample to be loaded on the gel was mixed with sample buffer and heated to 80 °C for 5 min. Samples were then loaded onto the gel along with a protein marker. The protocol by Studier (2005) was followed for the rapid staining of the gel. The gel was suspended in 50 ml distilled water of 50% ethanol, 10% acetic acid and heated to boiling point in the microwave oven. It was left for shaking for 5 min and the liquid was discarded. The gel was resuspended in 50 ml distilled water of 5% ethanol, 7.5% acetic acid, and 200 µl of 0.25% of Coomassie brilliant blue in 95% ethanol. After shaking for 5 min, it was heated again to the boiling point and left on the shaker until the bands were visible.

Reconstitution of Porin into Liposomes

L-α-PC (phospatidyl choline) was purchased from Sigma and used for reconstitution. 2 mg lipid was dissolved in choloroform and dried overnight in order to get uniform bilayers. 2 ml of protein solution (0.5 mg/ml) was added to the dried lipids and the solution was vortexed until there were no lipid traces attached to the walls of the glass tube. The mixture was then incubated at 37°C in the shaker for 30 min. In order to get rid of the detergent molecules attached to the protein, Bio-beads were used. Bio-beads were first treated with a methanol-water cycle, mixed with the protein-lipid solution and left for incubation at 37°C in the shaker for 30 min. The tube was frozen in liquid N_2 for 1 min and thawed again. This freeze-thaw method was repeated for 3 times more and the tube was kept at +8 °C overnight. The supernatant was sucked with a syringe to separate the protein+lipid solution from Bio-beads and ultracentrifuged at 35 kRPM for 3 hours (Sorvall ultracentrifuge, 60 Ti rotor). The supernatant was discarded and the pellet was used for spectroscopic analysis.

A freeze fracture electron microscopy image of porin reconstituted in L-α-lecithin is shown in Figure 2.2. In the figure, concave shapes are membrane surfaces and the small dots on the surface are porins. As a result of the reconstitution protocol applied in this study, porins are nicely embedded in the lipid bilayer.

Figure 2. 2 Freeze-fracture image taken by electron microscopy of the reconstituted OmpF porin in lecithin. The circle in the figure indicates one of the membrane surfaces and the point-like structures on the surface are porins embedded in the bilayer. Image taken by C. Ziegler, Max Planck Institute of Biophysics, Department of Structural Biology, Frankfurt am Main, Germany.

2.2.3 OmpG from *E. coli*

OmpG WT (wild type) and the mutants listed in Table 2.2 were kindly provided by Stefan Köster and Dr. Ö. Yildiz, Department of Structural Biology, Max Planck Institute of Biophysics, Frankfurt am Main, Germany. The OmpG WT protein provided as OG slubilized stock solutions (0.53% W/V OG in Tris buffer, pH 8) were provided as 10 µl aliquots at 50 mg/ml concentration for WT and 10mg/ml for the mutants. 2D crystal samples were provided in Tris buffer. The buffers of OG-solubilized protein samples were exchanged to 100 mM K-phosphate by ultrafiltration (Millipore Centricon, USA) at the desired pH prior to the spectroscopic analysis. OmpG in 2D crystals were buffer exchanged to 100 mM K-phosphate by a dialysis membrane overnight, which was floating inside a large volume

(100 ml) of the K-phosphate buffer. For lipid reconstitution, the method described above for porin was applied.

Table 2. 2 OmpG mutants and the stocks provided for the analysis in this study.

Name of mutant	Mutated residues	Provided stocks
OmpG-ALA	His231Ala His261Ala	Detergent solubilized & 2D crystals
OmpG-CYS	His231Cys His261Cys	Detergent solubilized & 2D crystals
OmpG-ΔL6	Deletion of ∆220-228	Detergent solubilized & 2D crystals

2.2.4 BetP from *C. glutamicum*

Purified BetP WT and mutants were kindly provided by Dr. C. Ziegler, Department of Structural Biology, Max Planck Institute of Biophysics, Frankfurt am Main, Germany. The mutants are listed in Table 2.3 below. The stocks were provided as 100 µl aliquots of 5 mg/ml, which then were divided to 20 µl fractions for long term storage at -80 °C. DDM (n-dodecyl-beta-D-maltoside) solubilized (0.1%) BetP buffer solution was exchanged by ultrafiltration to 100 mM K-phosphate buffer at pH 7.4. 2D crystals were provided in phosphate buffer and thus were directly used for analysis.

Table 2. 3 BetP mutants and the stocks provided for the analysis in this study

.

Name of Mutant	Mutation	Provided Stocks
BetP∆C45	Deletion of ∆551-595 from C -terminal	Detergent solubilized & 2D crystals
BetA	Deletion of ∆1-29 from N -terminal	Detergent solubilized
BetY	Tyr550Pro	Detergent solubilized

2.2.5 Spectroscopic Techniques

In this study, FTIR spectroscopy in transmission mode and Attenuated Total Reflection (ATR)-FTIR spectroscopy has been utilized.

FTIR Transmission Spectroscopy

Infrared measurements were carried out in transmission mode using a demountable thin-layer IR cell with CaF_2 windows developed in our institute (Fabian and Mäntele, 2002). CaF_2 windows are transparent in the mid-IR region used in this study. The optical path length was calculated to be 12 µm for the particular pair of cells in hand. In order to determine the optical path length, the cells are placed empty and the absorbance spectrum is taken with air as reference. Absorbance spectrum yields sinusoidal waves and the wavelength of one wave determined from the spectrum is equal to the optical path length of the cells. Approximately 2 µl of protein sample were used for each experiment. Transmission experiments were performed for proteins both in H_2O and ^2H_2O buffer. For experiments in ^2H_2O, 8 µl of 10mg/ml protein sample in 100 mM K-phosphate buffer was loaded onto the center of the cuvette and dried under vacuum. The sample was then resuspended in 2 µl of ^2H_2O and the cuvette was sealed by using an oil-ethanol mixture in the outer ring of the flat window to prevent loss of water upon heating. IR-transmission spectra were recorded with a Bruker VECTOR 22 FTIR spectrometer (Bruker, Germany) equipped with an MCT detector.

For temperature ramp experiments, 256 scans were averaged and zero-filled for a spectral resolution of 2 cm^{-1}. Computer-controlled heating and cooling was performed by a water bath circulating the cell holder. In order to achieve temperatures above 100 °C, the water reservoir was filled with commercially available antifreeze liquid. Additionally, in order to decrease the temperature difference between the circulating liquid and the sample, a brass sample holder was built for improved temperature conductivity. Temperature values were taken from a thermocouple sensor coupled directly to the cell. A temperature-excursion program with heating of the sample from room temperature to 115 °C and recording of spectra every 5 °C takes approximately 20 hours. In order to increase the long-term stability, a background

spectrum was taken from a blank sample before each measurement using a sample shuttle. Spectra processing, secondary derivative calculation and further mathematical operations were performed using the spectrometer software OPUS version 4.2 (Bruker, Germany).

H_2O vs. ^2H_2O Buffer

Water has strong absorbance in IR spectrum. It particularly overlaps with the amide I region due to the O-H bending mode and partially interferes with lipid C-H stretching region due to H-O-H stretching vibrations centered around 3400 cm^{-1}. Absorption spectra of H_2O and ^2H_2O are shown in Figure 2.3 below. Therefore in most cases, where appropriate, protein was suspended in ^2H_2O (or represented also as D_2O) buffer since the characteristic bands for water shift to lower wavenumbers due to the increased reduced mass (Eq. 2) and hence shifts down from the amide I region. However, the O-H bending mode at 1650 cm^{-1} shifts down to 1230 cm^{-1} as seen from the figure, which overlaps with the PO_2^- stretching mode originating from lipid headgroups. Therefore the buffer solution had to be correctly chosen and carefully subtracted if necessary.

Water subtraction from the spectra was achieved by taking the 1250-1800 cm^{-1} region as a reference. The respective water spectrum was multiplied by an appropriate factor so that this region became a straight line. For D_2O subtraction, the low frequency band at 1230 cm^{-1} was used as reference for detergent solubilized protein samples. For protein samples in 2D crystals, the high frequency band at 2500 cm^{-1} was used.

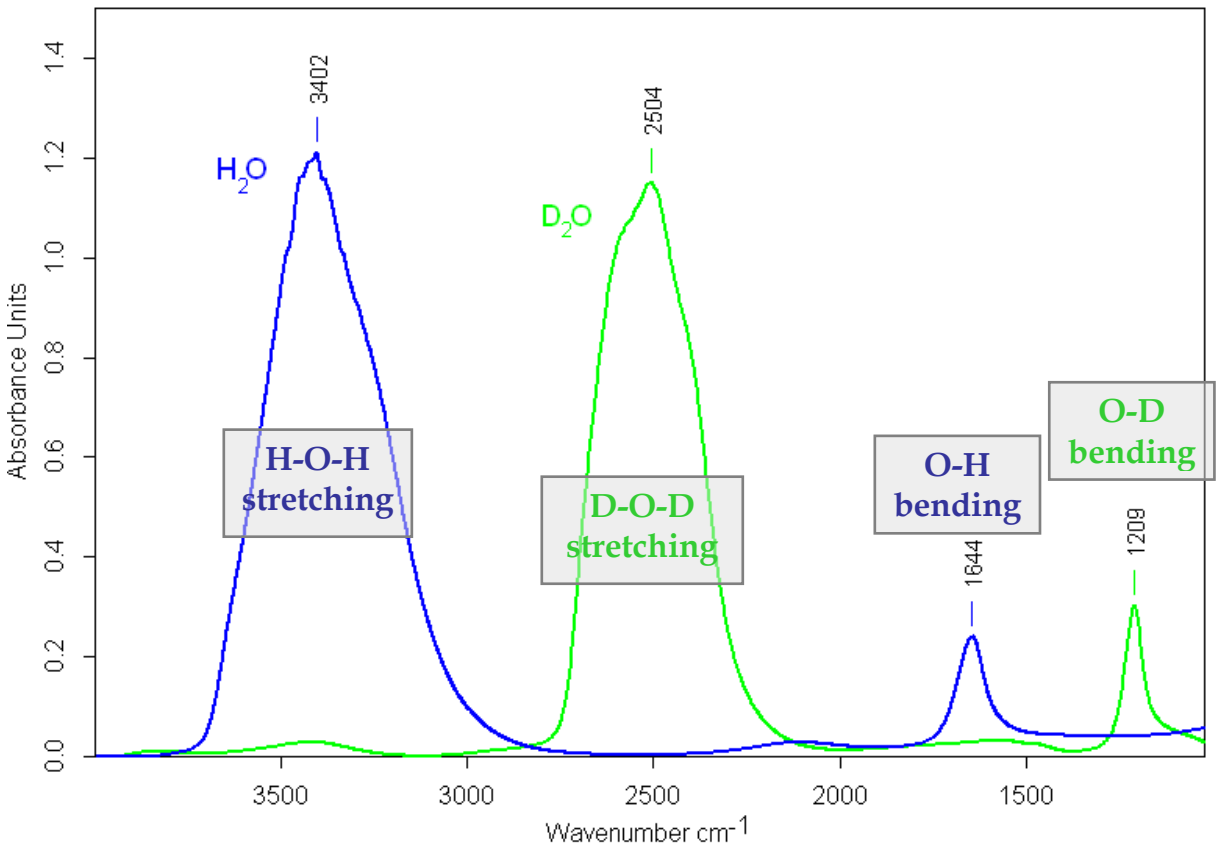

Figure 2. 3 IR-transmission spectrum of H_2O shown with blue and the spectrum of D_2O shown with green.

Protein Structure Analysis by FTIR

I- Second Derivative

Second derivative is the most widely used method for resolving overlapping bands, performed by the software OPUS 4.2. Local maxima are reflected as minima in the second derivative profile of a protein spectrum as shown in the figure below. Second derivative spectrum is especially useful for protein analysis in the amide I region since all secondary structure types appear in a 100 cm^{-1} spectral region (1700-1600 cm^{-1}) and hence overlap. A sample spectrum of porin in lecithin is shown in Figure 2.4. In the figure, although the main spectrum (continuous line) shows two peaks that are very close to each other, the second derivative spectrum (dashed line) shows many component bands as minima, which are not evident from the raw spectrum. While calculating the derivative of a spectrum, a

simultaneous smoothing of the spectrum is required to reduce the noise generated by the derivatization. Smoothing is basically the weighted mean of neighboring spectral data points. A smoothing factor of 5 means that five nearby data points are averaged and the resultant point replaces the five points in the spectrum.

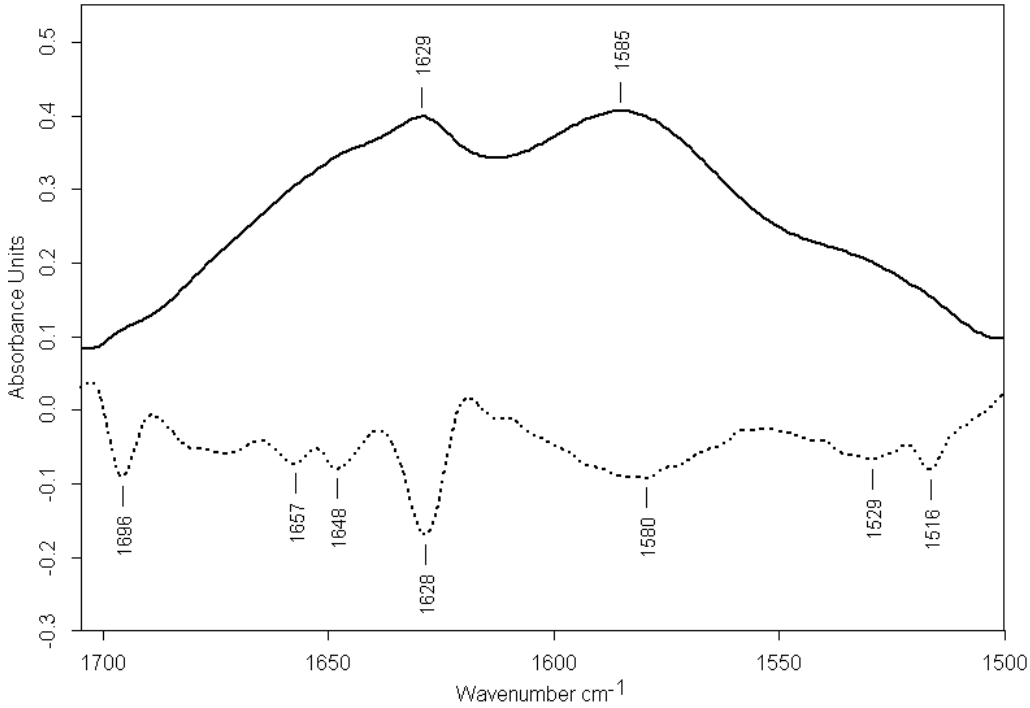

Figure 2. 4 IR spectrum of porin from *P. denitrificans.* The continuous line shows the raw spectrum and the dashed line represents the second derivative of the raw spectrum, calculated with a smoothing factor of 9.

II- Fourier Self Deconvolution (FSD)

Another way of determining the component band positions in an overlapping band is the FSD. Basically, it decreases the width of all lines contributing to the spectral range considered. As the lines get narrower, peaks are separated and become more distinguishable. The spectrum is deconvolved by multiplying the corresponding region of the interferogram with a function to amplify the signal amplitude and taking the Fourier transform again to get the deconvolved spectrum. The line shape function is the product of an increasing exponential function and a decreasing triangular apodisation function (Gronholz, 1985). In deconvolving the amide I region, a Lorentzian band shape of 29 cm^{-1} line width and

a noise reduction factor of 0.2 is applied using the Fourier Self Deconvolution built-in macro of the OPUS 4.2 software.

An example is shown for porin in lecithin in Figure 2.5. The same spectrum used in the second derivative calculation is shown here in order to be able to compare the results and the two methods for resolving overlapping bands. The continuous line (black) represents the raw spectrum and the dashed line (red) represents the resultant spectrum after FSD application. FSD amplifies an interferogram and also enhances the noise as a result of multiplying the inetrferogram with the deconvolution function, especially at the wings of the selected spectral region. This is the reason of obtaining higher amplitude after FSD application. However, the relative ratios of the peaks remain the same. Although many peaks are distinguished better with FSD, it is not as effective as the method of calculating the second derivative. Nevertheless, one can see the relative weights of individual peaks with FSD, which is not the case in second derivative spectrum. In most cases FSD and second derivative are used together to get information about the component bands.

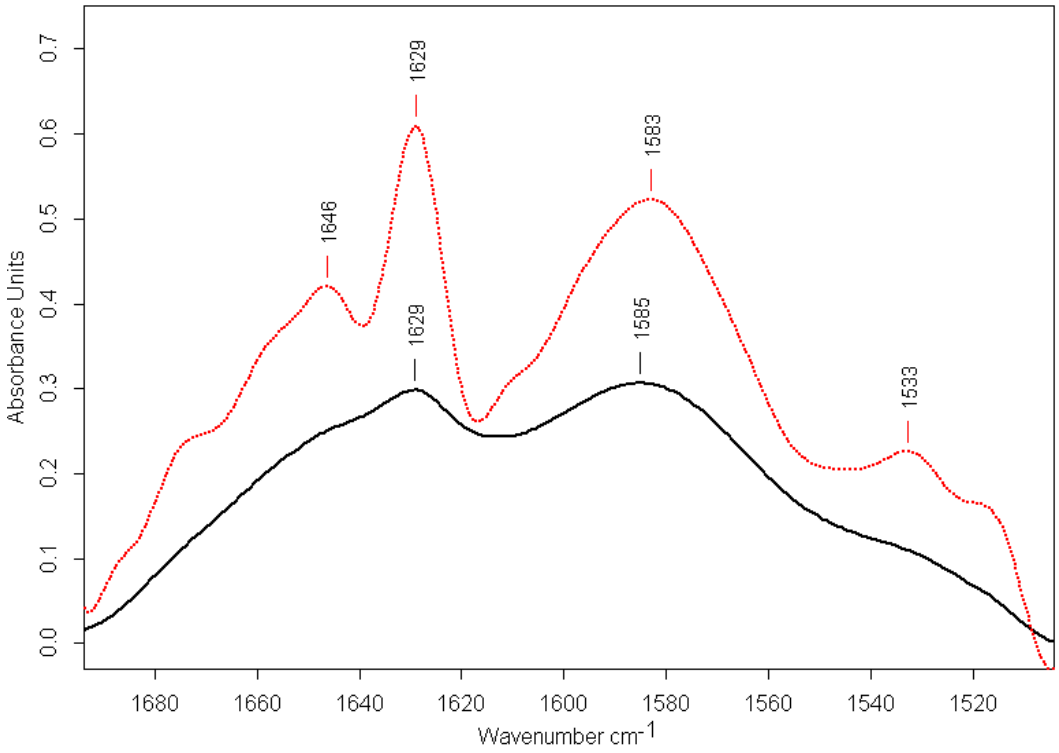

Figure 2. 5 IR spectrum of porin from *P. denitrificans.* Continuous line shows the raw spectrum and dashed line represents Fourier Self deconvoluted spectrum. Deconvolution was performed with a Lorentzian band shape with andwidth of 39 cm^{-1} and noise reduction factor of 0.19.

III- Curve Fitting

Curve fitting is the modeling of the broad envelope band by component bands. In this study, curve fitting has been performed by using a built-in macro based on least-square algorithm available with the software OPUS 4.2. There are four parameters concerning the fitting of an envelope band. They are the position, intensity, width and shape of each of the component bands. Positions are generally determined from the second derivative of the original spectrum. Relative intensities are determined from FSD results. The shape of a band can either be Lorentzian or a Gaussian or a combination of these two, called Voight function. A Lorentz function is defined as,

$$L(x;\gamma) = \frac{1}{\pi\gamma\left[1+\left(\frac{x-x_0}{\gamma}\right)^2\right]} \tag{5}$$

where, x_0 specifies the location of the peak and γ is the half-width at half-maximum (HWHM). The Lorenztian distribution shown in Figure 2.6 is calculated by setting the location parameter to zero and HWHM value to 0.5. A Gauss function, on the other hand, is defined as,

$$G(x;\sigma) = \frac{1}{\sigma\sqrt{2\pi}}\exp(-\frac{(x-\mu)^2}{2\sigma^2}) \tag{6}$$

where, μ is the location of the peak (mean) and σ defines the standart deviation (variance). The Gauss function shown in Figure 2.6 is calculated with a mean value of zero and a varience value of 1. Voight function is the convolution of Gauss and Lorentz functions, defined as,

$$V(x;\sigma,\gamma) = \int_{-\infty}^{\infty} G(x';\sigma)L(x-x';\gamma)dx' \tag{7}$$

where, x is the frequency of the line center. In the limiting cases where σ = 0, Voight function is a Lorentzian and for γ = 0, it is a Gaussian.

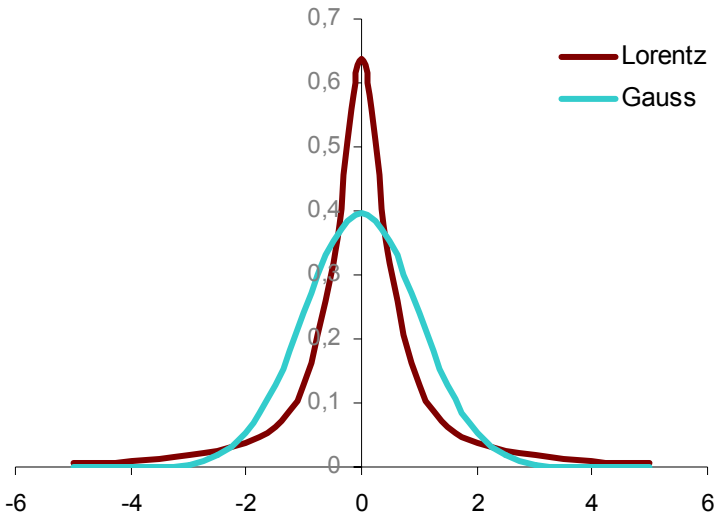

Figure 2. 6 An example of Gauss and Lorentz functions centered at x = 0.

The component bands under a broad envelope band, then, can have different band profiles. The location of the components and their relative intensities are entered in the curve-fitting program via an interactive user interface and the band profile was set to Voight function in this study. The program also can optimize these parameters by using a least square algorithm in order to get the best fit between the constructed envelope and the original one. This method is especially useful and is the sole method of determining the secondary structure weight percentages of proteins from FTIR spectroscopy. One simply calculates the area of each component band and finds the percentage of its contribution to the total amide I area. A fit example is shown in Figure 2.7 for porin in D_2O buffer.

A component band is defined with four parameters as described above. The curve-fitting method success then heavily depends on the user entries. Particularly the determination of the number of component bands is extremely crucial. Although second derivative profile resolves the overlapping bands in an envelope, some small contributions may still be hidden. In most practical cases, curve fit success is determined by taking the difference spectrum of the raw and constructed envelope (Anbazhagan et al., 2008; Chehin et al., 1999); however, this method does not discriminate between a successful fit and a fit with too many component bands. In this respect, we additionally compare the second derivative profiles of

the two envelopes since only the correct number and composition of component bands will give the same second derivative profile with the raw spectrum.

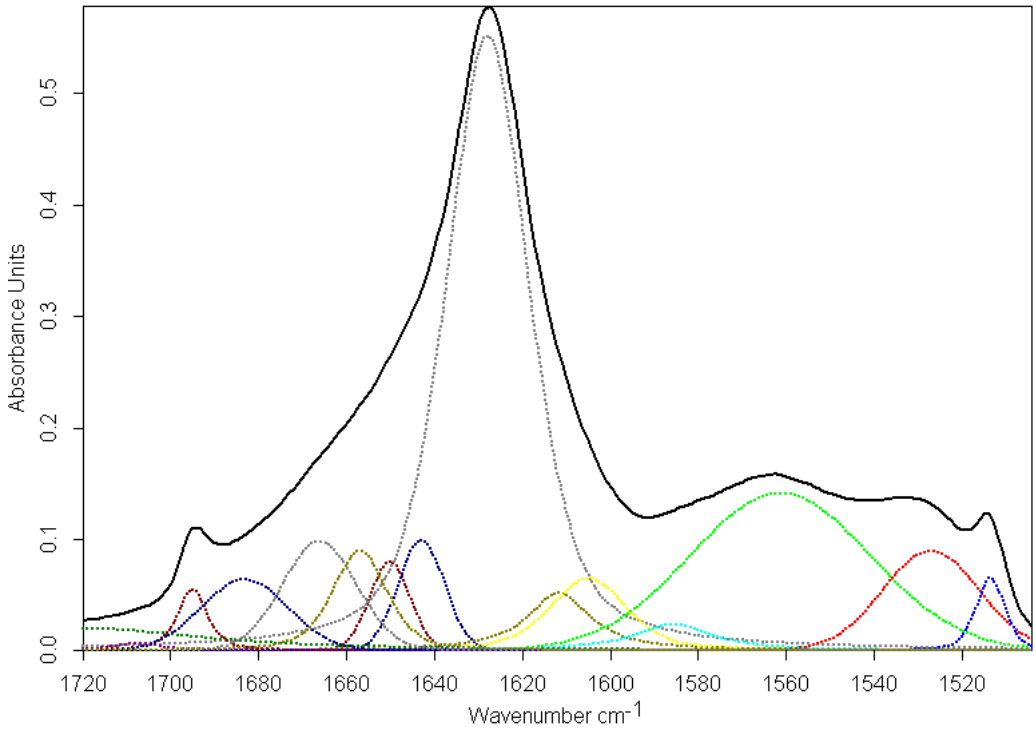

Figure 2. 7 Amide I and II region of OmpG WT pD5.4 in IR spectrum, represented by the continuous line and curve fitted bands using OPUS 4.2 represented by dashed lines.

FTIR-ATR Spectroscopy

FTIR ATR spectroscopy is a surface sensitive absorption spectroscopy method that is used to analyze small amounts of material close to an interface with IR radiation. In the ATR geometry, IR radiation is totally internally reflected at the interface between an internal total reflection element (IRE) and a less dense medium (air, liquid, solid or polymer). Each internal reflection results in the production of an evanescent field that extends a few microns into the coating layer and any IR absorbing species that approaches the interface will absorb radiation and attenuate the main beam, giving rise to a spectrum modified by the absorption properties of the material. The choise of the IRE material influences the specral intensity since the penetration depth of the evanescent wave depends on the refractive index, as given by

$$d_p = \frac{\lambda / n_1}{2\pi\sqrt{\sin^2\theta - \left(n_2 / n_1\right)^2}} \quad (8)$$

Where, λ is the wavelength of light within the IRE; n_1 and n_2 are the refractive indices of IRE and the sample, respectively; and θ is the incidence angle of the beam. IRE material can be germanium (n = 4), silicon (n= 3.42), ZnS (n= 2.42) or KRS-5 (n= 2.35) due to their high refractive indices indicated in paranthesis (Goormaghtigh et al., 1999).

The chemical specificity and surface sensitivity of this technique make it ideal for studying the adsorption of monolayers and ultra thin films of organic molecules such as polymers and proteins in combination with flow and perfusion techniques. ATR also enables to study the diffusion of individual chemical species through thin films and membranes.

In this study, a home-built ATR-FTIR microdialysis cell has been used (Dzafic et al., 2009). 5 µl of protein sample (1mM concentration) are placed on top of the ATR crsytal and the compartment is closed via a dialysis membrane of 25 kDa pore size. On top of the membrane, the compartment has an inlet tubing and an outlet tubing enabling to perfuse the protein sample with a buffer during the IR scan and hence study *in situ* changes in protein structure (Fig. 2.8). The buffer is circulated through the protein sample at a constant speed with a preristaltic pump. Speed of the pump was set to 0.3 ml/min for the experiments presented in this study. The influence of effector molecules, the change of solvent, or the switching from H_2O to D_2O buffer is possible while the protein is periodically scanned. In this study, we have performed activation experiments by changing the salt amount or pH of the solvent as well as H/D exchange.

I- H/D Exchange with ATR-FTIR Flow-Through Cell

It is a widely used technique in order to identify different domains of a protein. This method of revealing the molecular groups accessible by solution and simultaneous screening with IR spectroscopy is called H/D exchange experiment. The method is particularly useful in protein structure studies using the fact that some secondary structure groups do not exchange but some rapidly exchanges with deuterium. The protons on the surface of a protein, exposed to

buffer solution will exchange with deuterium upon dissolving in D_2O buffer. After these fast exchanging protons, relatively flexible regions (loops) buried in the protein exhibit slower exchange rates. On the other hand, protons from the protein core either exchange very slowly or remain unaffected from the changing buffer.

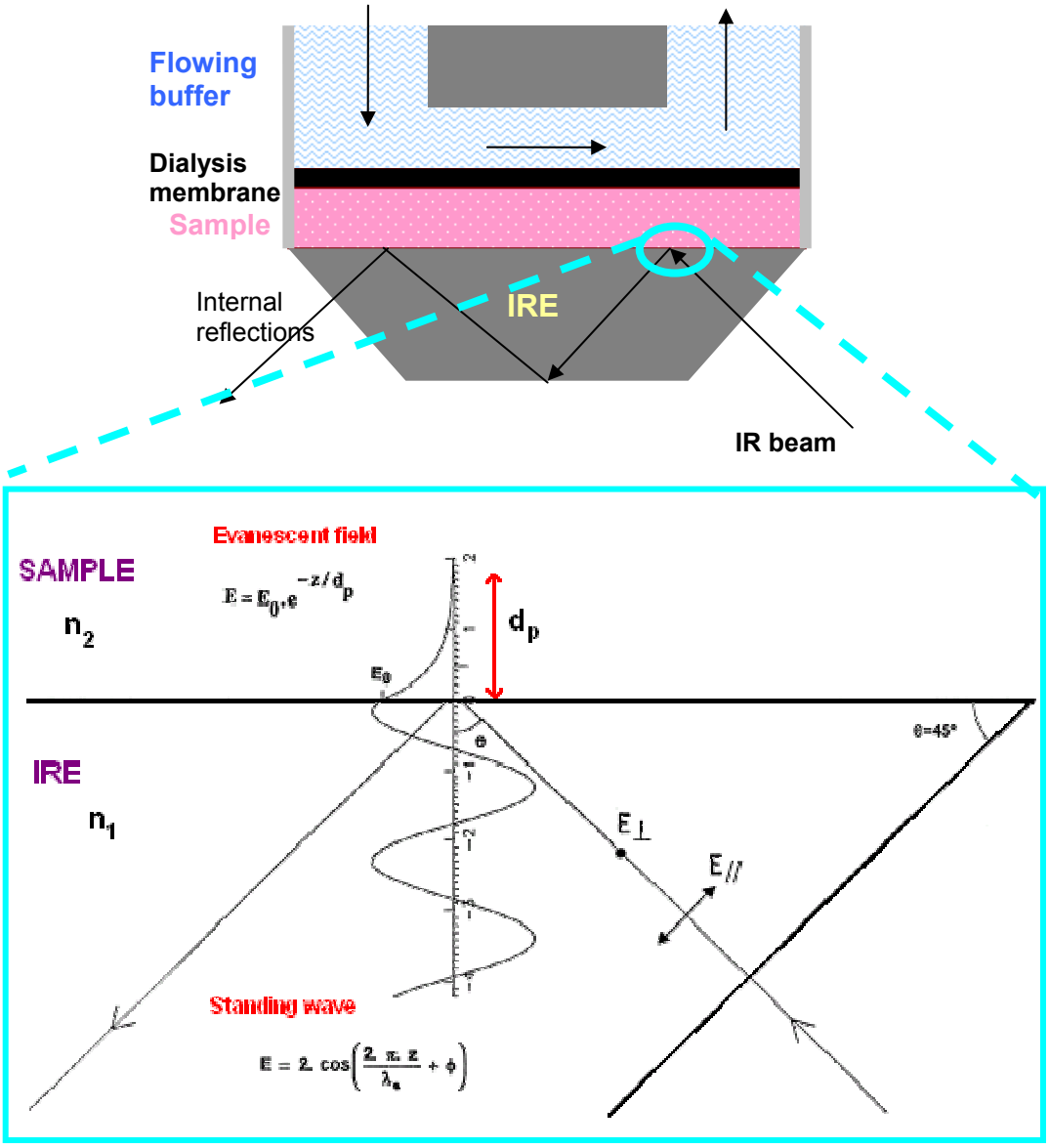

Figure 2. 8 Schematic drawing of the ATR-crystal (the IRE element) with a liquid sample that is shown atop on one side of the crystal. Perfusing buffer and the sample chamber are separated with a dialysis membrane. The internally reflected IR beam is producing an evanescent wave penetrating through the liquid sample. Incident and evanescent beams are shown in greater scale at the bottom of the figure, where the penetration depth is indicated by d_p. (Figure adapted from Goormaghtigh et al., 1999)

One advantage of incubating the protein in D_2O buffer is that it enables the discrimination of unordered structure and α-helix. Unordered structure in H_2O buffer solution has the characteristic band at around 1655 cm^{-1}; which is the same region for α-helix structure. However, after suspending the protein in D_2O, this frequency shifts down to 1640 cm^{-1}, while α-helix remains at ~1655 cm^{-1} in most cases, thus enabling better determination of secondary structure composition of a protein. One can also measure the time rate of shift of this frequency to get information about the parts of a protein facing the buffer solution, which is especially useful for membrane protein research.

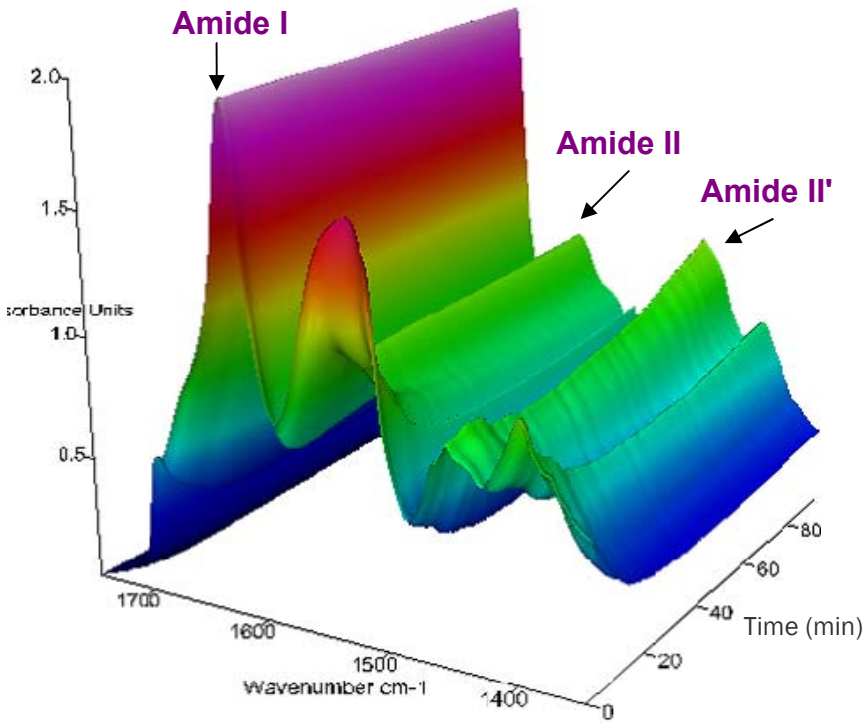

Figure 2. 9 3-D representation of *in situ* H/D exchange experiment performed with ATR-FTIR perfusion microdialysis cell. The protein sample is first incubated in H_2O buffer at time zero and it is changed to D_2O buffer by perfusion. Exchange is indicated by the intensity decrease of amide II (~1550 cm^{-1}) and simultaneous increase of amide II' (~1450 cm^{-1}) for the first 90 minutes of the exchange.

In the H/D exchange experiments, the process is followed by two major changes; gradual intensity loss of water bands and along with that the gradual raise of deuterium bands (Fig. 2.3). In the intermediates of the process, the H-O-D bending vibration appears at 1450 cm^{-1}. This band interferes with the fingerprint region of the spectrum and has to be carefully

subtracted. Together with the solvent absorbance changes in the spectrum, there are changes in the sample spectrum due to the exchanging hydrogens. The amide I region has a small contribution from N-H bending which becomes N-D and shifts down in D_2O. The amide II region (1600-1500 cm^{-1}) is however affected more from the N-H in plane bending vibrations and, upon dissolving the protein in D_2O, most of the band shifts down by about 100 cm^{-1}, thus creating another band called amide II'. On this basis, one can calculate the rate of H/D exchange by integrating the amide II band and analyzing the time course of this area change. Furthermore, amino acid side chains carrying exchangeable protons exposed to solution exchange with deuterium and will shift down in the spectrum. Studying the positions of these side chains in H_2O and D_2O will reveal whether they are in direct contact with the solvent and will help to identify these groups.

The protein sample is first equilibrated by flowing 100 mM H_2O K-phosphate buffer. After the sample is equilibrated so that the sample spectrum is stable over time, the buffer is switched to 100 mM D_2O K-phosphate buffer. 15 ml of D_2O buffer is used, from which 13 ml is discarded to make sure that the buffer in the tubings and the flow compartment is completely exchanged, while the remaining 2 ml is left for closed circulation. In order to observe the fast exchanging parts, 128 scans were averaged in every 150 seconds. After the first hour of exchange, 256 scans were averaged. Exchanging the ordered parts of a protein takes relatively longer time than for the unordered parts; therefore the exchange process has been followed for 24h for each of the samples.

For the analysis of spectra from H/D exchange experiments, the method described by Dzafic et. al (2009) was used.

II- Difference Spectra

Using the same microdialysis membrane, one can also study the conformational changes induced by different buffer contents. Since opening and closing of OmpG depends on the pH of the buffer, the ATR cell has also been used to observe minute changes accompanying

opening and closing. BetP activation on the other hand depends on the salt content. BetP is activated with high K^+ in the environment.

Absorbance spectra of a protein were generally taken against air or buffer solution to see the protein bands free from buffer absorbance in the same region of interest. If however, the inactive state of the protein is taken as background spectrum and active state as the sample spectrum, the result is a difference spectrum where ideally the positive bands represent the molecular groups in the active state and the negative bands represent those in the inactive state.

3. RESULTS AND DISCUSSION

3.1 Interaction of *P. denitrificans* Porin & OmpG from *E.coli* with Lipids

Similar to other members of porin family, *P.denitrificans* porin is extremely thermostable (Haltia and Freire, 1995; Sukumaran et al., 2005; Sukumaran et al., 2004). It was found that OmpF aggregates in detergent micelles when heated above 86 °C. However, if reconstituted into liposomes, there is no change in its global secondary structure up to 90 °C. It was also reported previously that it has different structural stability in different lipid environments. Among the various pure lipids tested, a non-uniform lipid bilayer is found to be the most appropriate in mimicking the natural environment (Sukumaran et al., 2005). This difference in structural stability between solubilized porin and porin in pure or mixed lipid environments has been attributed to the specific interaction between the aromatic girdle of porin (Fig. 3.1) and its immediate lipid environment (Sukumaran et al., 2004). Tyrosine OH groups and tryptophan indol groups point toward the lipid headgroups, while phenylalanins are located in the lipid core. Altogether, they form the part of the protein interacting with the membrane by forming H-bonds in the bilayer-water interface. The role of tyrosine deprotonation for porin unfolding at alkaline pH has already been reported (Sukumaran et al., 2004).

Previous functional studies and SDS-PAGE anlaysis have shown that when porin in detergent micelles is heated above 50 °C, it starts monomerizing and looses its function already by >90%, yet the secondary structure of the protein is unaffected. As the temperature is further increased the function is completely lost as the fraction of monomer/trimer increases (Sukumaran et al., 2006a).

FTIR spectroscopy provides access to several reporter groups with IR signatures that can be used to probe different depths of the lipid bilayer and their interaction with specific parts of proteins (Fig. 3.2). In detail, these are the lipid CH_2 and CH_3 antisymmetric and symmetric stretching modes in width and position (Cameron et al., 1980; Mantsch and Mcelhaney, 1991), the lipid C=O stretching mode, the lipid PO_2^- antisymmetric stretching mode as well

as the amide I mode for the protein backbone and the tyrosine side chain C=C mode (Fringeli and Gunthard, 1976; Korkmaz and Severcan, 2005; Zscherp et al., 2003). For these modes, the temperature-dependent band positions and, partly, the half widths can be taken. These reporter groups have been extensively used in previous IR studies on model membranes and proteins (Beck et al., 1998; Toyran et al., 2007).

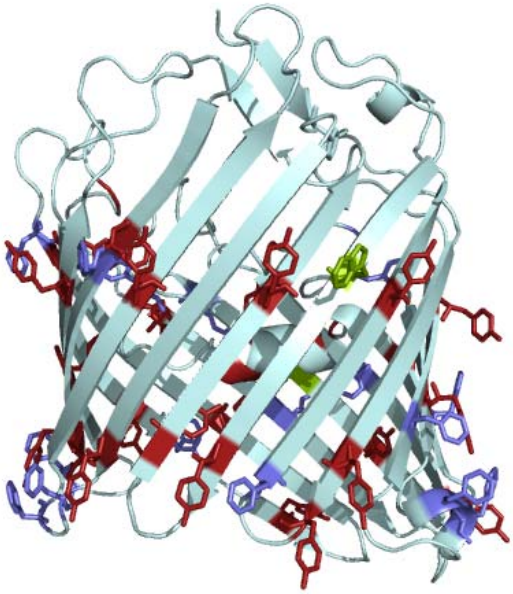

Figure 3. 1 Porin monomer aromatic girdle. Tyrosines are shown in red, trptophanes are in green and phenylalanins are in violet.

The structure, thermal stability and porin—lipid interaction were monitored by FTIR spectroscopy. The first reporter groups addressed are the tyrosine side chains at the protein-lipid interface. Aromatic amino acids play a key role in protein-lipid interaction since they are known to lock the protein into its correct position in the lipid bilayer (de Planque et al., 2003; Yau et al., 1998). Aromatic side chains of tryptophan and tyrosine preferably point towards either the membrane-water interface or the hydrophilic region. The X-ray crystal structures showed that detergent molecules are populated around these belts (Hirsch et al., 1997; Yildiz et al., 2006). Tyrosine side chains give rise to a characteristic C=C vibrational mode which peaks at around 1515 cm^{-1} in the protonated form. As a remarkable property, this mode shows only a small variation from 1513 cm^{-1} to 1517 cm^{-1} even among very different proteins (Zscherp et al., 2003). It is evident in absorbance and second derivative spectra and its

position can be determined to < 0.1 cm^{-1} precision for FTIR spectra by second derivative formation. In the deprotonated form, this mode shifts to around 1498 cm^{-1} (Sukumaran et al., 2006b).

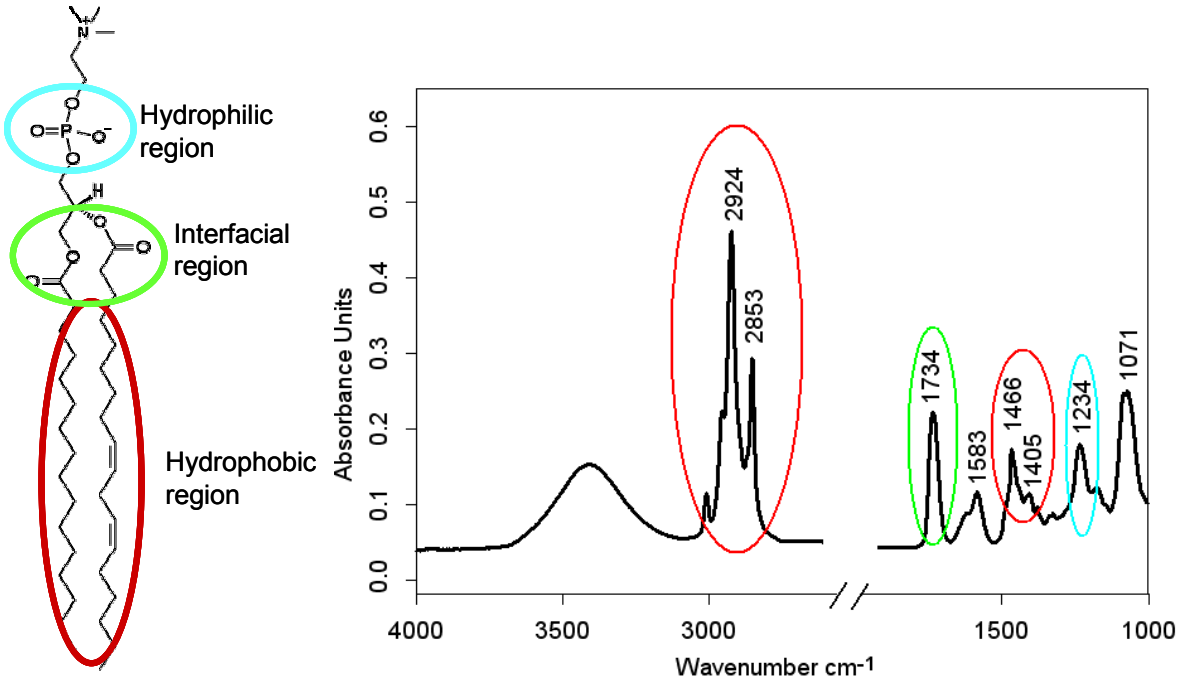

Figure 3. 2 FTIR reporter groups used in screening the different depths of a bilayer shown on the phospholipid molecule scheme on the left and on the IR spectrum of lecithin on the right, encircled with the same colors.

The peak position of Tyr as determined from second derivative spectra with respect to temperature obtained in a temperature excursion experiment is shown in Figure 3.3. Overall, a two-step transition is evident for OmpF as shown by the divisions in the figure. From room temperature up to 55 °C, the Tyr peak position is almost constant, averaging at around 1514.4 cm^{-1}. Between 55 °C and 77 °C, the C=C mode position gradually shifts to 1512.7 cm^{-1}. At around 82 °C, a second phase of downshift starts and continues up to 90 °C where the Tyr band appears at around 1511 cm^{-1}. Notably, the first phase covers a temperature range of about 20 °C, while the second phase is much sharper and is complete in a temperature span of only 8 °C. Nevertheless, both involve comparable shifts of the C=C mode. OmpG displays an upshift with increasing temperature in the overall graph; however, does not show this two step transition. The tyrosine peak position remains the same up to ~77 °C and then shifts to higher wavenumbers with further increasing temperature.

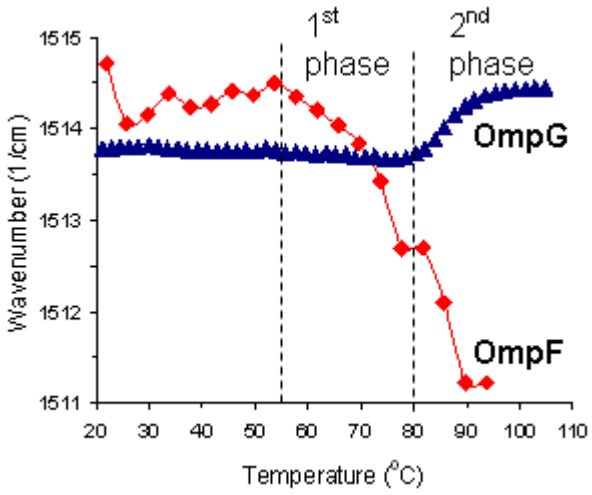

Figure 3. 3 IR signal of tyrosine C=C mode as a function of temperature for reconstituted OmpF (red diamonds) and OmpG (blue triangles).

Since the tyrosine side chains of the aromatic girdle face towards the membrane-water interface, an interaction of the OH group with the C=O group of the lipid molecules in the interfacial region of the membrane is probable. This lipid C=O group gives rise to a stretching mode, which is located around 1730 cm^{-1} in the IR spectra. Lipid samples used in this study are a mixture of saturated and unsaturated lipids with different acyl chain lengths adapted to the natural lipid environment of porin. Differences in lipid structure result in slightly different positioning of C=O modes from different *sn*-chains. Depending on their hydration status, these bands further split in positions that are only a few wavenumbers apart. Therefore C=O groups of bound lipids and bulk lipids give rise to a single superposed signal between 1770 and 1700 cm^{-1}; however, the component bands can still be discriminated by taking second derivative of the spectrum (Blume et al., 1988; Fringeli and Gunthard, 1976). Component bands at lower wavenumbers are attributed to hydrogen-bonded ester groups. A component band at higher wavenumbers indicates the lack of H-bonding. Measuring only the peak position gives information about the overall behavior of the band and this may not be sensitive enough for probing small changes in lipid-water interface of membrane bilayer or even be misleading (Hubner et al., 1990). Therefore we measure the band position of C=O stretching band from half-height and compare with individual component behavior with respect to temperature. To achieve this, we have normalized the band intensity to 1 among

different samples and different temperatures. We then measured the midpoint of the horizontal line dividing the band at its half-height. In the analysis of the C=O stretching mode, with homogeneous lipid samples, curve fitting helps better understanding the individual component response to the external variable such as the presence of an interacting molecule or the temperature (Lewis and McElhaney, 2000; Zhang et al., 1992a). In our study, curve fitting has been attempted in order to be able to identify each component and which lipid groups they belong to. As seen from the second derivative profile of the C=O mode for all the samples (Fig. 3.4), there are at least 6 components and the number increases with increasing temperature. We found that an interpretation of the behavior of each component was too speculative and was not supported by the data. Thus, we preferred to measure the overall C=O stretching band position.

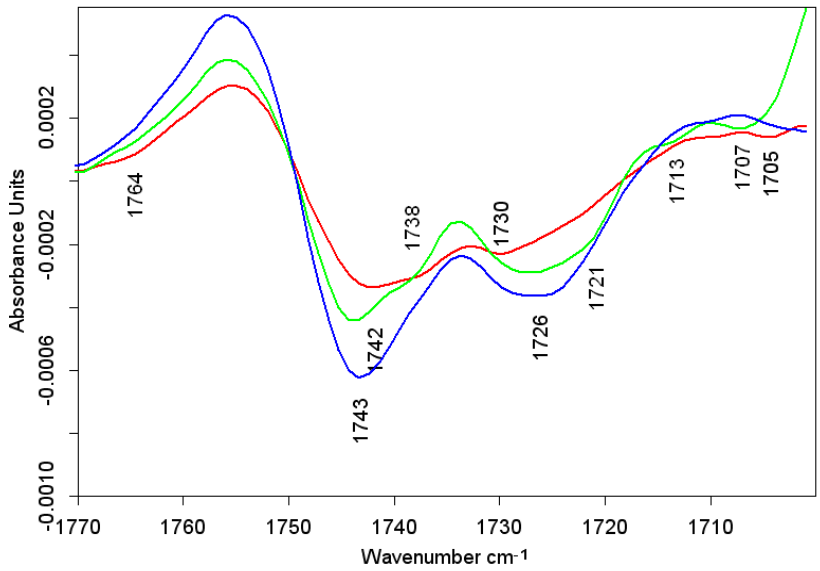

Figure 3. 4 Second derivative profile of C=O ester stretching mode of blank lipid (blue), OmpG (green) and OmpF (red) in lipids at 20 °C.

The temperature dependence of the C=O stretching mode during the temperature excursion experiment for reconstituted OmpF and OmpG is determined from the corresponding band position at ~1730 cm^{-1}. Three sample spectra are selected from OmpF and OmpG experiments at RT, 60 and 80 °C and shown in Figure 3.5A. The C=O band position for OmpF, shown on the left, at RT and 60 °C is almost the same and hence can not be

distinguished well in the figure. However, at 80 °C the band shifts remarkably, as shown by the dotted line. The same band for OmpG, shown on the right, is not affected by the temperature excursion for RT-80 °C region.

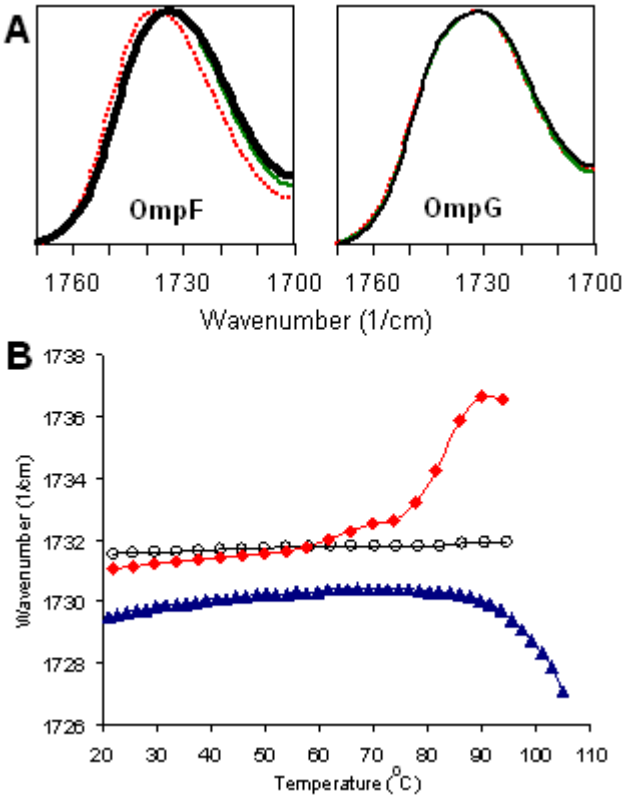

Figure 3. 5 (**A**) FTIR spectrum of lecithin C=O stretching region (1780-1700 cm^{-1}) in the presence of OmpF on the left and OmpG on the right. In both spectra, straight bold line (**—**), straight line (—) and dotted line (·····) represent the spectra at RT, 65 and 80 °C. (**B**) Graph of the C=O band position as a function of temperature for blank lipid sample (open circle) and reconstituted OmpF (red diamond) and OmpG (blue triangle).

Temperature dependence of the C=O band for the entire experiment for blank lipid, reconstituted OmpF and OmpG are shown together in Figure 3.5B. For the blank lipid sample, the band position does not show any significant change. For OmpF reconstituted into lipids, there is an overall upshift with increasing temperature. While the upshift of the band between RT and approximately 50-55 °C is very small (≈ 0.5 cm^{-1}), this shift increases between 55 and 70 °C and further between 75 and 90 °C. Overall, the band shifts from about 1731 cm^{-1} to 1737 cm^{-1}, thus indicating a less H-bonded C=O group. Notably, this shift occurs in two phases in temperature regions comparable to the shift of the tyrosine C=C mode discussed above. For the pure lipid sample without porin, the overall shift over the

temperature range amounts to less than 0.2 cm^{-1}. For reconstituted OmpG samples, the band position remains at around 1730 cm^{-1} from RT up to 80 °C. However, above 80 °C, it shifts to lower wavenumbers.

An upshift of the C=O band position for OmpF as observed here is consistent with the strengthening of the double bond character, for example by weakening or loss of H-bonding (Fringeli and Gunthard, 1976; Korkmaz and Severcan, 2005). As seen in the figure, the H-bonding state of the C=O group is not affected at temperatures below 50 °C for both porin samples. Above this temperature, a general upshift is seen in two steps between approximately 55 and 75 °C and approximately 75 and 90 °C. The case for OmpG however is opposite where the downshift above 80 °C indicates the weakening of the double bond character.

Deeper in the membrane, the CH_2 symmetric stretching vibration of the lipids can give information about dynamics and order-disorder state of the hydrophobic tails of the membrane (Cameron et al., 1980). There are also CH_2 vibrations from protein side chains; however, considering the protein-to-lipid ratios used in this study (~1:120) and protein amino acid composition, protein contribution to the CH_2 modes is calculated to be less than 1%. Thus, lipid CH_2 modes significantly overweigh the protein CH_2 modes. The asymmetric mode at ~2950 cm^{-1} can also be used; however, it is partially overlapped with CH_3 asymmetric stretching mode, therefore CH_2 symmetric stretching mode is a better candidate for determining conformational disorder and packing of lipid acyl chains. This mode is found at approximately 2850 cm^{-1} in the IR spectra. The order-disorder state of the bilayer can be monitored by following the band position with respect to temperature.

The position of the CH_2 symmetric stretching mode and its full width at half-maximum (FWHM) are shown as a function of temperature in Figure 3.6 on the left and right, respectively. The position and width of this band was determined from the absorbance spectra by reading the values from half-height. In both cases, a lipid blank is added for comparison. The lipid bilayer system is essentially a closely packed system. If an external

perturbation leads to disordering of this packing, it is reflected by an upshift in the position of CH_2 symmetric stretching mode, while a downshift indicates ordering of the bilayer.

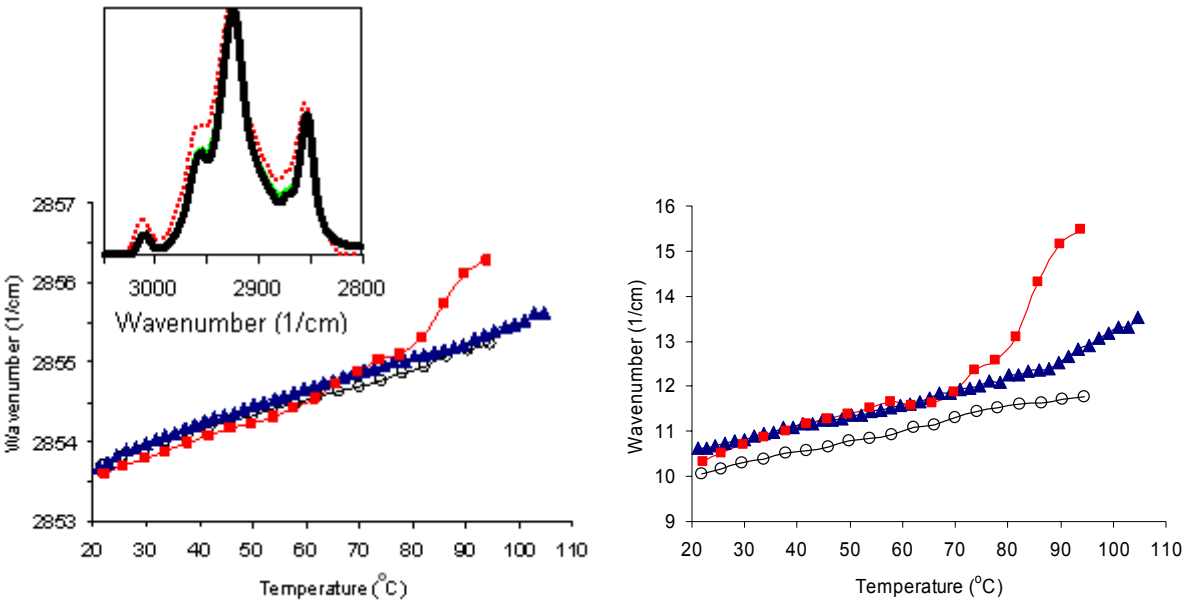

Figure 3. 6 (Left) Lecithin CH_2 symmetric stretching mode as a function of temperature for blank lipid sample (○) and reconstituted OmpF (◆) and OmpG(▲). Inset figure: C-H stretching region (2800-3050 cm^{-1}) of the FTIR spectra of OmpF at RT (**—**), 65 °C (—) and 80 °C (·····). **(Right)** FWHM of lipid CH_2 symmetric stretching mode as a function of temperature for blank lipid sample (o), reconstituted OmpF (■) and OmpG(▲).

For the temperature range from RT to 60 °C, the position of the CH_2 mode for the lipid-protein system for OmpF is at slightly lower position as compared to the pure lipid membrane, thus indicating that OmpF porin has a slight ordering effect on the lipid bilayer. When the temperature increases above 60 °C, the hydrophobic tails of the lipids are disordered in a two-step phase. The first phase is observed between 60 and 80 °C and the second phase between 80 and 90 °C. OmpG does not induce a significant change in packing of hydrophobic tails throughout the entire temperature-profiling.

The temperature dependence of the bandwidth of the CH_2 symmetric stretching shown in Figure 3.6 (on the right) provides information about the freedom of motion of hydrophobic tails of lipids. An increase in the bandwidth is an indication for an increase in dynamics. It is important to note that the dynamics of acyl chains together with the order-disorder state determines the degree and kind of interaction between protein and lipid, and may consequently be indicative for a hydrophobic mismatch (Zhang et al., 1992b).

Throughout the entire temperature range, the lipid-protein complex exhibits a higher bandwidth for the CH_2 symmetric stretching mode as compared to the blank lipid for both porin samples. For reconstituted OmpF, this difference becomes more pronounced above 70 °C and significantly more above 80 °C. The CH_2 scissoring mode at around 1467 cm^{-1} gives similar information about the mobility of acyl chains. Blank lipid and porin reconstituted samples behave very much the same up to 60 °C, however OmpF has a much broader scissoring band at higher temperature values, suggesting that hydrophobic packing of tails is considerably disturbed above 60 °C. Reconstituted OmpG shows also slight increase in bandwidth above ~85 °C similar to the second phase of OmpF.

The headgroups of the lipids can be monitored via the PO_2^- antisymmetric stretching mode, which appears at about 1220–1245 cm^{-1}. The phosphate group provides hydrogen bonding acceptors; the spectral position of the corresponding mode is thus strongly affected by the hydration state of the headgroup. Upon hydration, the antisymmetric PO_2^- stretching frequency decreases (Fringeli and Gunthard, 1976). Figure 3.7 shows the temperature dependent behavior of the phosphate group of a lipid blank and of reconstituted OmpG and OmpF. For the analysis of this band, the ^2H_2O contribution to the sample spectrum at 1210 cm^{-1} had to be subtracted. For a successful subtraction, the main O-^{2}H stretching mode at 2550 cm^{-1} is taken as reference. In Figure 3.7, the blank lipid sample shows a gradual decrease in frequency as the temperature is raised from RT up to 70 °C. Above 70 °C, the O-P-O mode remains at a constant frequency. For reconstituted OmpF and OmpG samples, a sharp decrease is seen upon heating up to 55 °C with no further alteration at higher temperature values. In order to investigate a possible hydrogen bonding among protein aromatic girdle and lipid headgroups we have also analyzed the band composition and temperature-dependent progression of each unit.

PC from soybean is a mixed lipid having 17% (C16:0), 4% (C18:0), 9% (C18:1), 60% (C18:2) and 7% (C18:3). The shift of band position to lower wavenumbers has been attributed to hydrogen bonding of the phosphate headgroup, whereas broadening of the band has been used as an indicator of polar headgroup mobility (Lewis and McElhaney, 2000; Lopez-Garcia

et al., 1993; Severcan et al., 2005). For blank lipid sample, as the temperature is increased, the band is clearly split into components (Fig. 3.8) and the one located at the lower wavenumber position is gradually downshifting to 1211 cm^{-1} as the temperature is increased from 20 to 70 °C. Band progression is almost linear with increasing temperature up to 70 °C; above that there is no change in the band position of this component. On the other hand, the higher frequency component remains to be located around 1238 cm^{-1}. Taking into account the temperature-induced changes in both components, it is clear that the degree of hydration of some lipid headgroups is increasing with increasing temperature; however, there are also certain lipid groups preserving their hydration status.

OmpG and OmpF reconstitution does not induce a wavenumber shift of the O-P-O antisymmetric stretching mode at 20 °C; nevertheless, reconstitution broadens the band (Fig. 3.8). When measured from half-height, the blank lipid sample has a bandwidth of approx. 44 cm^{-1}, while it is 46 cm^{-1} and 51 cm^{-1} for OmpF and OmpG reconstituted samples, respectively. Broadening of the band suggests increased mobility of polar headgroups in the presence of both protein samples but the effect is more pronounced with OmpG reconstitution.

The band splitting seen with the blank lipid sample as the temperature is increased is also evident in protein reconstituted samples. The downshift of the lower frequency component to ~1210 cm^{-1} is completed at 60 °C for both protein samples. The high frequency component is again positioned at 1240 cm^{-1} throughout the whole temperature range, although it is less pronounced as compared to the blank lipid profile. Nevertheless, the number and positions of individual components are common under the O-P-O antisymmetric stretching mode as seen from the second derivative profiles of the three samples at 20 °C and 90 °C in Figure 3.9.

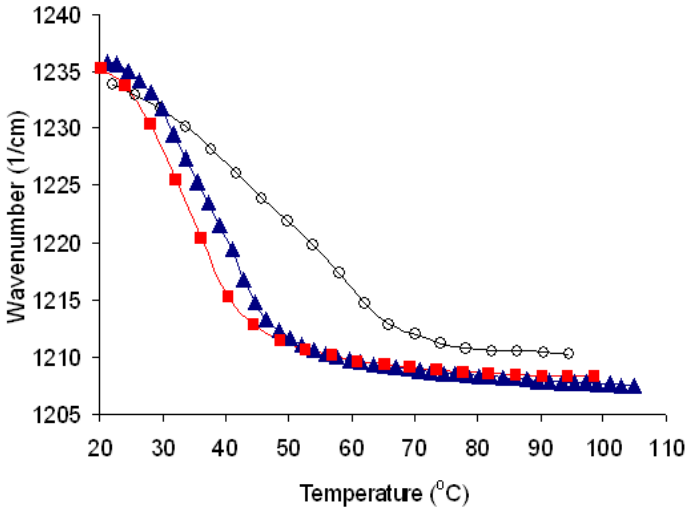

Figure 3. 7 Lecithin PO_2^- antisymmetric stretching mode as a function of temperature for blank lipid sample (○), reconstituted OmpF (■) and OmpG(▲).

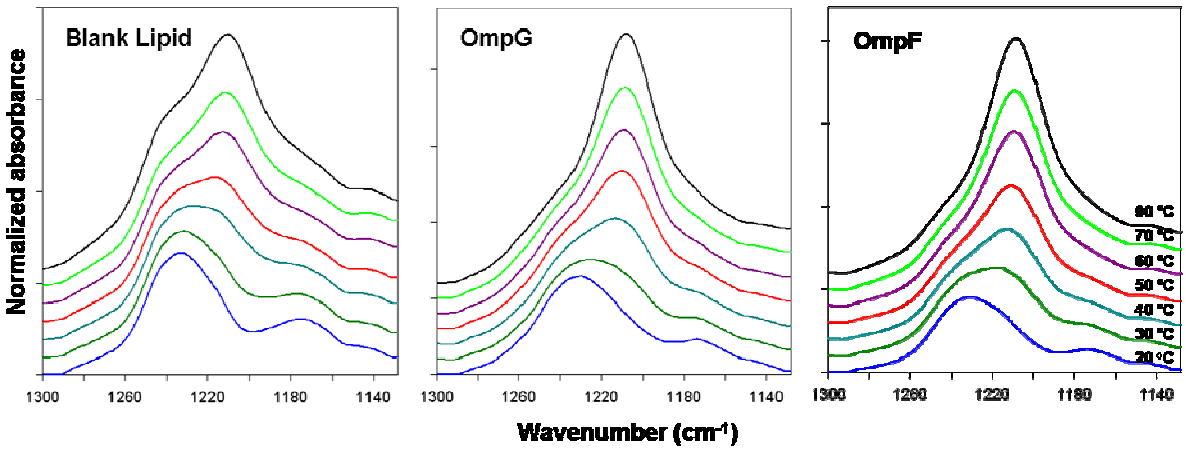

Figure 3. 8 IR absorbance spectra of O-P-O asymmetric stretching mode with increasing temperature for blank lipid (left panel), lipid reconstituted OmpG (middle panel) and OmpF (right panel). Temperature values are indicated on the right panel. Spectra are offset corrected for comparison.

In order to understand the temperature-dependent progression of these two component bands and to see whether there is an effect induced by protein insertian, we have performed some calculations based on the component band areas. The O-P-O band was integrated for the range 1260-1230 cm^{-1} and 1230-1190 cm^{-1}. These spectral ranges roughly correspond to the high frequency component, which is unaffected by temperature or protein insertian, and the downshifting lower frequency component, respectively. Their integrated areas are then compared to the total area of O-P-O antisymmetric stretching band integrated between 1260

and 1190 cm^{-1}. The results are represented in terms of relative percentage of each component with respect to the total band area and plotted against increasing temperature in Figure 3.10.

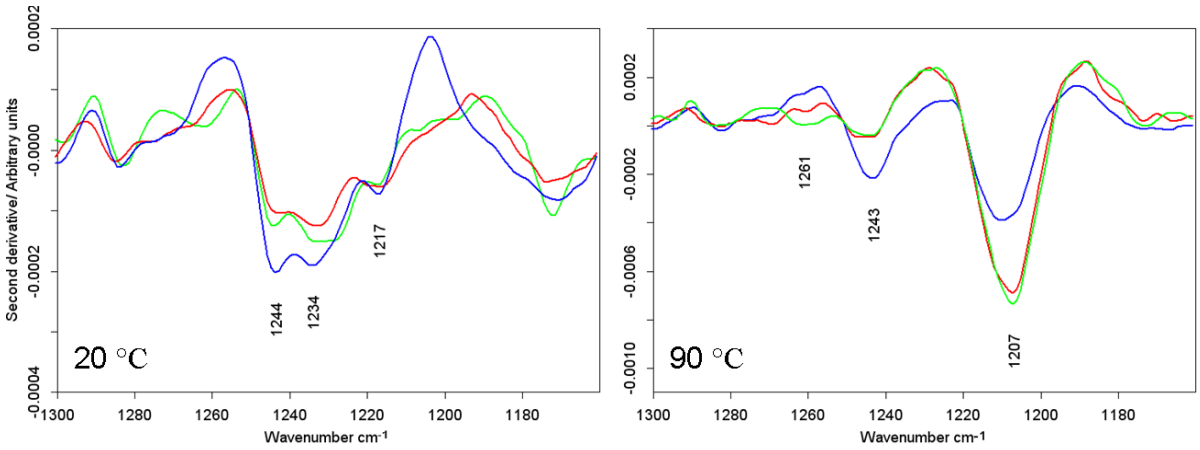

Figure 3. 9 Second derivative profile of P-O-P asymmetric stretching mode for blank lipid (blue), lipid reconstituted OmpG (green) and OmpF (red) at 20 °C (left panel) and 90 °C (right panel).

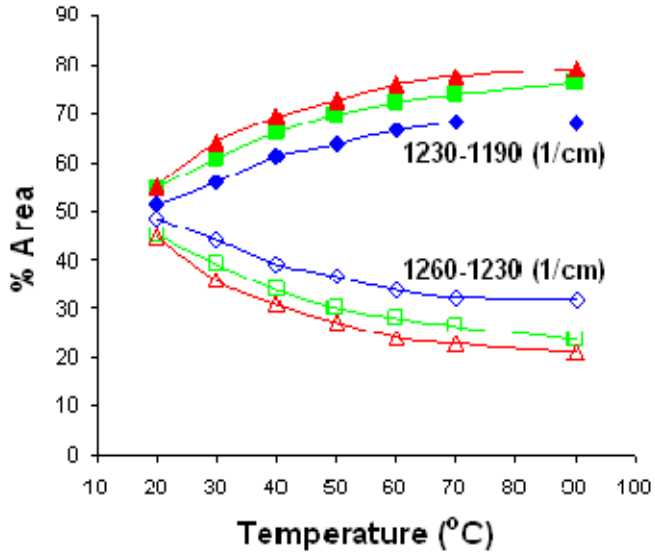

Figure 3. 10 Percentage of integrated areas between 1260-1230 cm^{-1} and 1230-1190 cm^{-1} relative to the total integrated area of O-P-O asymmetric stretching mode between 1260-1190 cm^{-1} for blank lipid (blue diamonds), OmpG (green squares) and OmpF (red triangles) reconstituted samples.

As the graph clearly shows, the two components have almost equal share from the total band area for blank lipid sample at room temperature. The slight increase in the presence of both proteins (3%) is in the range of error. When the temperature is increased to 90 °C, the

blank lipid sample has 32% of lipid headgroups in the high frequency region and 62% in the low frequency region. However, these values are 24% - 76% for OmpG and 21% - 79% for OmpF, respectively. Protein incorporation induces ~10% more of the lipid headgroups to shift to lower wavenumbers, which is indicative of an increased number of lipid molecules forming hydrogen bonds. This could be caused by the increased mobility of headgroups induced by protein insertian. It should be noted here that the number of lipid headgroups in the low frequency region is increased mainly between 20 and 30 °C in the presence of both proteins. Above 30 °C, we could not detect a monomerization/aggregation-related increase or discontinuity, which would lead to the idea of a possible hydrogen bonding between lipid headgroups and protein aromatic girdle.

The lipid reporter groups exhibit changes which can help to explain the activity loss of porin above 50 °C. A possible scenario is that the OmpF—lipid system is reacting to temperature in two steps. We thus divide whole temperature-ramp series into three regions:

From room temperature to 55 °C, the tyrosine C=C mode shows essentially a constant position around 1514.4 cm^{-1}, which is characteristic for the protonated form of tyrosine (Fig. 3.3). The lipid C=O group shows a stronger H-bonding relative to the blank lipid sample for both porins. This H-bonding strength slowly decreases as the temperature is raised for OmpF (Fig. 3.4). The hydrophilic part of the bilayer in the blank lipid sample shows a gradual downshift with increasing temperature (Fig. 3.8). Analysis has shown that there are two groups of lipid molecules; in one the degree of hydration is preserved (high frequency component) and in the other (low frequency component) increasing temperature induces higher degree of hydration (Arrondo et al., 1984). Hydrated groups of lipids are located around 1210 cm^{-1} in the presence and absence of protein. Therefore the presence of protein does not induce an additional shift but increases the number of lipid molecules undergoing the shift. On the other hand, it is difficult to correlate the hydration profile of lipid headgroups with respect to temperature with protein structure/function alterations. Although OmpG does not undergo any structural or functional change up to 80 °C, its presence affects the fraction of hydrated lipid molecules, especially between 20 and 30 °C (Fig. 3.10). Since OmpG and

OmpF affect the hydrophilic region in the same way, changes in the hydrophilic region are not a result of protein aggregation/monomerization. In addition, the mobility of headgroups is increased in the presence of both proteins; however, the bandwidth is increased by 7 cm^{-1} in the vicinity of OmpG while it is 2 cm^{-1} for OmpF.

In this temperature range the hydrophobic part of the membrane is slightly more fluid than the blank lipid sample (Fig. 3.6), thus suggesting that the cooperativity of hydrophobic part of the bilayer is slightly altered (Korkmaz and Severcan, 2005). In view of the above information the protein is stabilizing its position inside the membrane bilayer in this temperature range by forming hydrogen-bonds between aromatic side chains and lipid ester C=O groups at room temperature, which was also suggested by previous studies (Lee, 2003). OmpG is also mainly affecting the interfacial region of the bilayer and has the properties of protonated tyrosine side chain. Lipid hydrophobic tails are not affected much by the presence of OmpG. If the effect on lipid headgroup molecules is also taken into account, this altogether leads to the conclusion that both porins are interacting with the interfacial region of the bilayer.

Between 55 and 75 °C, which is the first step in alteration of protein—lipid interaction, the tyrosine C=C mode of OmpF shows a downshift and the lipid C=O mode shows an upshift, both suggesting that H-bonds existing before between OmpF and the lipid interfacial region are weakening. In this temperature range, hydrophobic tails become slightly more disordered. Disordered tails consequently result in shortening of the hydrophobic length of the bilayer, which is the normal behavior of most lipids with increasing temperature (Zhang et al., 1992b). However, reconstituted OmpF shows an upshift at 55 °C both in CH_2 symmetric stretching band position and bandwidth values within this temperature range, thus suggesting that the shortening of lipid bilayer is related to the loss of H-bonds between OmpF and lipid molecules in the interfacial region. In this first stage, where a series of changes are seen between porin and lipid molecules, starting at the same temperature value, OmpF also starts monomerization according to SDS-PAGE study of samples pre-incubated at different temperatures (Sukumaran et al., 2004). In this study we provide evidence that trimeric and monomeric units of OmpF are different in terms of the interaction

that it is showing with its immediate environment. This property of porin must in turn affect the functionality because it was reported that porin looses 90% of its pore activity at 50 °C and conductivity loss has been related to monomerization since both occur at the same temperature value in detergent environment. In this study we show that porin is more stable in oligomeric form if reconstituted in lipids. Although OmpF does not show any secondary structure change, its interactions with lipids are changing remarkably at the level of the aromatic girdle starting at 55 °C, which then leads to monomerization and loss of function. In this temperature range, OmpG does not show any significant change in terms of its interaction with neighboring lipid molecules with increasing temperature in any of the protein/lipid regions analyzed with FTIR. This is also in accordance with the fact that SDS-PAGE analysis does not imply any significant structural or organizational change from RT up to ~90 °C and also the black lipid membrane experiments show that OmpG is fully functional until the secondary structure is completely lost (Korkmaz et al., 2008).

Between 75 and 100°C, the tyrosine C=C mode shows further downshift and the lipid C=O stretching mode shows further upshift, suggesting that protein—lipid interaction is further weakened for OmpF. This is also reflected in the hydrophobic region of the bilayer by dramatic disordering and increased mobility of acyl chains. It is common to all these four reporter groups that this second phase is more pronounced than the first one. The lipid headgroup region does not show any significant difference between blank lipid and reconstituted porins, which probably means that porins have little or no interaction with interfacial region of the bilayer. Previous studies have shown that monomerization of trimeric OmpF still takes place and it is completed at the late stages of this phase. Nevertheless, it is mostly the ‘monomeric porin’—lipid interaction that is reflected by the data. Further weakening of this interaction indicates that the OmpF-monomer is not stable in lipid environment, and aggregates as the temperature is further raised. The tyrosine C=C mode and lipid C=O modes indicate stronger H-bonding for OmpG. Hydrophobic tail order is not influenced but the fluidity increases starting from 90 °C. At later stages of this temperature

range OmpG in detergent micelles unfolds with increasing temperature and looses its function (Korkmaz et al., 2008).

For both OmpF and OmpG, temperature dependent profiles of hydrogen bond donors in proteins (tyrosines) show a better correlation with the lipid interfacial region than with the phosphate headgroup region. It has been shown in this study that structural and functional changes induced by increasing temperature are directly related with protein—lipid interactions. It turns out that, in spite of the observed stability of porin in terms of global secondary structure, its functional integrity depends on environmental composition. It is thus conceivable that for proteins with a relatively rigid structure and aromatic side chains pointing towards the lipid chains as in the case of the porin aromatic girdle, lipid chain length and polarity become essential points to be considered for correct folding and functionality.

3.2 OmpG-WT and the Mutants OmpG-CYS, OmpG-ALA and OmpG-ΔL6

3.2.1 Structural Characteristics

First structural data of OmpG came from the projection maps at 6 Å obtained by electron cryo-microscopy from two-dimensional (2D) crystals. The structure showed a monomeric ring-shaped density with a diameter of 2.5 nm (Behlau et al., 2001). By X-ray crystallography Yildiz and coworkers were able to get molecular information at acidic and neutral pH values. The difference in pH went along with conformational changes in the loop regions of the porin (Yildiz et al., 2006). While the loop L6 extends outwards at neutral pH, it folds inward into the OmpG channel and is thought to block the entrance at acidic pH. This goes along with unzipping of a few hydrogen bonds between neighboring β-strands S12 and S14. The proposed mechanism of this pH gating involves two histidine residues at the end of the loop L6 and beginning of the neighboring loop L7 (Fig.3.11). Thus the histidine pair triggers opening and closure of OmpG in response to pH by protonation at alkaline pH and deprotonation at basic pH.

In order to be able to interpret and correlate the experimental data, three mutants were used. OmpG lacking the amino acids 220-228, called OmpG-ΔL6, was expressed and purified anologue to the wild type OmpG (Yildiz et al., 2006). This mutant lacks the loop L6, which blocks the channel entrance at acidic pH. It is designed in order to understand the role of histidine protonation/deprotonation in opening and closure of the channel. This mutant is, in principle, constitutively open at all pH values although the histidines can still be protonated or deprotonated at different pH values. Another mutant is OmpG-ALA, where the histidines at positions 231 and 261 are replaced with alanines so that they presumably stay neutral at all pH values and therefore the pH dependence due to the two histidines is abolished. Another mutant is OmpG-CYS, in which the histidines at the positions 231 and 261 are replaced by cysteine residues. These two residues form a disulfide bridge in oxidizing conditions and hence act like H-bonded histidines in WT protein at pH>7.5. This mutation should decrease the mobility of L6 due to the disulfide bridge and therefore should be more in the open

conformation than the WT protein independent of the pH. OmpG WT protein, OmpG-ΔL6, OmpG-CYS and OmpG-ALA mutants incubated at different pH values are compared in terms of secondary structure, thermal stability and H/D exchange rates. Experiments were performed both for 2D crystals and detergent OG solubilized forms for all the protein samples.

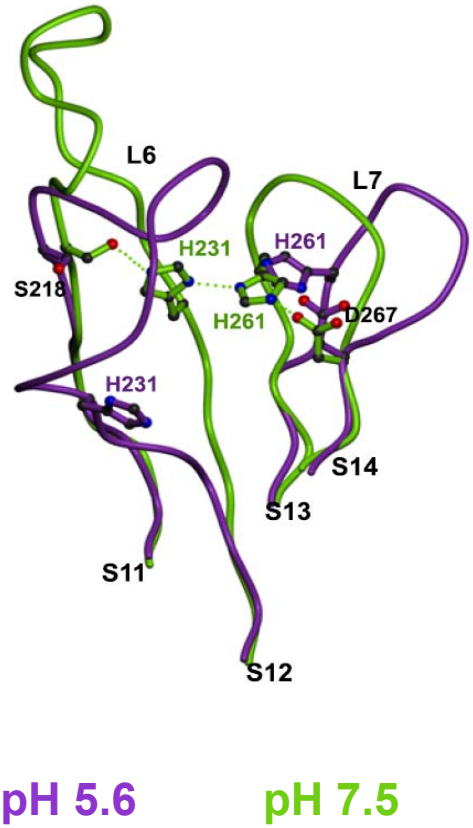

Figure 3. 11 Loops L6 and L7 in the open (green) and closed (purple) conformation of OmpG WT. Figure adapted from Yildiz et. al. (2001).

The structural properties of OmpG have been investigated by FTIR spectroscopy using the amide I region between 1700-1600 cm^{-1}. The amide I region is sensitive to backbone conformations like β-sheet, α-helix, turns and loops. OmpG-WT exhibits the amide I peak position around 1627 cm^{-1} which is indicative of mainly β-sheet conformation. This is in accordance with the X-ray crystal structure of the protein in open and closed forms, according to which OmpG-WT is composed of 67% (71%) β-sheet, 1% (1%) α-helix, 25% (21%) coil and 8% (8%) turns connecting the β-strands in the closed conformation (open

form) (PDB id: 2iww and 2iwv). The structure is composed of 14 strands, 4 residues forming α-helix, 9 loops in extracellular region and 6 turns in cytoplasmic region.

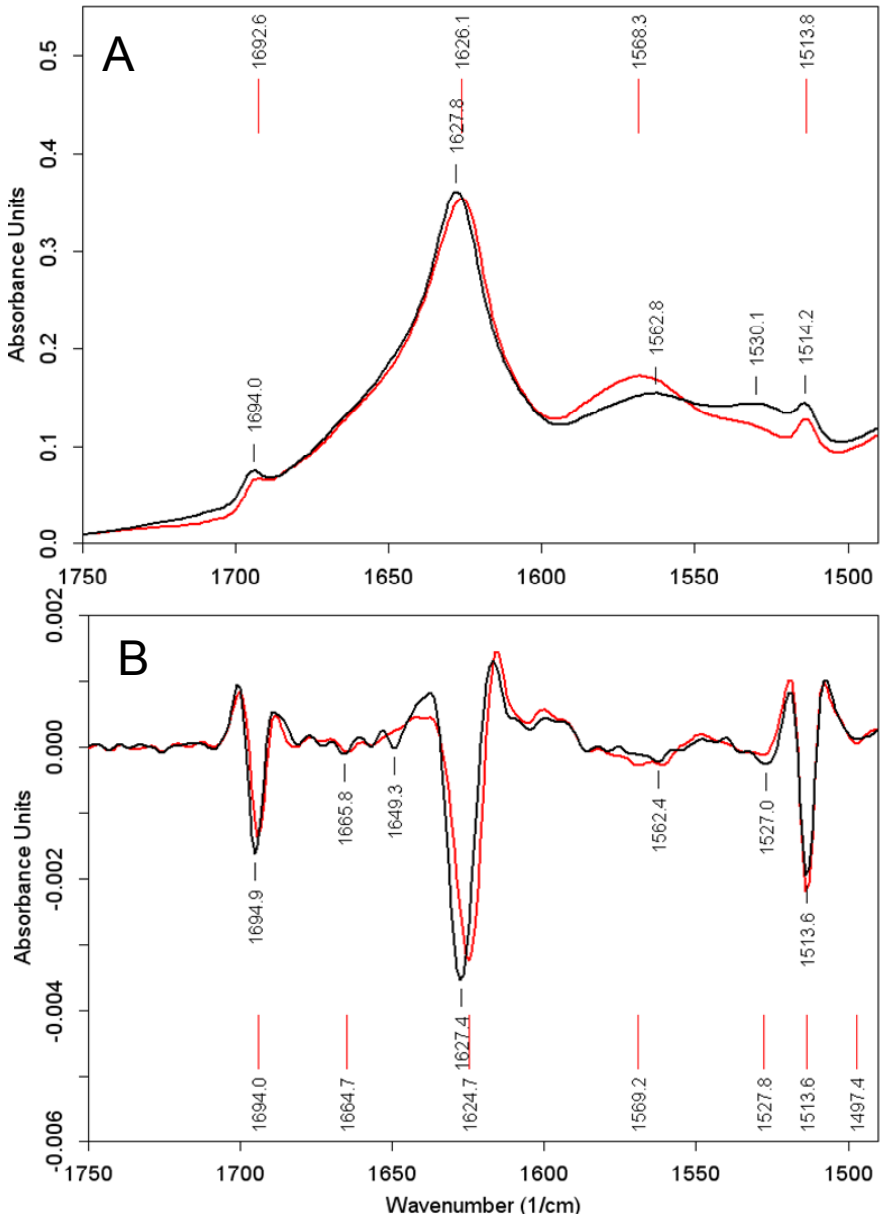

Figure 3. 12 (A) FTIR absorbance of OmpG-WT at pD 5 (black) and pD 7.5 (red) and (B) second derivative of spectra in (A).

The amide I and II regions from OmpG-WT spectra at pD 5.4 and 8 and their corresponding second derivatives are shown in Figure 3.12. OmpG-WT and the mutants exhibit the typical amide I band positions centered at around 1627 cm^{-1} both for the 2D crystals and detergent (OG) solubilized protein. The second derivative profile of WT protein shows two distinct

bands as indicated in Figure 3.12B at around 1628 cm^{-1} and 1694 cm^{-1} in the amide I region, which can be attributed to the low and high frequency β-sheet component based on the X-ray structure of the protein and previous FTIR studies with proteins having high β–sheet content (Arrondo et al., 1988; Sukumaran et al., 2004; Susi and Byler, 1987). When the spectra of the WT protein incubated at different pD conditions are compared from the second derivative (Fig.3.12B), β–sheet band positions differ in closed (pD 5.4-black line) and open (pD 7.5-red line) states. This is also evident from the slightly different amide I band positions in the absorbance spectra (Fig.3.12A). In order to understand the nature of this shift in the β–sheet position, IR absorbance spectra of the WT protein in detergent were taken at increasing pD values between 5 and 8. For this experiment, six WT protein samples were taken from the same parent stock and all samples were freshly prepared under the same conditions before the experiment. High and low frequency β-sheet positions from the second derivative of amide I region are extrapolated against the corresponding pD values in Figure 3.13. The β-sheet position stays almost constant at ~1695 cm^{-1} for the high frequency and at 1627.5 cm^{-1} for the low frequency mode between pD 5 and 6; however afterwards, it gradually starts shifting down with increasing pD values. It has also been reported that the protein is in a conformationally transition state at pH 6, where it fluctuates between open and closed states (Conlan and Bayley, 2003). In terms of the β-sheet positions, there is no difference between pD 5 and pD 6. Above pD 7.5, both positions reach a constant value, i.e., the high frequency mode at 1694 cm^{-1} and the low frequency mode at 1625 cm^{-1}. The results clearly indicate that the β-sheet band position is related with the opening of the channel. According to the X-ray structure (Yildiz et al., 2006), the open state at pD 8 exhibits more β-sheet content (approximately 12 residues), which are formed as extensions to strands S8, S11-S14. We suggest that the shift of β-sheet position in the IR spectrum can be explained by these new β-sheet extensions and that the protein has more rigid β-barrel structure upon opening of the channel with loop L6 pointing outward. In previous IR studies, it was shown that β-type folding can have different positions and in some cases multiple bands appear in the amide I region between 1640-1620 cm^{-1} (Arrondo et al., 1988; Naumann et al., 1993;

Zandomeneghi et al., 2004). The band position depends on the hydrogen bond strength (Naumann et al., 1993), the number of strands in the protein and the twist angle between the strands (Zandomeneghi et al., 2004). Stronger hydrogen bonding, less number of strands and narrower twist angles all result the IR vibrational frequency to be shifted to lower wavenumbers in the amide I region.

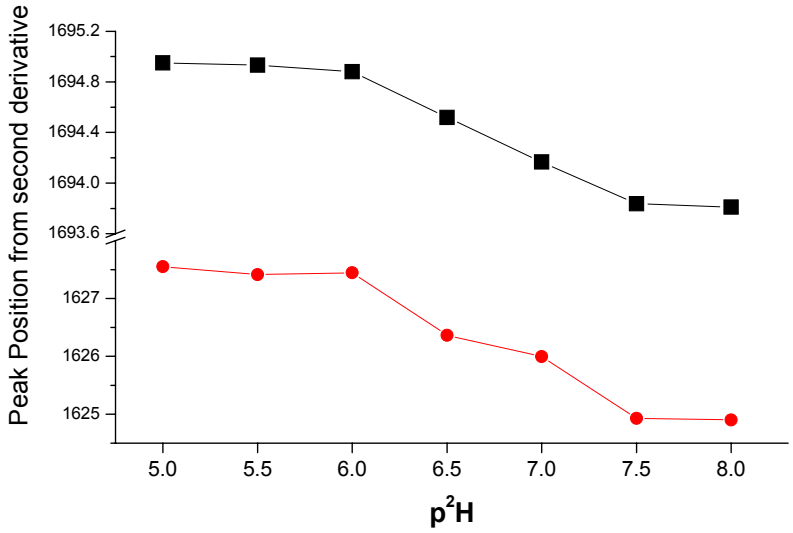

Figure 3. 13 OmpG-WT β-sheet positions from second derivative profiles with respect to increasing buffer pD.

In determining the backbone conformation of OmpG, Fourier self deconvolution and second derivative were used together to determine the exact number of underlying components and band half-widths. However, even these enhancing methods were not enough to resolve some small and strongly overlapping bands. As a measure of the band-fitting success, the original spectrum and fit envelope were compared from their respective second derivative profiles. We suggest that only the exact number of fitted bands and correct intensity and half-width will give a second derivative profile that is the same with the second derivative of the raw spectrum. Therefore, although the band-narrowing techniques do not resolve some small and overlapping components, one can still find them by comparing the second derivatives. In all the cases, where the user should introduce one or two additional bands to the band-fitting program, they turned out to be very close to another larger band and in most cases

completely overlapped. In curve fitting program, protein samples in D_2O buffer gave more successful results as deduced from the second derivative comparison than the samples in H_2O buffer because of two reasons; (i) the amide I band is less crowded in D_2O than in H_2O buffer. Some side chain modes like Arg shift to the amide II border in the spectrum (~1600 cm^{-1}), hence allowing the determination of component bands with higher accuracy. (ii) Subtraction of buffer from the spectrum is very important before the band-fitting procedure and water has a strong absorbance in amide I region. There have been many suggestions in literature on the correct water subtraction methods; however the problem is that the bound water molecules can never be completely subtracted and thus, the amide I band will always bare sub-bands that do not originate from the protein structure. On the other hand, subtraction of D_2O buffer, even with a wrong subtraction coefficient, does not cause serious problems like water does. Correct estimation of a protein structure requires the comparison of the IR spectrum in H_2O and D_2O buffer and in dry state. Therefore the buffer subtraction plays an extremely important role for a successful band-fitting routine. However, the band-fitting results for the protein in H_2O buffer can still be used to determine the position of loops, although there may be variations in β–sheet fractions due to residual water.

Band-fitting routine has been performed for OmpG-WT in pD/pH 5,4 and pD/pH 8 and the results are summarized in Table 3.1. Each component band has been integrated and the relative percentage of integrated areas have been calculated with respect to the total amide I area. The two bands at ~1611 and ~1605 cm^{-1} were not taken into consideration during the calculations, since this region of amide I (1600-1615 cm^{-1}) is due to side chain vibrations, which will be discussed later in this section. Figure 3.14 shows the fitted components for the amide I region only, however the fit procedure has been performed for both amide I and II regions.

Table 3. 1 OmpG-WT curve fit results for pD/pH 5.4 and pD/pH 8.

pD/pH 5,4			pD/pH 8		
Band position (cm^{-1})	Band area (%) in H_2O	Band area (%) in D_2O	Band position (cm^{-1})	Band area (%) in H_2O	Band area (%) in D_2O
-	-	-	1619	-	7
1623	31	35	1623	40	36.2
1635	21	25	1634.5	17	16
1640	-	2.5	1643	1.5	8
1642	5	1.4	1645	-	1
1650	2	12.8	1650	7	8.7
1658	20	4.2	1658	13	5.6
1666	-	7.7	1666	2	5
1673	7	2.4	1673	5	3.7
1681	-	5.7	1681	-	5.5
1688	9	0.7	1691.6	11	1.8
1694	4	2.8	1694	4	1.3

For the band assignments, calculated percentages were compared with the published X-ray structure. A previous FTIR study for OmpF (Nabedryk et al., 1988) has also been used for band assignments, since the two proteins, OmpF and OmpG, are very similar in composition and FTIR band components. Comparison of data between the protein incubated in H_2O and D_2O buffers at pH/pD 5 indicate that upon deuteration, the signal for loops is shifted from ~1660 cm^{-1} to ~1650 cm^{-1}. On the other hand the band at 1642 cm^{-1} remains at the same spectral position in both H_2O and D_2O buffers. Therefore we assign this band to weakly interacting β–sheets. Similarly, in the open state, the signals for loops are located at ~1660 cm^{-1}; however, upon exchange with D_2O, they shift down to 1650 cm^{-1} and 1643 cm^{-1} as the percentages indicate. The overall assignments, thus, for the protein in D_2O buffer are as follows; the bands 1643-1620 cm^{-1} and 1688-1695 cm^{-1} are assigned to β–sheet, the spectral region 1681-1670 cm^{-1} is assigned to β-turn and the region 1666-1645 cm^{-1} is assigned to loops and α-helix (Chehin et al., 1999; Naumann et al., 1993). According to these band assignments, OmpG is calculated to be composed of 70.3% β -sheet, 20.5% loops & α-helix, 9.2% β-turn in the open state at pD 8 . In the closed state at pD 5.4, WT protein has 67.4% β–sheet, 24.5% loop & α-helix structure, 8.1% β-turn structure. Although

they do not exactly match the X-ray structures of the two states, they are quite close with a maximum deviation of 1% for β–turn at pD 8. Therefore the band assignment can be used for the next sections in the analysis of OmpG dynamics.

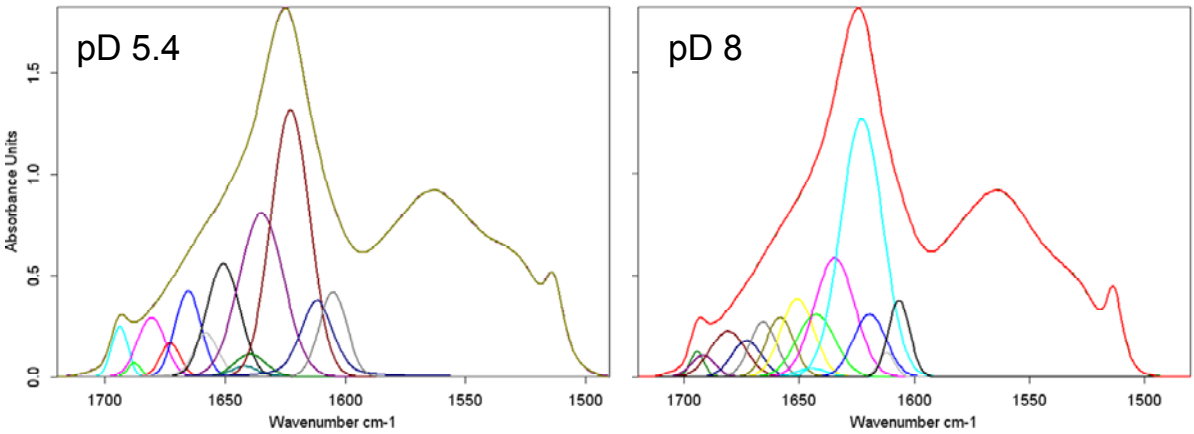

Figure 3. 14 Curve-fit results for the amide I region of OmpG-WT in detergent solubilized form at pD 5.4 and pD 8.

It is interesting to note that there are four low frequency and two high frequency β–sheet components at pD 5.4. When the protein is at pD 8, the fraction of the band at 1635 cm^{-1}, which contributed to 25% to the total amide I signal, decreases to 16%, while the contribution of the band at 1623 cm^{-1} stays almost constant. On the other hand, a new band rises at 1619 cm^{-1} with 7% contribution. Also the band at 1694 cm^{-1} decreases in intensity and the band at 1688 cm^{-1} shifts to 1691 cm^{-1} (Fig. 3.16). Upon opening of the channel the small contributions between 1643-1640 cm^{-1} increases from 4% to 8%. This increment is consistent with the additional 12 residues, involved in hydrogen bridges of the strands S8, S11-S14 when the channel is in the open state (Fig. 3.15). The high wavenumber position of this component suggests that the hydrogen bonds involved in these extracellular regions are more weakly interacting than the rest of the strand. This could be due to the flexibility of this part of the backbone. Here we can see both the splitting of β–sheet components and shifting of their positions at different states of the protein. Splitting of the bands can be attributed to the presence of β–sheet components with different hydrogen bonding properties. As indicated earlier, hydrogen bond strengths can cause similar folding types to be positioned at slightly different wavenumbers (Naumann et al., 1993).

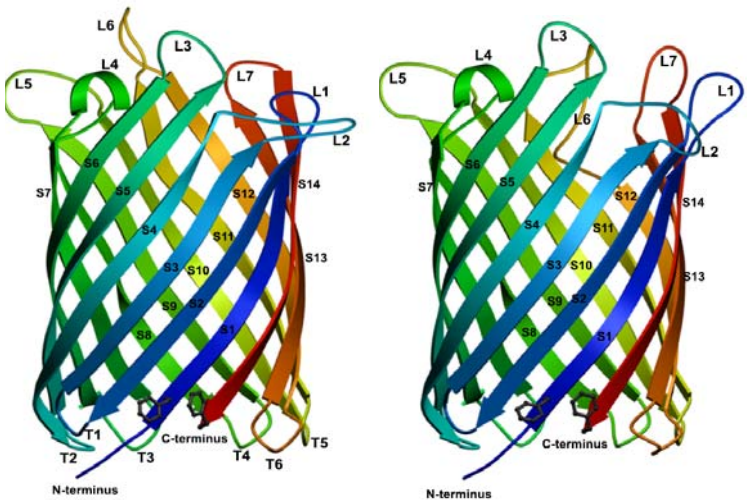

Figure 3. 15 OmpG-WT secondary structure at open state (left) and closed state (right) with strands (S), turns (T) and loops (L) numbered.

In a previous study with concanavalin A, which is the lectin from jack bean, it has been reported to have 60% β-structure in overall (Becker et al., 1975). In an IR spectroscopy study of this protein, the band at 1620 cm^{-1} has been assigned to β-edge together with 1685 cm^{-1} (Arrondo et al., 1988). It was described as the carbonyl groups at the edge of a β-sheet, which are followed by a different inter-/intramolecular structure. Later the same band was found in a hairpin-forming peptide and described as a more rigid connection between the strands (Arrondo et al., 1996; Chehin et al., 1999). In OmpG structure, the strands are connected with loops on the extracellular side that are shortened by 12 residues in total, by forming additional hydrogen bridges at the ends of the strands S8, S11-14 above pD 7.5 (Fig. 3.15). By forming such extensions and repositioning of the loops along with opening of the channel, it is possible that there are different hydrogen bond strengths involved within one β–strand. Although the appearance of a low-frequency component is indicative of opening of the channel, we do not think that they are originating from the extended strands. This is also in accordance with the relative contributions of the 1635 cm^{-1} component, since the fraction of 1635 cm^{-1} band at pD 5.4 is almost equal to the addition of the splitted bands, i.e., 1635 cm^{-1} and 1619 cm^{-1}, at pD 8, only with a small variation (Tab. 3.1). The downshift of the band position with opening of the channel can be due to the shortened loops; L6 and L7 (see Fig. 3.15). The extended strands correlate better with the band at ~1640 cm^{-1}, which

increases by 4% at high pD. The curve fit results suggest that the band at 1650 cm^{-1} decreases from 13% to 9% and the fraction of 1640-1643 cm^{-1} region increases from 4% to 8% in amide I contribution as the channel opens at pD 8.

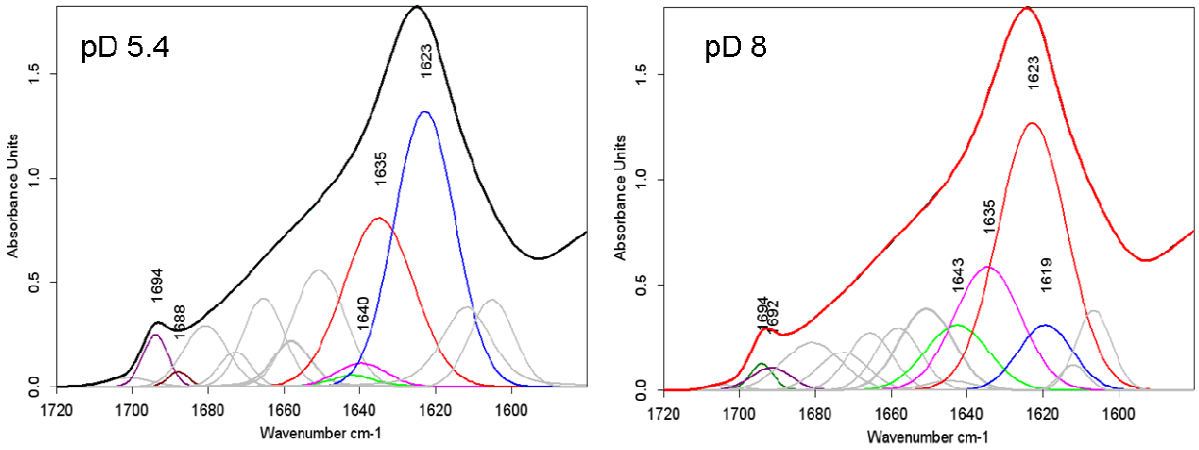

Figure 3. 16 The bands assigned for β-sheet are colored for OmpG-WT in pD 5.4 and pD 8.

Mutants were also compared in terms of band positions in open and closed states. Figure 3.17 shows the second derivative profiles of the open and closed states for the mutants OmpG-ΔL6, OmpG-CYS and OmpG-ALA. Incubating at different pD values had only affected the second derivative profile of OmpG-ΔL6. For the others, the two states have a very good match in terms of the band positions. The low frequency β-sheet band appears at almost the same position for OmpG-CYS and OmpG-ALA, which is around ~1623.5 cm^{-1}. However, the same band is found at ~1628 cm^{-1} in the closed state and 1626.8 cm^{-1} in the open state for OmpG-ΔL6.

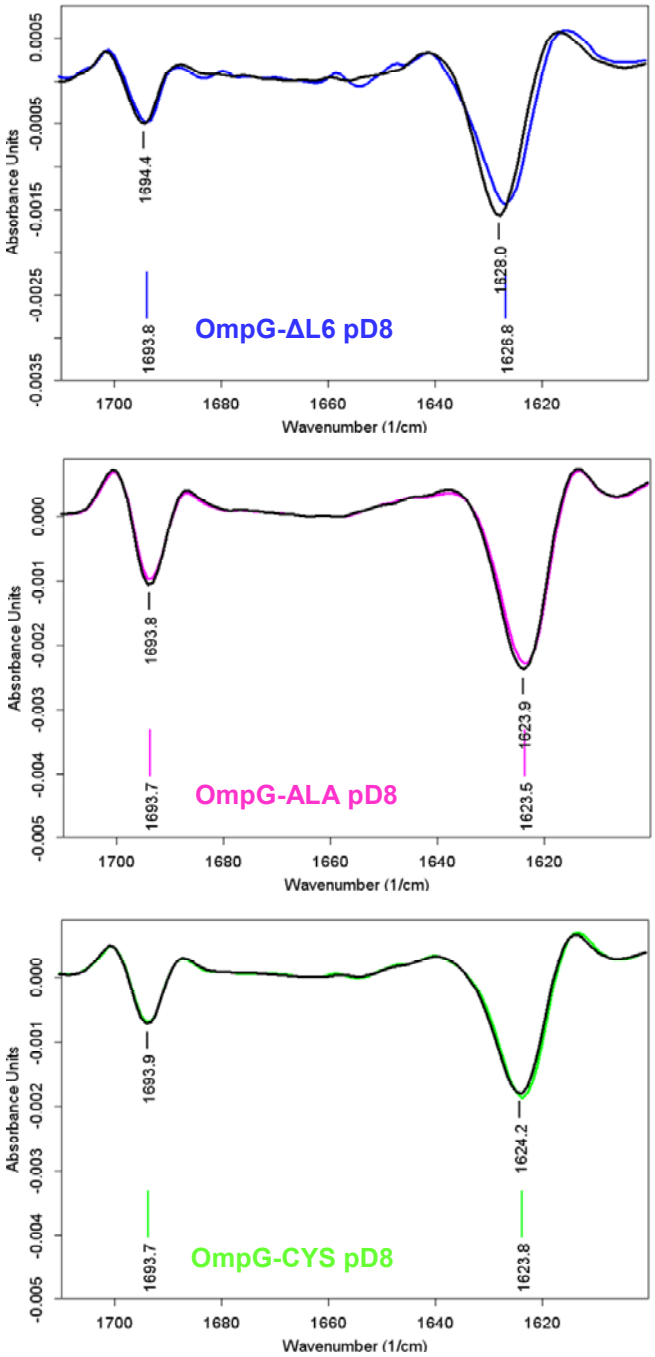

Figure 3. 17 Second derivative profiles of the mutants at pD 8 (colored) and pD 5.4 (black).

A similar shift of β-sheet modes with changing pD was also seen with WT protein; however, the shift was from 1627.4 cm^{-1} to 1624.7 cm^{-1}, which is slightly more than the shift of OmpG-ΔL6. As discussed in detail above, this shift has been attributed to the changing hydrogen bonding strengths of β-sheets with opening and closing of the channel. OmpG-ΔL6 lacks only the loop L6 but the histidines are still in position and therefore can still be protonated at acidic pH. Since the histidines were suggested to play the switch role between the open and closed

states of the protein, this mutant supports our argument that the positions of the β-sheet signals are related with the state of the protein. In the case of OmpG-CYS and OmpG-ALA mutants, the mutations were made to the histidines to immobilize them either by permanently bridging them with cysteines or by canceling the electrostatic interaction by means of neutral amino acid replacements with alanine. Therefore with both mutants opening and closing of the channel are successfully canceled although the loop L6 is still intact and free to move, if it has a secondary triggering mechanism, other than the histidines, in pH-gating of the channel. Based on the direct relationship we observed between the β-sheet signal position and the rigidity of the barrel as suggested by the experimental data, one can also argue that OmpG-CYS and OmpG-ALA mutants exhibit a more rigid barrel structure. In both mutants, the β-sheet band position is at least 1 cm^{-1} downshifted with respect to the open state of the WT protein. It is, thus, possible to argue that these mutants can adapt a more rigid conformation, which is energetically the most favored one, since the pH-dependent flexibility is no longer needed.

Previously, the increased fraction of 1643 cm^{-1} by 4% at pD 8 has been attributed to the new hydrogen bridge formations on the extracellular edges of S8, S11-S14. It has been argued that the signal for loops absorbing at 1650 cm^{-1} shift down to 1643 cm^{-1} at pD 8. The difference in the secondary structure between the different states of the WT protein is also evident from the second derivative profile of WT presented in Figure 3.12B. In the figure while there is a clearly distinguished band at ~1650 cm^{-1} at pD 5, it is less obvious at pD 7.5. A similar effect in the same IR region of OmpG-ΔL6 mutant is also evident from the second derivative profile, while no such change is observed with the other mutants (Fig. 3.17). However, OmpG-ΔL6 is truncated between 220 and 228, corresponding to the loop L6. Nevertheless, the second derivative profile still shows a signal at 1653 cm^{-1} at pD5, which then shifts down to 1645 cm^{-1} at pD 8. Therefore, we suggest that this shift corresponds to the formation of new hydrogen bridges with the opening of the channel.

3.2.2 Thermal Stability of OmpG WT and Mutants

In order to have a better understanding of the structural stability differences between OmpG WT, OmpG-ALA, OmpG-CYS and OmpG-ΔL6 mutants, temperature dependent experiments were performed with FTIR in transmission mode for the temperature range 20-110°C. As a result of increasing temperature, proteins undergo temperature-induced transition, which is a measure of their thermal stability. It is possible to compare proteins in terms of thermal stability based on the transition temperature value and transition profile, since the more stable ones will make the transition at higher temperatures due to the differences in secondary structure properties and/or the location of the protein in a bilayer system.

Figure 3.18 shows the IR spectra for the entire temperature range collected for OmpG WT 2D crystals in the region 1750-1500 cm^{-1}. Absorbance is shown with black lines before the transition and with red lines during and after the transition. Peak positions are indicated for RT (black) and 110°C (red). The figure on the right shows the second derivative profile of the absorbance spectra for the same region. As the temperature is raised from RT to 110°C, the high and low frequency β-sheet signals shift down by ~10 cm^{-1} and simultaneously another signal rises at 1650 cm^{-1}, shown by the red arrows in Fig. 3.18 on the left. Appearance of this band indicates unfolding of the protein with increasing temperature together with the protein-protein contacts reflected by the presence of the band at 1619 cm^{-1}. Taken together, they all point to a denatured protein at elevated temperatures. Peptide backbone amide I components and/or a specific side chain absorption band can be used to characterize a temperature-induced conformational changes in proteins. Extrapolation of the selected band position or intensity with respect to temperature enables the determination of the transition temperature of a specific secondary structure unit in the protein.

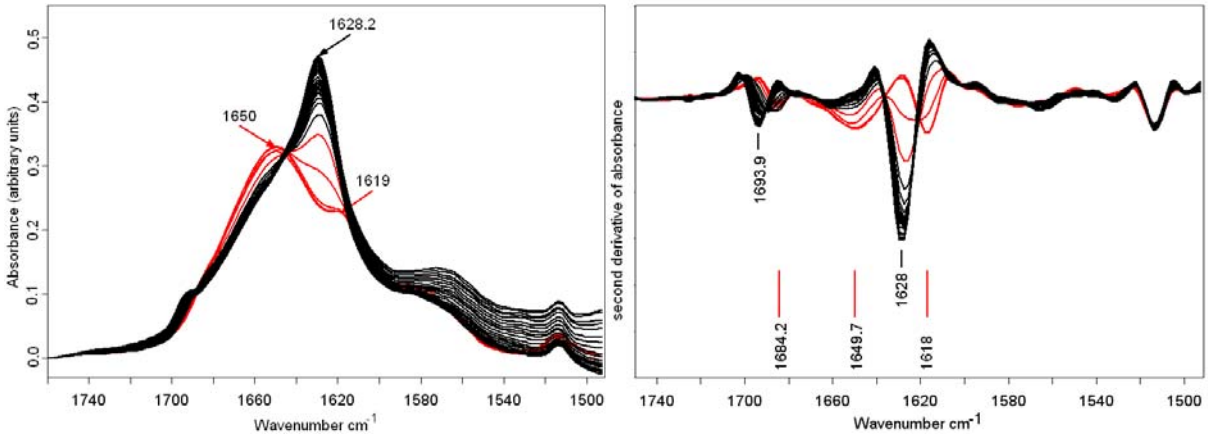

Figure 3. 18 Thermal profiling of OmpG-WT 2D crystals. IR absorbance spectra (on the left) and their respective second derivatives (on the right) of amide I and II regions are shown in black from RT to the transition state. Above the transition point, spectra are shown in red.

Temperature ramp experiments were first performed for the detergent solubilized WT protein and the mutants at increasing pD values. Figure 3.19 shows the plot of the amide I peak position versus the temperature for OmpG-WT in hydrated and deuterated forms. As seen in the figure, the detergent solubilized sample form aggregates at around 80 °C in H_2O buffer, independent of the pH. It is a common property among porins that they have a remarkable thermal stability (Haltia and Freire, 1995; Heinz et al., 2003; Sukumaran et al., 2004). The temperature-dependent transitions are better distinguished with D_2O buffer and they are scattered between 75 and 85 °C. However, there is no linear correlation between increasing pD and transition temperature values. Different D_2O exchange levels or different concentrations of sample may have contributed to the irregular transition temperature values here. Such a direct relationship is also not observed for the samples in H_2O buffer. A direct conclusion would be that the protein has very little or no stability difference between the open and closed states. It could also be due to the detergent environment since porins are known to have increased structural stability due to their interaction with the membrane bilayer. Although detergents are used to shield the hydrophobic surface of the membrane proteins against water; at extreme temperatures values, detergent micelles are less protective. Another reason for not having a direct relationship between different states and the transition temperature values can be the structural fluctuation between the two states between pD 6 - 7.5 as described in the previous section (Fig. 3.13). However, the protein attains a

closed state between pD 5 and 6, and an open state above pD 7.5; but the transition temperatures show slight differences even among the same states. When only the acidic and basic values are compared, samples in H_2O buffer are seen to be more stable at pH 5 than at pH 7.5. On the other hand, although the intermediate pD values show diversity in transition temperature values; samples in D_2O at pD 5 and 8 have the same temperature-induced transition profile.

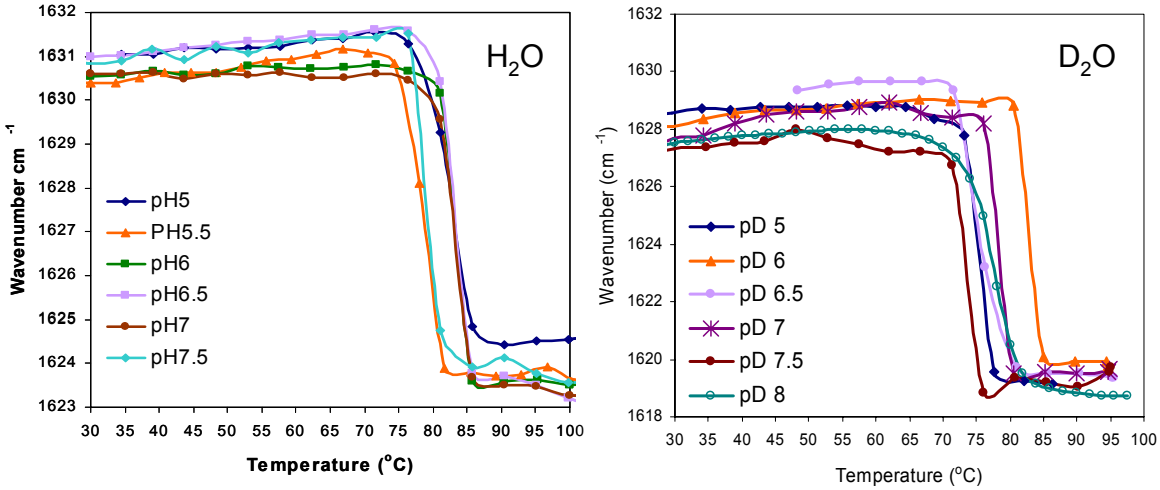

Figure 3. 19 Temperature dependent change of amide I peak position for detergent solubilized OmpG-WT (KPi buffer with 0.1% OG) at different pH values (left) and different pD values (right) from 5 to 7.5.

The mutants were also subjected to temperature-ramp (T-ramp) experiments in the open and the closed states of the protein corresponding to pD 5.4 and pD 8. The results are shown in Figure 3.20. All mutants show transition temperatures around 80 °C, comparable to the WT. All the mutants were designed to study either the role of histidines or of loop L6 in attaining different states. Hence similar transition temperature values confirm that in detergent environment there is no structural stability difference between the different states of the protein. The transition temperatures of ALA and CYS mutant are very close to each other; on the other hand there is a slight difference between the two pD values for ΔL6; the mutant is slightly more stable at pD 5.4.

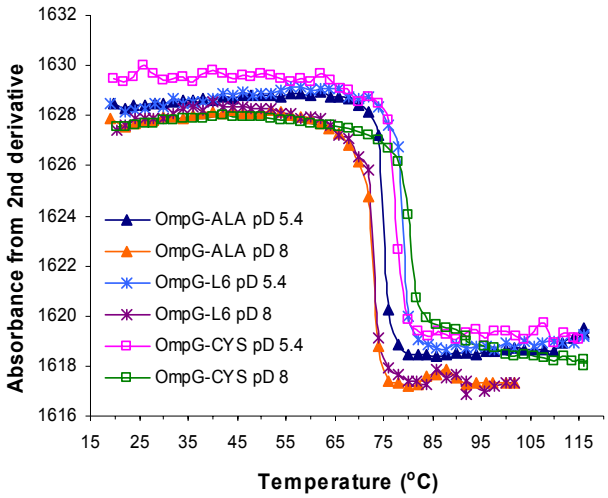

Figure 3. 20 Temperature dependent change of the amide I peak position for detergent solubilized OmpG-WT at different pD values from 5 to 7.5 on the left panel and mutants at pD 5.4 and pD 8 on the right panel.

When the experiments are performed with WT in 2D crystals, the transition temperature values are elevated to 97 °C at pD 5.5 and to 105 °C at pD 8 (Fig. 3.21a). Increased structural stability can be attributed to the more ordered structure of lipid bilayer that acts like a protective shield for the protein. There are also similar studies proving that the lipids form a more structured environment than the detergent micelles (Sukumaran et al., 2005). Also the rigid packing of OmpG in 2D crystals forming strong interaction with the lipid molecules and among themselves enabled us to observe not only the increased stability but also a difference between the open and closed states of the protein unlike the detergent solubilized WT protein. The data suggest that when the protein is in the open state it is more stable than the closed one. As stated above, WT protein in detergent solution in H_2O buffer shows an opposite result, i.e., the closed state is more stable. Here the difference between the transition temperature values is more pronounced in the 2D crystals. It is possible that in the open state stability is related with the protein-lipid interactions so that the stability difference diminishes with detergent micelles; however, the protein-lipid interaction does not explain the reason of a more stable OmpG in detergent in the closed state. It has been reported previously that OG molecules bind in the channel interior in the closed state, most likely indicating the positions of sugar binding sites (Yildiz et al., 2006). It could be that such an

interaction between OmpG and OG molecules in the closed state increase the thermal stability of the protein in the closed state.

We have also performed T-ramp experiments for OmpG-CYS, OmpG-ALA and OmpG-ΔL6 (Fig. 3.15 b-d) in 2D crystal form, incubated in pD 5.5 and pD 8. The most interesting case here is the CYS mutant since no temperature-induced transition is detected within the temperature range tested. The maximum temperature value in the experimental set-up is limited to the boiling point of the circulating anti-freeze liquid and stability of the equipment, like the tubings, to the extreme temperature values. Therefore in the experiments the maximum temperature value was set to 116 °C. This remarkable stability of the mutant can be attributed to the S-bridge stabilizing the protein conformation. It has been shown for the WT protein in 2D crystals that if the two histidines are H-bonded to each other, the protein has an increased stability evident by an increase of the transition temperature by 8 °C. For the CYS mutant instead of this H-bonding there is a S-bridge. Also there is no difference between the two samples of CYS mutant in different pD values in terms of the temperature-dependent profile. Apart from the role in pH-gating of the protein, the histidine pair also stabilizes the globular structure in its neutral form and the hydrogen bond network is thus established among S218-H231-H261-D267 (Fig. 3.11). Also the β-sheet extension to S8, S11-14 in the open state must have contributed to the increased stability.

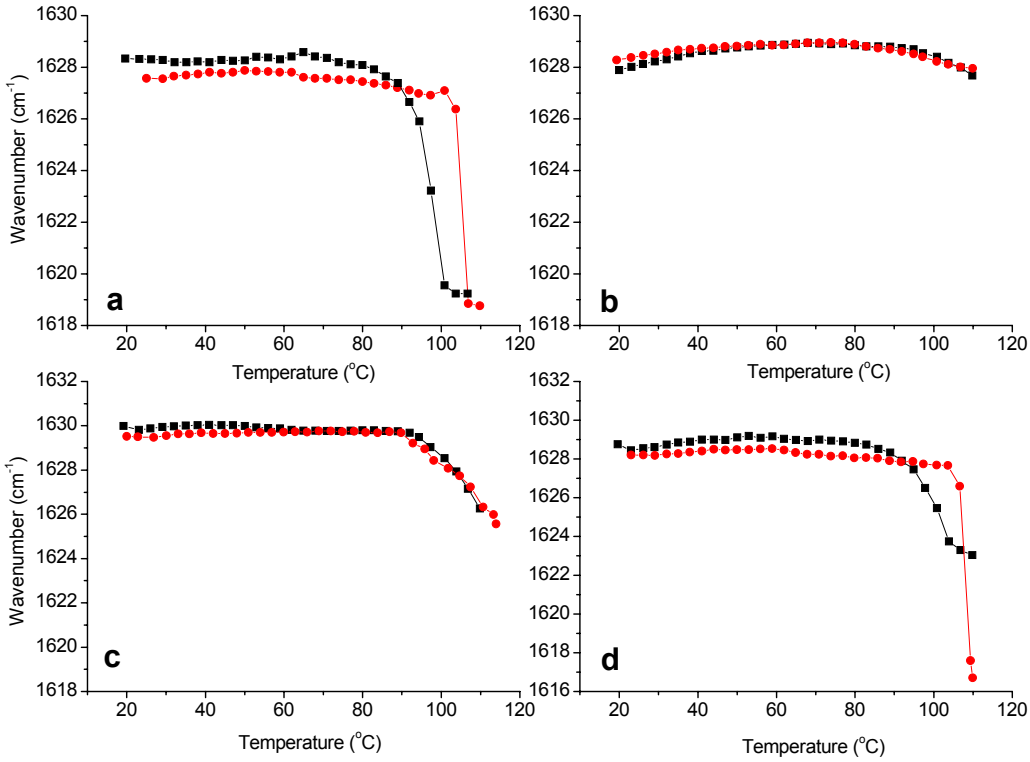

Figure 3. 21 β-sheet position followed from second derivative of OmpG-WT (a), OmpG-CYS (b), OmpG-ALA (c) and OmpG-ΔL6 (d) 2D crystals plotted against temperature. Closed states of the proteins (pD 5.4) are shown with black line (squares) and open states (pD 8) with red line (circles).

In the case of the ALA mutant, the transition temperatures of the two states are almost the same; at pD 5.5 being 103 °C and at pD 8 being 104 °C. This mutant does not show a difference in structural stability at different pD values, i.e., open and closed states of the mutant are not really distinguishable unlike for the WT. This can be explained by the fact that this mutant is no longer sensitive to pH changes in the environment. Since the histidines at the positions 231 and 261 inside the channel are replaced by alanines, they can no longer undergo an electrostatic interaction with each other. This should leave the protein between the open and closed states because neither they can attract each other and open the channel nor are they protonated and induce closure of the channel. However, the transition temperature values are closer to the open state of the WT protein, which means that OmpG-ALA has the structural integrity properties similar to the open state of the WT due to the strong backbone interactions of β-strands. Rigidity of the β-barrel and hence the increased stability has been attributed to the β-sheet extension in the open state of the WT. From this

point we can further argue that the β-sheet extensions to these strands are formed in the OmpG-ALA mutant and they are not altered with different pD values. Therefore the loop L6 should point outward from the channel entrance, leaving the channel permanently open at least partially if not completely.

OmpG-ΔL6 mutant has similar transition temperature values as compared to the WT protein, which are 98 °C at pD 5.5 and 108 °C at pD 8 (Fig. 3.21b). There is a difference in the structural stability at different pD values as for the WT, since histidines are still in place and hence respond to pD changes. However the transition temperature for the open state is slightly elevated as compared to the open state of WT. This can be explained by the fact that the loop L6, which is one of the flexible parts of the protein, is missing and hence the protein is no longer as dynamic and flexible as the WT. Although at basic pH values OmpG-WT channel is open most of the time, there are spontaneous closures observed in channel conductance measurements (unpublished data, Yildiz and co-workers). The overall position of L6 is dependent on the histidine protonation states; nevertheless L6 is still flexible and is able to move independent of histidines. Removal of this part may have increased the stability of L6 microenvironment. On the other hand the loops are the first parts of the protein affected from the increasing temperature simply because they are in the hydrophilic region and hence are not protected by the lipid bilayer. Removal of this long loop may have started the denaturation of the protein at later stages of the T-ramp.

The results of temperature dependent experiments are actually consistent with the role of histidines in the opening of the pore. In the open state they are attracted to each other and form a more stable pore. Therefore the open form of the protein is more rigid and stable as compared to the closed form. However, the detergent OG solubilized WT protein does not show such a difference in the D_2O incubated form and shows an opposite effect in the H_2O incubated form. Also there is no linear relationship between the transition temperature and pH values (Fig. 3.19). Although the protein undergoes the same structural alterations while opening and closing in detergent micelles as well; structural stability is different in different

environments. It is possible that the open state of the protein has stronger lipid interaction than the closed state, which can not be satisfied by detergent micelles.

3.2.3 H/D Exchange Profile of OmpG

In order to compare the solvent accessibility of OmpG WT and mutants, we have performed H/D exchange experiments with ATR perfusion microcell. N-H bending vibrations from the protein backbone appear in the amide II region (1600-1500 cm^{-1}). Upon deuteration, this band shifts down by about ~100 cm^{-1} and it is then called amide II'. A protein, mostly buried in the hydrophobic core of the bilayer, is accessed less by the buffer solution as compared to a solubilized protein. D_2O only affects the regions of protein backbone that are exposed to solution. When the buffer is changed from H_2O to D_2O, the time course and different phases of the decrease of the amide II band intensity gives information about the tertiary structure of a protein and the solvent accessibility of the protein backbone. It is even possible to determine the H/D exchange kinetics for different secondary structure types.

Figure 3.22 shows the calculated difference spectra by subtracting the spectrum of the protein in D_2O buffer at different times from the spectrum of the initial state of the protein in H_2O buffer for OmpG-WT in detergent. The negative absorbance values indicate the bands shifted with deuteration, while the positive absorbances are the signals appearing when deuterated. The removal of the 1535 cm^{-1} band from the amide II region is an indication of the degree of deuteration. In the figure, this band appears as a shoulder since it overlaps with the negative signal at 1518 cm^{-1}, which will be discussed later. The negative absorbance at 1535 cm^{-1} increases as the H/D exchange is proceeded. In the first hour of deuteration we see a fast decrease of this band; however, after 3 hours it reaches a constant value. At the same time and the same rate another band rises at ~1453 cm^{-1}. This is the N-H bending vibration becoming N-D bending and thus shifted from 1535 cm^{-1} to 1450 cm^{-1} upon deuteration. This vibration arises from the protein backbone regions exposed to solution.

Another characteristic change in proteins incubated in D_2O buffer is the shift of tyrosine band at 1519 to 1512 cm^{-1}. Although this band is due to the C=C stretching mode of the aromatic

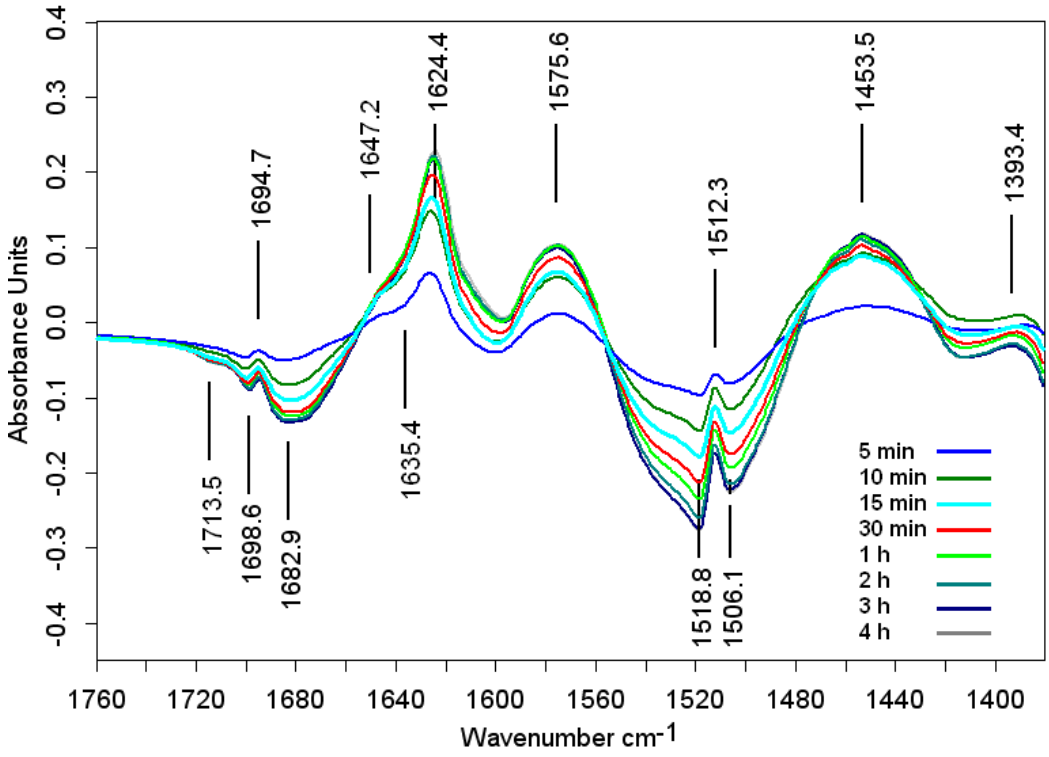

Figure 3. 22 Difference spectra calculated at indicated times from the H/D exchange experiment of OmpG-WT at pH/D 5. The negative absorbance values indicate the bands shifted with deuteration, while the positive absorbances are the signals appearing when deuterated.

ring, it is highly susceptible to the protonation state of the O-H group attached to it. Deuteration causes the hydrogen to be replaced with deuterium and the C-C mode shifts by ~5 cm^{-1} (Chirgadze et al., 1975; Zscherp et al., 2003). In the amide I region of the protein it is seen that secondary structure changes occur in the first 15 minutes of deuteration. The broad negative band in the region 1680-1660 cm^{-1} shifts to 1647 cm^{-1} upon deuteration. This large shift indicates the unordered structure most probably originating from the loops in the hydrophilic region of the protein. A small shift of 1698.5 cm^{-1} to 1695 cm^{-1} is also evident from the figure. This goes along with the shift of 1635 cm^{-1} to 1624.5 cm^{-1}. Simultaneous shift of these two bands suggest that these signals are indicative of the β-sheet structures exposed to solution. In previous studies, a β-sheet type of folding was shown to be only weakly affected from deuteration due to the strong backbone interaction (Fabian and Mäntele, 2002; Goormaghtigh et al., 1994a).

However, we should discriminate between the β-sheet forming rigid hydrophobic wall of OmpG and the sheets that are formed in the open state of the channel. In the closed state,

the extracellular ends of the strands S12 and S13 are distorted due to the attraction between the histidines (231 and 261). Neutralization of histidines at higher pH values changes their alignment and additional hydrogen bridges are formed. Curve fit routines performed with deuterated protein suggested that 7% β-sheet part of the backbone, corresponding to approximately 20 a.a., are directly involved in the dynamic transition between open and closed states. It was shown by the decrease in intensity of 1635 cm^{-1} and the simultaneous appearance of 1619 cm^{-1} upon channel opening (Fig. 3.16). The difference spectra above show the H/D exchange dynamics of the WT protein in the closed state. Therefore we suggest that β-sheet signals shifting upon deuteration originate from these dynamic regions.

We calculated the difference spectra after 3 hours of deuteration for WT protein in detergent in the open and the closed state. Since the fast phase of the H/D exchange process is due to the loops in the hydrophilic region, which is basically the same in both states of the protein, the first 10 minutes of deuteration were subtracted from each spectrum to simplify the spectra and the results are shown in Figure 3.23A. Generally the two states have the same profile of exchange but the degree of exchange is greater with the open state. In order to see the difference between them, the spectrum of the closed state is subtracted from the spectrum of the open state as presented in Figure 3.23B. The negative band at 1670 cm^{-1} is tentatively assigned to arginine residues being deuterated and shifted to 1607 cm^{-1}. This signal is originating from the antisymmetric stretching mode of the arginine side chain $CN_3H_5^+$. The corresponding symmetric stretching mode then should appear at 1635 cm^{-1} in H_2O and at 1586 cm^{-1} in D_2O based on the previously tabulated vibrational modes of arginine and their IR frequencies (Chirgadze and Nevskaya, 1976). In Fig. 3.23B, a signal at 1585 cm^{-1} is visible; however, the negative band at 1635 cm^{-1} is less clear. This could be because of the overlap of a relatively larger 1624 cm^{-1} band. It is however reasonable that arginines are deuterated since the lumen has 13 arginine residues restricting the eyelet of the channel as shown with highlighted arginines in Figure 3.24.

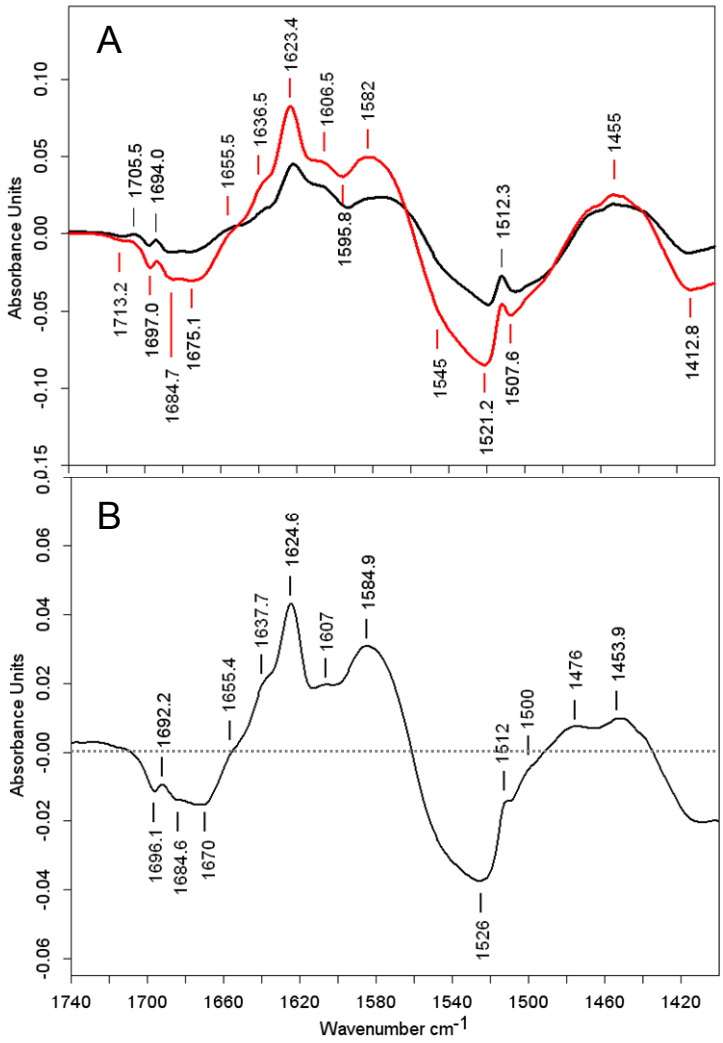

Figure 3. 23 (**A**) OmpG-WT open state (3 hours *minus* 15 min in D_2O) shown in red. Closed state (3 hours *minus* 15 min in D_2O) shown in black.
(**B**) Difference spectra of [open state] minus [closed state].

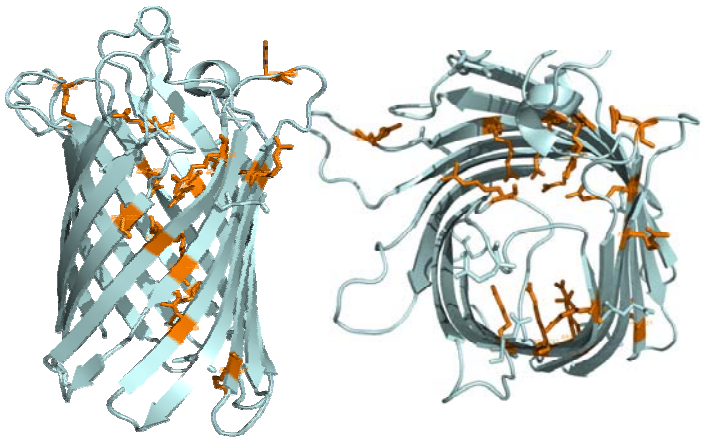

Figure 3. 24 OmpG-WT closed state side (left) and top (right) views. Arginines are highlighted as orange residues.

When the absorbance at 1606 cm^{-1} is integrated, it corresponds to 1-2 additional arginine residues deuterated in the open state. These should be one of the residues in the greasy slide region inside the lumen, because in the hydrophilic region they are readily accessible to the solvent regardless of the state of the protein.

H/D exchange experiments were performed for the open and the closed state of the WT protein and the mutants separately by arranging the pH value of the flow-through buffer. The results are summarized in Table 3.2 for 24 hours of exposure to D_2O buffer. The first three hours of exchange dynamics are shown in Figure 3.25. In the figure, only the exchange profile at pH/pD 5.5 is shown for the mutants since there was no difference in exchange rate for the open state at pH/pD 8. For the sake of clarity in the figure, we excluded the data.

Table 3. 2 H/D exchange rate percentages after 24h of exposure to D_2O buffer of OmpG-WT and mutants in detergent at pD 5.4 and 8, corresponding to closed and open state.

	H/D Exchange Rate (%)	
	pD 5.5	*pD 8*
OmpG-WT	25	37
OmpG-CYS	37	37
OmpG-ALA	36	37
OmpG-Δ L6	37	38

In the first 10 minutes of the experiment, there is no significant difference between the open and closed states of OmpG-WT in terms of the solvent accessibility (Figure 3.25). However the mutants CYS, ALA and ΔL6 show faster exchange rates (~25% for ALA and ΔL6 mutants; 18% for CYS mutant and ~13% for WT after 10 minutes). This difference in the fast phase of exchange can be attributed to the different folding pattern of the loops and turns in the hydrophilic region of the mutants. While the ALA and ΔL6 mutants and closed state of the WT reach a plateau after half an hour, the CYS mutant and the open WT continue exchanging at an almost constant rate. This second phase of exchange must be due to the parts that are not in immediate solvent contact, which could be the interior parts of the

protein or more ordered secondary structure parts. In this sense, the channel walls are relatively more accessible in ALA and ΔL6 mutants.

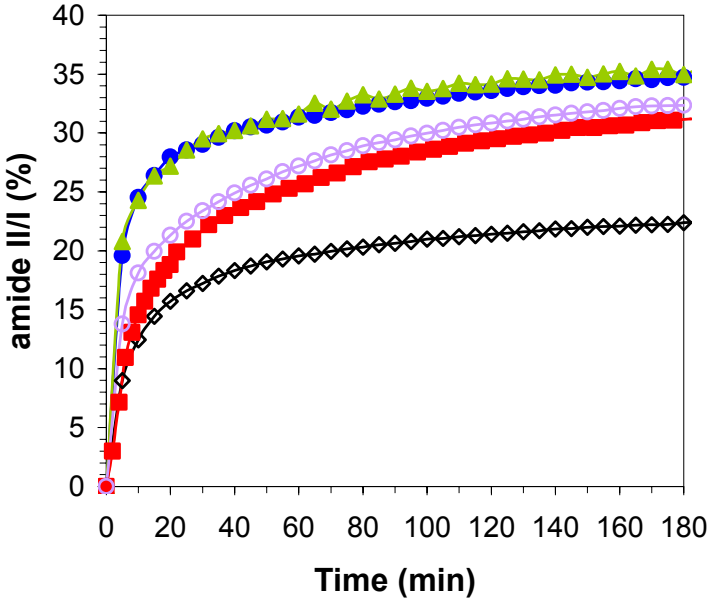

Figure 3. 25 Relative percentage rates of H/D exchange for OmpG-WT at pH/pD 5.4 (◊) and at pH/pD 8 (■). OmpG-CYS (○), OmpG-ALA (▲) and OmpG-ΔL6 (●) are at pH/pD 5.4 for the first three hours of exchange.

Accessibility is the same in all mutants and the open WT as can be seen from the overall exchange rates from the table. However, data show that ALA and ΔL6 mutants have the channel interior directly accessible to the buffer solution based on the fast exchange kinetics (Fig. 3.25). It is possible that these mutations slightly disturbed the electric potential inside the lumen so that the water molecules can get in rather easily as compared to the WT protein. The loop L6 includes four acidic residues (D221, D224, D225 and E227), one basic residue (R228) and one polar residue (Q223). Deletion of this loop may have changed the electric potential at the channel mouth. Replacement of histidines at position 231 and 261 with alanines may have changed the charge distribution at the channel entrance as well. Eventually they all resulted in an easily accessible pore lumen.

After 24 hours of exposure to D_2O buffer, open state of WT and all the mutants in both states exchange at the same rates. Although there is 12% accessibility difference between the open and closed states of WT protein, no such difference is observed for the mutants (Tab. 3.2).

Closed state of the WT protein exchanges 25%, which agrees well with the number of amino acids in the hydrophilic region, i.e. the loops and turns (78 a.a.). However the open state of WT protein has 12% more in exchangeable parts, which then adds up to 37%. Considering that WT protein has 281 a.a., 12% difference corresponds to 33 a.a.. Most probably the difference is related with the interior part of the channel, being more accessible in the open state and shielded in the closed state. Figure 3.26 shows the equipotential surfaces of OmpG in the open and closed state. The top views show clearly that the interior part of the protein is not accessible to the buffer solution for the protein in the closed state. On the other hand, the fact that mutants do not show such a difference might be evaluated as there is no major difference in structure of the mutants at different pH values and they all have the characteristics similar to the open state of the WT protein. Among the mutants, OmpG-CYS is the closest one to the open WT protein in terms of the H/D exchange profile. This could be evaluated as the neutralized histidines in the open state are well mimicked by the cysteines having S-bridges.

OmpG-ALA and OmpG-ΔL6 mutants have almost the same H/D exchange rate with the open state of the WT protein. Although the mutant OmpG-ΔL6 is sensitive to pH changes by protonation/deprotonation of histidines, there is in principle no functional opening and closure of the channel entrance since the loop L6 itself is missing. In the case of OmpG-ALA, the loop L6 is intact; however, it is presumably always at the same position, independent of the pH. Therefore the H/D exchange profile differences are due to the accessibility of the channel interior, which is related with the position of the loop L6. When the loop blocks the channel entrance, it does not only do it for maltodextrins but it effectively does it also for water molecules. This could be a defense mechanism adapted by *E. coli* to prevent the acidification of the cell. In the overall, secondary structure analysis, t-ramp and H/D exchange experiments all lead to the conclusion that OmpG attains a closed state at acidic pH values, where the channel lumen is not accessible by the solvent. This pH-gating is controlled by the hydrogen bond network among S218-H231-H261-D267, which leads to

different positioning of the loop L6. While the histidine pair at positions H231 and H261 plays the pH sensitive switch role, loop L6 controls the channel entrance.

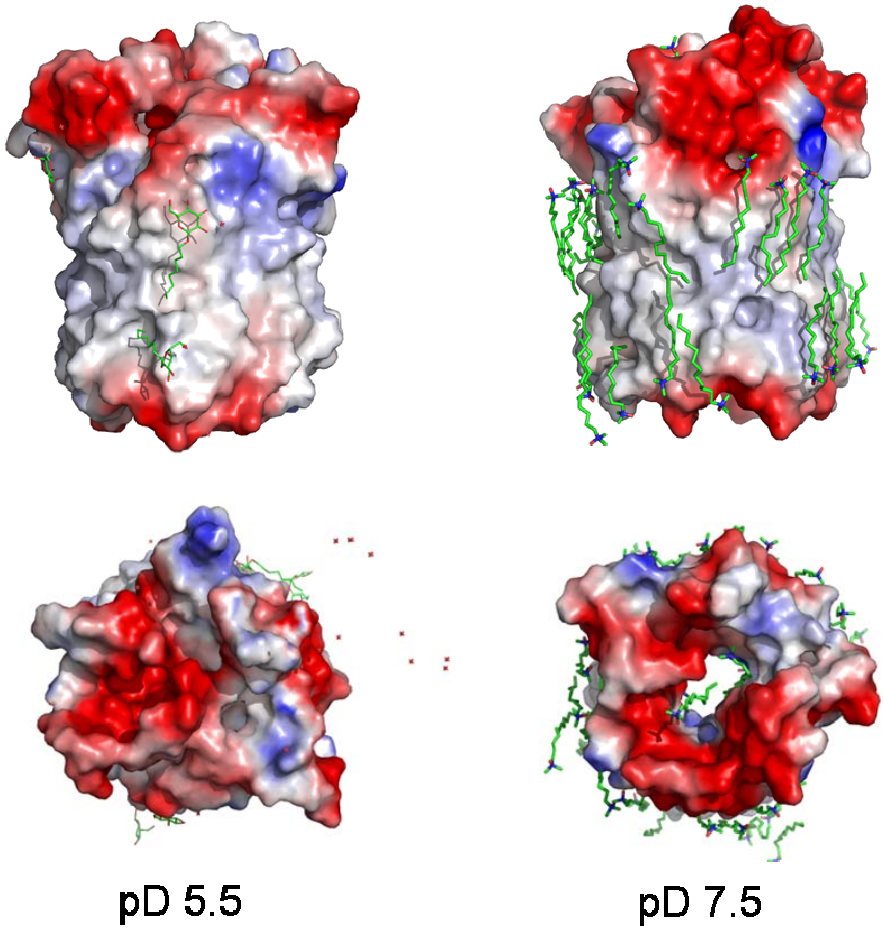

Figure 3. 26 Equipotential surfaces of OmpG with bound detergent molecules in the closed and open state viewed from side (top) and extracellular side (bottom). Surface areas having negative charge at neutral pH are red, positively charged areas are blue, uncharged areas are colorless. Picture generated by using PyMOL 0.99beta33.

3.2.4 *In situ* Opening/Closing of the Channel

The ATR perfusion microcell enables us to change the flow by means of a perfusion buffer while the protein sample is being scanned as previously performed for H/D exchange experiments. Using the same setup, we have investigated the structural differences revealed in the amide I and II regions while the pH of the buffer is changed. We have used so far the absorbance spectra in order to get information about the structure of a protein and the interaction with its surrounding molecules. On the other hand, when the activation of protein

causes only small changes in the structure of a protein, it may not be possible to distinguish them from the absorbance spectra. In such cases, the absorbance spectra of the protein in inactive state are subtracted from the active state. Such difference spectra enable us to probe small changes.

By switching the sample buffer back and forth several times, a series of difference spectra are collected and compared. Figure 3.27 shows two difference spectra of WT protein in H_2O buffer, representing the transition from the open to the closed state (black) and from closed to the open state (red), respectively. pH 8 *minus* pH 5 spectrum has the positive bands associated with opening of the channel and negative bands with closing. pH 5 *minus* pH 8 is the control spectrum to look for the bands that are reversing together with the reversing buffer conditions. Ideally, the difference spectra are mirror images of each other. *In situ* opening-closure experiments lasted generally around 24 hours in order to ensure the stability of the sample. In such long term experiments water vapor can be a problem. The green line at the bottom of Figure 3.27 shows the bands arising from water vapor. This disturbance can be successfully subtracted from the sample spectrum if necessary. If the difference spectra and the noise are compared, it is clear that none of the reversing bands is originating from noise.

The bands at positions 1697, 1691, 1639, 1629.5, 1624 and 1620 cm^{-1} are assigned to β-sheet structure. The shift of 1697 cm^{-1} to 1691 cm^{-1}, the positive signal at 1639 cm^{-1} together with the shift of 1629.5 and 1624 cm^{-1} to 1620 cm^{-1} are consistent with the formation of new β-sheet and/or the overall structure being more rigid with opening of the channel. The signal at the position 1639 cm^{-1} can be also partially attributed to arginine residues. However, the symmetric stretching mode that is supposed to be at 1670 cm^{-1} is not clearly distinguished from the spectra. H/D experiments showed the shift of this antisymmetric stretching mode to 1586 cm^{-1}. Therefore 1639 cm^{-1} is mainly assigned to the additional hydrogen bridges upon formation of weakly interacting β-sheets.

β-sheet proteins have the typical amide II positions at 1530 cm^{-1} (Nabedryk et al., 1988; Venyaminov and Kalnin, 1990b). Therefore we assign the positive signal at 1535 cm^{-1} to the

C-N, N-H and C-C modes from the backbone of β-strands in the open state of the protein. The reversal is marked by the dashed line IX in Figure 3.27. This band is associated to the β-sheet changes in different states of the protein that are also reflected in the amide I region. There is a positive correlation among the signals at 1691, 1639, 1620 and 1535 cm^{-1}.

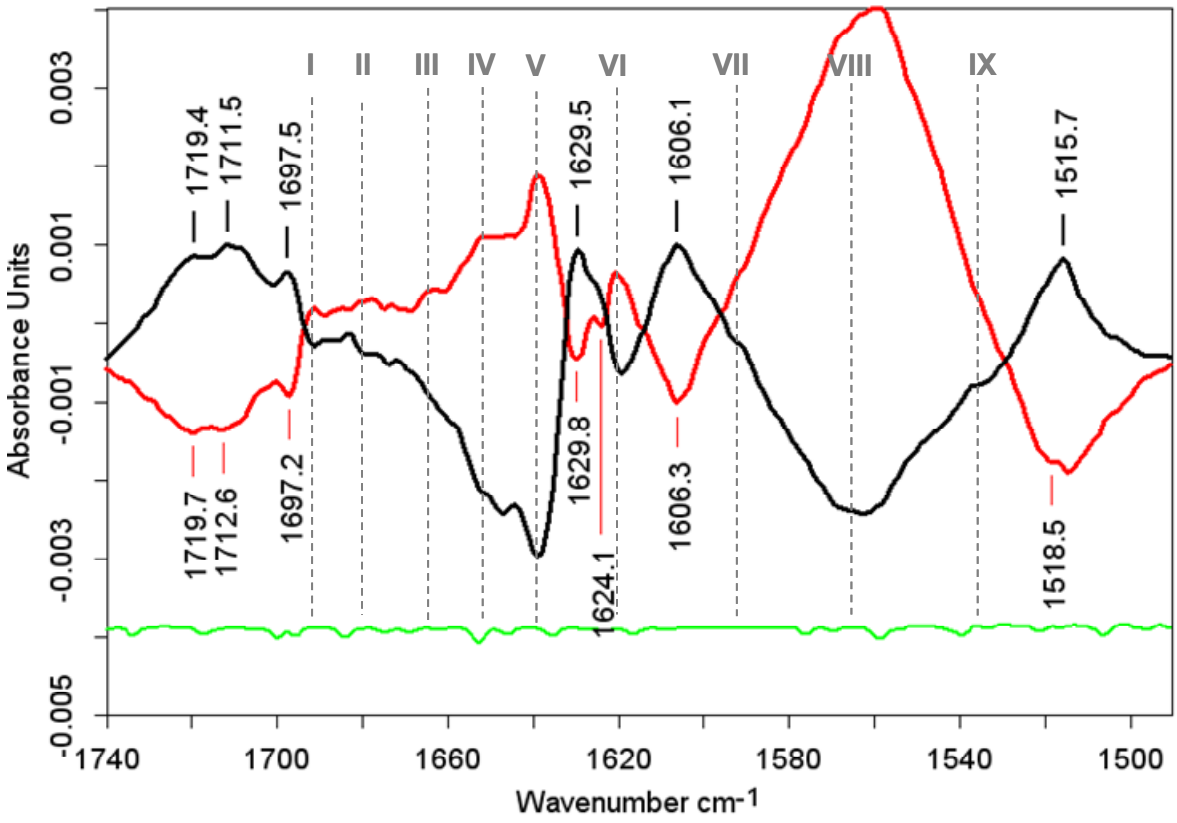

Figure 3. 27 Difference spectra of OmpG-WT in H_2O-buffer in detergent. Red spectrum is pH 8 *minus* pH 5 and the black is pH 5 *minus* pH 8. Green is the atmospheric interference, shown for comparison. Band positions of the numbered lines are; I:1691.5 cm^{-1}| II: 1679 cm^{-1}| III: 1665 cm^{-1}| IV:1652 cm^{-1}| V:1638.8 cm^{-1}| VI: 1619.8 cm^{-1}| VII: 1592 cm^{-1}| VIII: 1562 cm^{-1}| IX: 1535 cm^{-1}.

The bands at 1592 and 1516 cm^{-1} are assigned to protonated tyrosine C-C stretching modes. Therefore, data from the difference spectrum suggests that tyrosines are involved in opening and closure of the channel. The signal does not indicate a deprotonation; it is rather the strength of the C-C mode attached to OH group changing with opening of the channel. These can be the tyrosines that are part of the aromatic girdle of the protein or the ones that are inside the channel lumen. These residues could be stretched out and relaxed with opening

and closure of the channel. This can be initiated by the repositioning of the charged loop L6 and the realignment of the strands S12-S14.

The negative signal at 1606 cm^{-1} in the open state is generally assigned to arginines (Ortiz et al., 2005); however, there is no explanation as to whether it is assigned to the protonated or deprotonated form. In studies with model compounds, such a low frequency is not detected in H_2O buffer (Venyaminov and Kalnin, 1990a). Therefore we prefer to leave the signal unassigned.

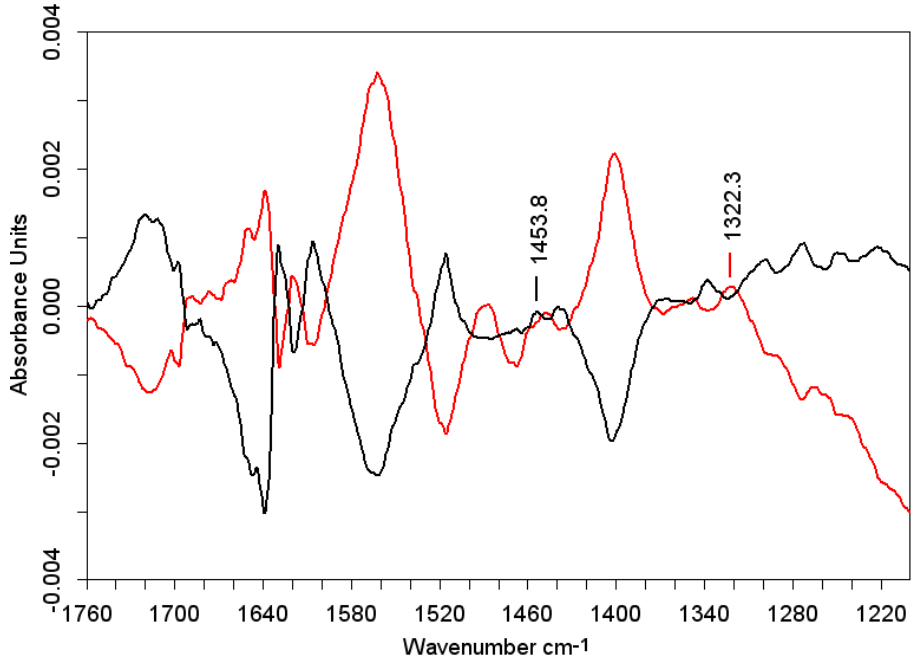

Figure 3. 28 Difference spectra of OmpG-WT in H_2O-buffer in detergent. Black spectrum in the figure represents the transition from open to closed state and the red spectrum represents the transition from closed to open state. Potential signals for histidine protonation are labeled.

In Figure 3.28, the negative signal at 1453.8 cm^{-1} and the positive signal at 1322.3 cm^{-1} in the open state of the protein are assigned to protonated histidines (Iwaki et al., 2005). The C-N stretching vibration of the side chain ring giving rise to the band at 1451 cm^{-1} has been calculated to have a molar extinction coefficient of 260 M^{-1} cm^{-1}, which disappears upon protonation. Here the absorptions of the bands are on the order of 0.1 mOD and the deprotonated histidine band at 1453.8 cm^{-1} is slightly shifted as compared to the published data in the study of Iwaki and co-workers. Nevertheless, the band at 1322 cm^{-1} is in good agreement with the data, where the transition from imidazole to imidazolate forms of

L-histidine in H_2O gives rise to a signal at 1323 cm^{-1}. OmpG WT has the opening/closing mechanism triggered by the two histidines. In the open conformation, they are connected via a H-bond network among S218-H231-H261-D267. Closing of the channel starts with the protonation of the histidines at acidic pH and thus the H-bond network is abolished. This is confirmed by the negative band at 1453.8 cm^{-1} and the positive band appearing at ~1322 cm^{-1}. In the difference spectra of the deuterated form, the same band at 1453.8 cm^{-1} is seen at exactly the same position (Fig. 3.23B). Due to the broad N-D deformation in D_2O, this band is overlapped and could not be compared due to different exchange rates observed for the two states of the protein.

At 1679 cm^{-1} and 1665 cm^{-1} the C=O stretching vibrations from asparagines and glutamines are detected. However, it is difficult to identify them in the difference spectra in D_2O buffer (Fig. 3.23B). Upon deuteration, the corresponding signals of both side chains should exhibit a downshift by about 30 cm^{-1}. However, the region of the amide I between 1650 cm^{-1} and 1630 cm^{-1} is also populated by the signals originating from short helices, loops and β-sheet (Susi and Byler, 1987; Van Wart and Scheraga, 1978). WT protein includes 21 asparagines and 8 glutamines. Their molar extinction coefficients are roughly the same (~310 M^{-1} cm^{-1} for asparagine and ~360 M^{-1} cm^{-1} for glutamine). In this sense, one would expect the band at 1679 cm^{-1} to be three times stronger as compared to the 1665 cm^{-1} band, which is not the case here. The region of the amide I between 1680 cm^{-1} and 1665 cm^{-1} is assigned to β-turns and this is more likely the case for the difference spectra in H_2O-buffer for two reasons; (i) we know from the structure that in the open and closed state of the protein, channel opening involves the repositioning of the turns and loops and (ii) the intensity of spectral changes are small. Therefore we assign this region to β-turns and loops. The situation at 1652 cm^{-1} is even less clear. To the best of our knowledge, this region is free of side chain absorbance in H_2O buffer. In terms of the secondary structure, it can be assigned to loops or α-helix. Although the loops should be positioned between 1670 and 1660 cm^{-1}, it is known that solvent-exposed and/or short α-helix segments absorb at lower wavenumbers around 1650. Therefore 1652 cm^{-1} band is less likely to be due to loops. Therefore, we suggest that the

short α-helical structure is affected from the changing ionic strength of the buffer. As we infer from the IR studies so far, the helix structure does not play a role in opening and closing of the channel. Thus it could be a hydrogen bond strength difference of the backbone as the pH changes in the buffer.

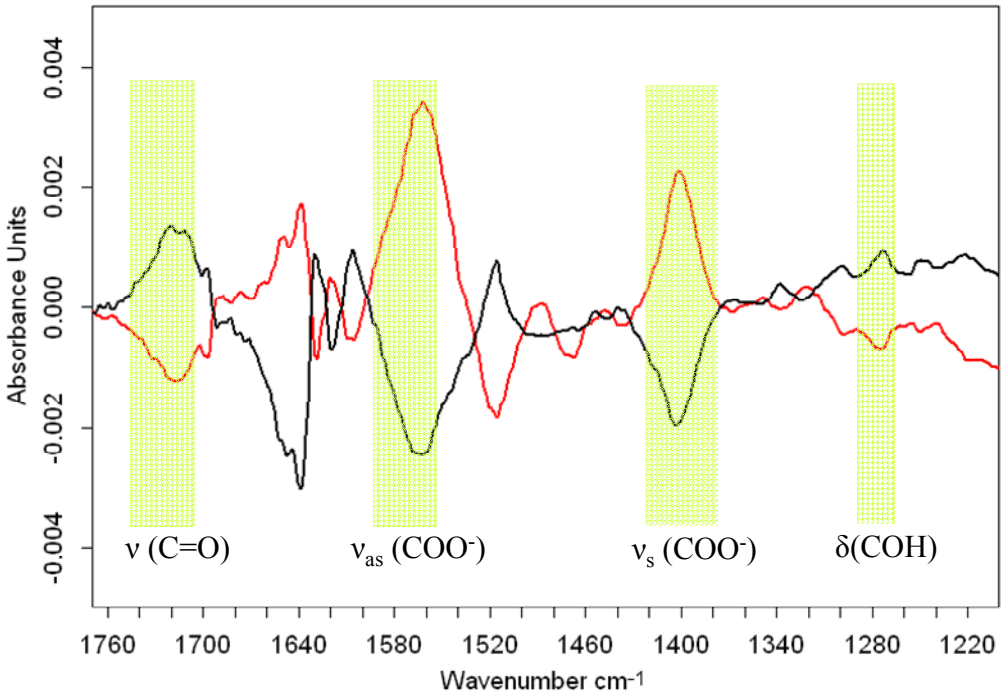

Figure 3. 29 Difference spectra of OmpG-WT in detergent. Black spectrum in the figure represents the transition from open to closed state and the red spectrum represents the transition from closed to open state. Protonated and deprotonated carboxyl group signals are shown with shaded areas.

The region above 1700 cm^{-1} is assigned to the C=O stretching mode from the side chains of aspartic and glutamic acids. WT protein has 26 aspartic and 23 glutamic acid residues distributed mostly inside the lumen of the channel and at the entrance. The signals at 1719 and 1712 cm^{-1} are assigned to these negatively charges residues. They are positioned at 1713 and 1705 cm^{-1} upon deuteration (Fig. 3.17A). Based on the frequency shifts upon deuteration, these bands can be attributed to the protonated C=O groups. Since these residues are relatively numerous as compared to other amino acids, and exhibit high molar extinction coefficients, (Chirgadze et al., 1975) the corresponding signals are very well distinguished. Figure 3.29 shows the spectral regions characteristic for these molecular groups as shaded areas. The antisymmetric and symmetric stretching modes of COO^- group are positioned at ~1570 and 1405 cm^{-1} respectively. These positions are in very good

agreement with published values (Barth, 2000). They correspond to the deprotonated side chains and are positive in the open state. We assign the protonated COH bending mode to the band at 1274 cm^{-1} that is positive in the closed state of the protein. It is likely that some negatively charged amino acids are protonated upon closure of the channel and deprotonated in the open state. This would effectively prevent the diffusion of the nutrients at acidic pHs. Protonation may occur via the positively charges amino acids like arginine, which are also located inside the lumen and the channel entrance. Therefore hydrogen bonding among the arginines and aspartic/glutamic acid residues is possible. The signal at 1639 cm^{-1}, previously assigned to arginine, should then correspond to the noninteracting residues in the open state of the protein.

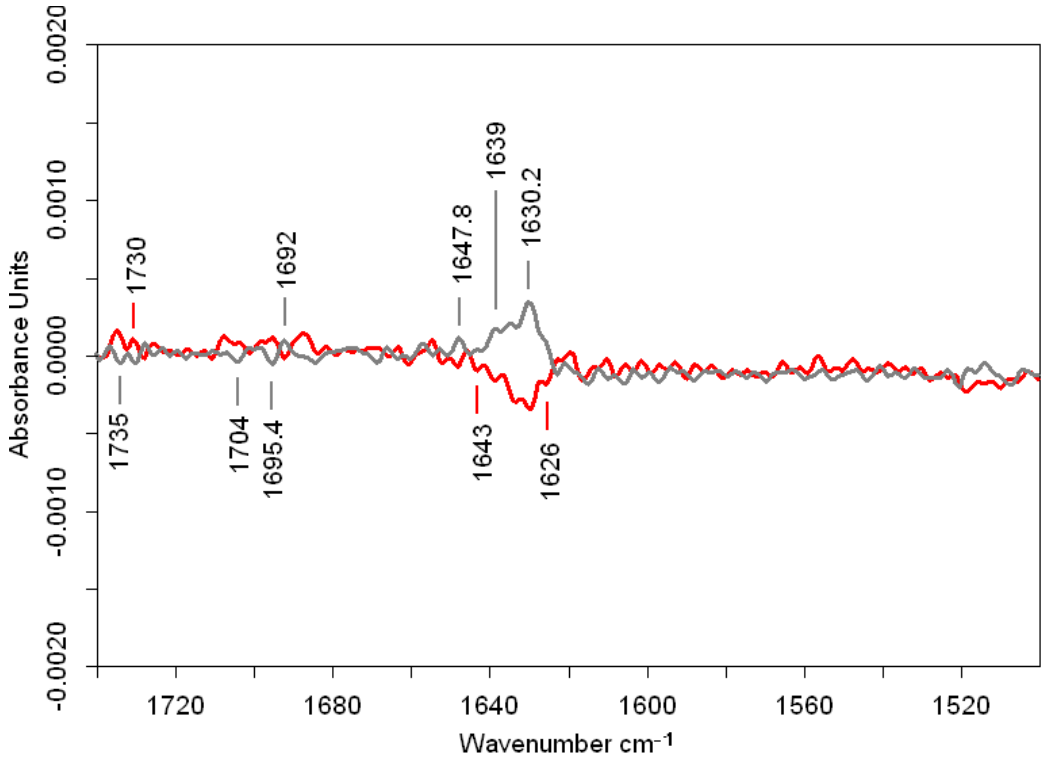

Figure 3. 30 Difference spectra of OmpG-ΔL6. Red line represents open *minus* closed state and grey represents closed *minus* open state.

Difference spectra of OmpG-ΔL6 mutant reveals fewer signals with smaller intensities as seen in Figure 3.30. Signal strengths are very weak, yet some reversible changes can still be seen. The open state of the protein (shown in red) exhibits the positive signals at 1735 and 1730 cm^{-1}, most probably arising from the C=O stretching modes of the aspartic and glutamic

acid side chains. These were negative signals in the open state of the WT protein. As discussed above, their protonation state could be related with their interaction with positively charged residues like arginine. In the case of the ΔL6 mutant the charged loop is missing and most of the side chain effects that were listed above are also cancelled. Here we can assume that repositioning of the loop L6 affects the interaction of charged residues. The arginine signal previously assigned to the band at 1639 cm^{-1} is also opposite as compared to WT protein but consistent with the aspartic/glutamic acid signal protonation state. The band shift of 1695 to 1692 cm^{-1} and 1630 & 1626 to 1622 cm^{-1} are consistent with the assignment to β-sheet structures.

The difference spectra of WT show mostly the changes from side chains rather than from secondary structure elements. The role of side chains in opening and closing the channel is less efficient in the case of ΔL6 mutant. However, there are differences in the β-sheet parts between the two states. This was also reflected by T-ramp experiments (Sect. 3.2.2). While the mutants ALA and CYS did not show differences in terms of thermal stability, the ΔL6 mutant and WT showed increased stability in the open state. Meanwhile, the lack of side chain effects explains the similar H/D exchange rates between the open and closed state of the ΔL6 mutant.

3.3 Structure of BetP WT and Mutants

BetP is a glycine betaine transporter from *Corynebacterium glutamicum*. It is an inner membrane protein and like the other members of betaine/carnitine/choline transporter (BCCT) family of transporters, it is predicted to be in α-helical structure (Peter et al., 1998). BetP responds to the hyperosmotic stress by transporting glycine betaine together with two Na^+ ions. It has an exquisite specificity for glycine betaine with an affinity about 10 μM and an affinity for Na^+ about 10-40 mM (Rubenhagen et al., 2000). Changes in external osmolaritiy and chill stress lead to the activation of BetP and the activation mechanism is considered to involve lipid stimulus (Morbach and Kramer, 2005). On the other hand, BetP is activated by the high luminal K^+ (and Rb^+ or Cs^+) concentration in proteoliposomes (Rubenhagen et al., 2001; Schiller et al., 2004). Interestingly BetP does not respond to other cations like ammonium or choline. K^+ activation requires a certain conformation of the long C-terminus, which is predicted to be in α-helical structure (Ott et al., 2008). Truncations from the C-terminal domain or mutations to the residues positioned downstream of Tyr550 in order to restrict its flexibility or to disrupt the helical structure resulted in an always active protein with reduced betaine uptake rates in proteoliposomes. However, these mutants can still be regulated by external osmolarity in cells.

Proteins having mostly α-helical or β plated sheet structure as the main folding motif differ in the amide I and II peak positions in the IR spectrum. BetP has the amide I peak position centered on 1654.5 cm^{-1} and the amide II position at 1545 cm^{-1} as shown in Figure 3.30. 500 mM K^+ is used in order to investigate the structural changes in the active state of the protein. 100 mM KPi buffer was used for the FTIR measurements. The free K^+ ions in the final buffer solution were counted together with the addition of KCl salt. 100 mM KPi buffer includes roughly 190 mM K^+ ions ($[K^+]$) when the appropriate amounts of acid and base salts are mixed to get pH 7.4. An additional 300 mM KCl dissolved in the buffer results in ~500 mM $[K^+]$, which is considered to be sufficient for activation. Henceforth, figure legends indicate the calculated total concentration of $[K^+]$. Figure 3.30 shows the IR absorbance

spectra and the corresponding second derivative spectra of the active (red) and inactive (grey) states of BetP-WT in reconstituted into 2D crystals in D_2O. The overall profiles of amide I' and II' do not show diversities except for a slight shoulder on the lower frequency region of amide I band in the active state. In order to clearly demonstrate the amide I region, the protein pre-incubated in D_2O is shown here. Although the shape of amide I band contour changes, the peak position does not change between H_2O and D_2O buffers, which confirms that the amide I band is dominated by the α-helical type of folding.

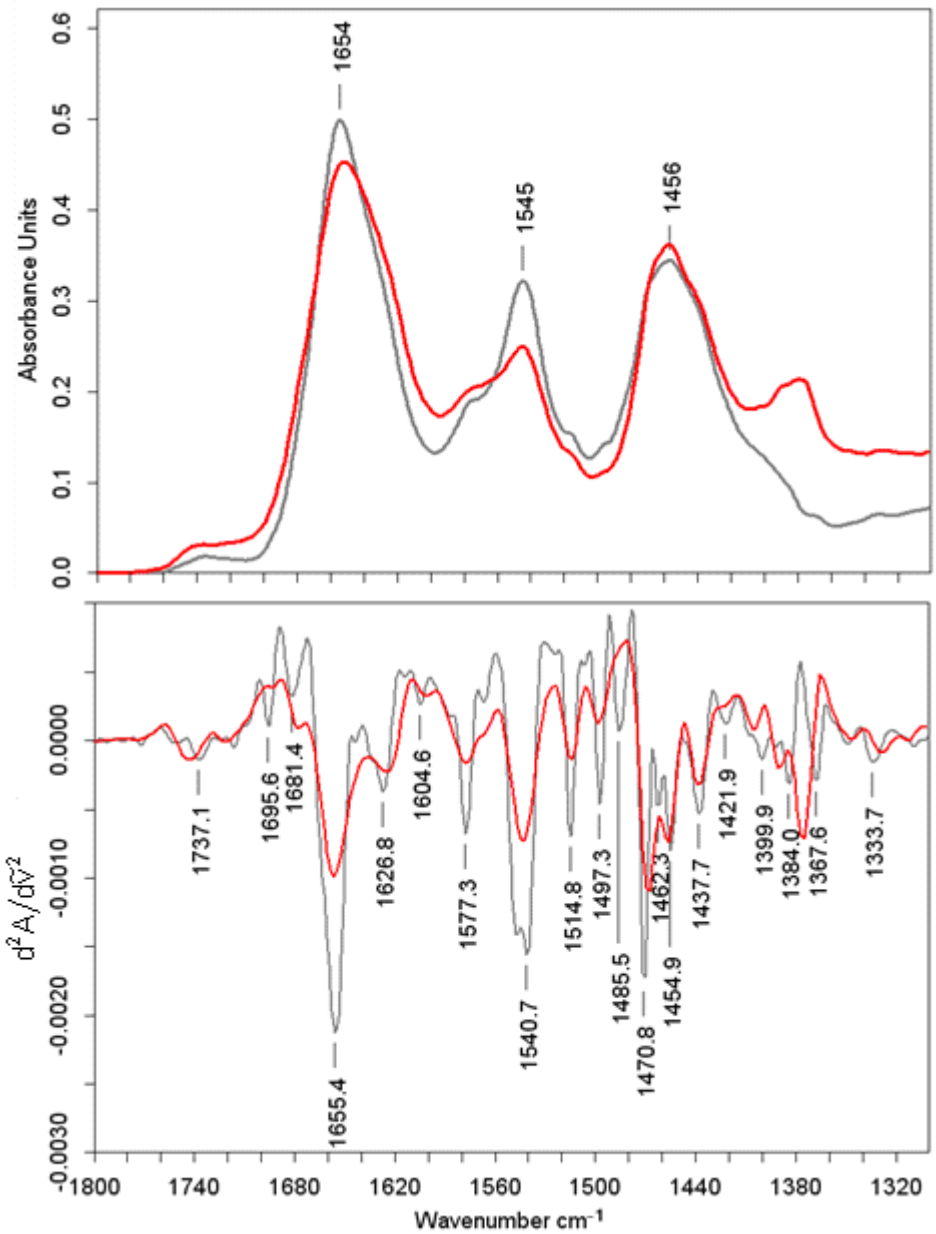

Figure 3. 31 Infrared absorbance of BetP WT in D_2O buffer in active (red line) and inactive (grey line) state (top figure) and their corresponding second derivative profiles.

The second derivative profile of both the active and inactive states of the WT protein shows a significant α-helix contribution located at 1656 cm^{-1} together with unordered structure around 1640 cm^{-1}. The unordered structure is not resolved in the second derivative since it is characterized by broad bands. There are also contributions from turns located at 1680 cm^{-1}. Although the protein consists of loops of varying lengths, we suggest that the signal originates from restricted parts of the loops. The appearance of two simultaneous bands at 1696 and 1627 cm^{-1} confirms the existence of intermolecular β-sheet in both states of the WT protein. This is to be expected since the protein was shown to be a trimer in detergent solution as well as in the membrane (Ziegler et al., 2004).

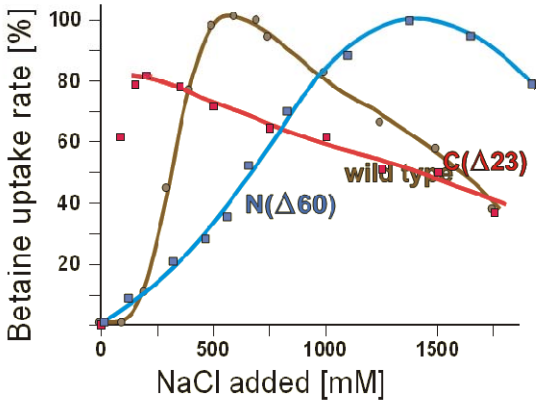

Figure 3. 32 Betaine uptake activity of BetP WT, C-terminus truncated mutant, C(Δ23) and N-terminus truncated, N(Δ60), mutant in response to increasing hyperosmotic stress (Figure adapted from Kramer and Morbach, 2004).

Hyperosmotic stress leads to the elevated level of cytoplasmic [K^+], which is the major stimulus for BetP activation in proteoliposomes (Schiller et al., 2004). The C-terminal region of the protein was shown to play the key role in osmosensing (Peter et al., 1998). C-terminal truncation of 45 a.a. led to the loss of response to osmotic stress resulting in a continuous glycine betaine uptake. This mutant is always in the active form. On the other hand, 12-23 a.a. truncations from the C-terminus led to partial deregulation of the mutant. These mutants still respond to changing osmotic stress, however at lower values of external osmolarity, where the WT protein is still inactive. Deletions from the N-terminal extension of BetP cause a shift of the activation optimum to higher osmolarities in *C. glutamicum* cells

(Fig. 3.32). 2-fold higher external osmolarities had to be applied in order to activate these mutants as compared to the WT protein. The structural changes upon activation and glycine betaine transport mechanism are still not clear. Previously, BetP reconstituted in *E. coli* lipids has been reported to reach half-maximum activity at 221±23 mM K^+ (Rubenhagen et al., 2000). However *E. coli* lipids only have <25% phosphatidylglycerol in composition (Prasad, 1996) and the critical value of [K^+] in order to activate BetP increases as the fraction of anionic lipids increases (Rubenhagen et al., 2000). *C. glutamicum* has ~87% anionic lipids (Hoischen and Kramer, 1990) and therefore higher [K^+] is needed to activate BetP. In 2D crystal samples, BetP is reconstituted in POPG lipids and in detergent solubilized samples, the protein was enriched with POPG during the purification steps. In perfusion cell experiments, the protein is continuously washed with KPi buffer including the detergent DDM, thus the free lipid molecules are removed and only the ones that are bound to proteins remain.

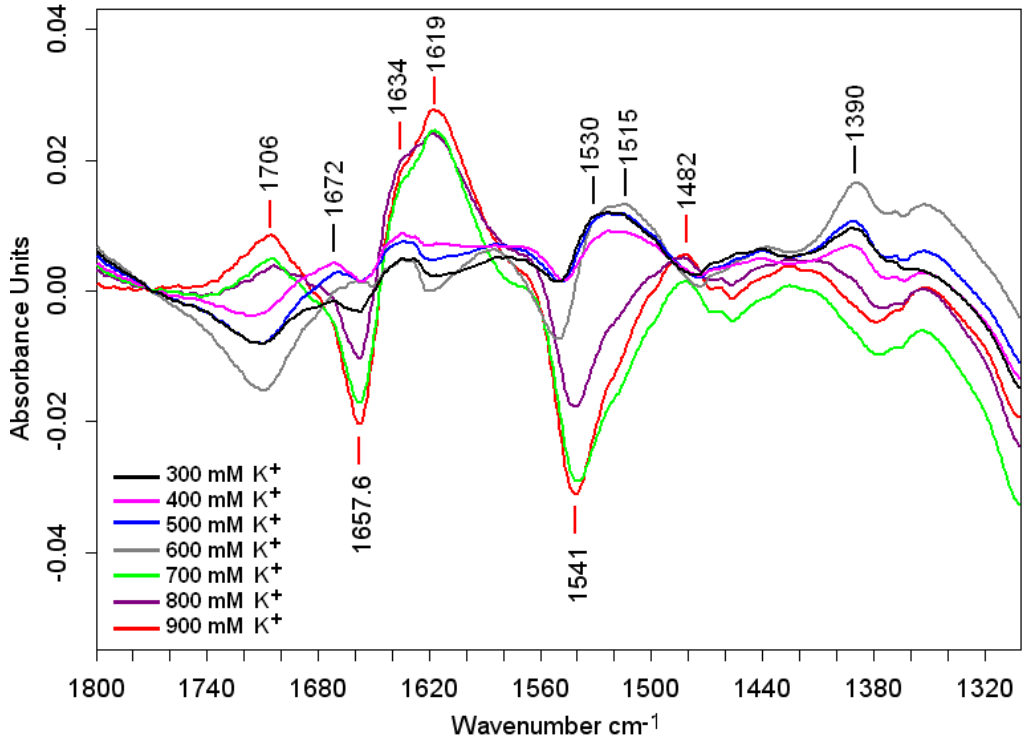

Figure 3. 33 Difference spectra of BetP WT in 2D crystals in 100mM KPi-H_2O buffer with increasing K^+. Protein in 100mM KPi buffer is taken as reference in difference spectra calculations.

We have first investigated the threshold ionic strength for activation by linearly increasing [K^+] via adding KCl salt to the sample buffer. Figure 3.33 shows the difference spectra of BetP

WT in 2D crystals in 100mM KPi pH 7.5 - H_2O buffer with increasing KCl concentration. As described above, calculated values of [K^+] are given in the figure legend. Difference spectra are taken with respect to the protein in KPi buffer with no extra KCl salt, which then corresponds to 190 mM K^+. Since ~200 mM K^+ leads to half-maximal activity of the protein in *E.coli* lipids, the changes in the protein structure, as the [K^+] is increased, may reflect the conformational changes induced by activation of the protein. Increasing the [K^+] from 300 to 500 mM did not induce significant changes in the protein difference spectra. However starting from 700 mM [K^+] dramatic structural changes are seen. In this respect 600 mM [K^+] is more like a transition state based on the peak position shifts. Positive peaks at 1706 cm^{-1} and 1619 cm^{-1}, and negative peaks at 1657 cm^{-1} and 1541 cm^{-1} are the most pronounced signals.

The band at 1706 cm^{-1} can be attributed to the C=O stretching group of either from the lipid interfacial region or from the aspartic and glutamic acid or a combined effect coming from both the lipid moiety and a group of side chains.

The decrease in the intensity of 1657 cm^{-1} can originate from ordering of some coils or it can as well be a decrease in the α-helix content of the protein. In H_2O buffer, the IR signature of random coil structures and α-helical structures overlap in the amide I region, hence the original molecular group/groups can not be identified at this point. Another positive peak at 1619 cm^{-1} is most probably due to a side chain like tyrosine aromatic ring stretching vibration or an asparagine NH_2 bending mode. Both residues were reported to absorb at this region in H_2O buffer (Venyaminov and Kalnin, 1990a). BetP WT has 9 Tyr and 21 Asp residues. According to the calculation method given in the study of Chirgadze and co-workers, it is possible to calculate the number of residues giving rise to a side chain signal at a specific spectral position (Chirgadze et al., 1975). Using the provided molar extinction coefficients of residues at 1620 cm^{-1}, it is calculated that either 1 Tyr or 0.2 Asp gave rise to the positive band at 1619 cm^{-1} in Figure 3.33. We conclude that the Tyr residue is the more plausible option.

The negative peak at 1541 cm^{-1} can not be directly attributed to side chain absorptions according to the available data so far. Although the frequency is close to the asymmetric stretching mode of COO^- from aspartic or glutamic acid, we propose that the signal is related with tertiary structure changes upon activation of the protein. In a previous study, the signal at 1545 cm^{-1} was correlated with the α-helical content of the protein, while the random coil structure content was correlated with the signal at 1553 cm^{-1} (Goormaghtigh et al., 2006). Also the negative amplitude of this signal is halfway with 600 mM $[K^+]$ together with the signal at 1657 cm^{-1}. This suggests that both signals at 1657 and 1545 cm^{-1} represent changes in the α-helical regions taking part in activation. The position of 1657 cm^{-1} signal is observed to shift to lower wavenumbers, to ~1640 cm^{-1}. A signal at 1640 cm^{-1} has been attributed to fully/partially hydrated helices, or hydrated short helices or 3_{10} helix (Haris and Chapman, 1995; Mukherjee et al., 2007). Therefore, it is possible that some helices are solvent exposed upon activation.

It can be concluded that activation of BetP WT in 2D crystals is achieved by 700 mM $[K^+]$, which corresponds to 100 mM KPi buffer with 500 mM KCl and that the activation causes changes in α-helical moiety together with changes in ester groups and a Tyr residue. In 2D crystals, where BetP is reconstituted in POPG lipids, this value of $[K^+]$ is in agreement with previous functional data that showed that activation of BetP requires almost three-fold more $[K^+]$ in phosphatidylglycerol lipids than the ~220 mM $[K^+]$ in *E. coli* polar lipids.

Activation of the protein with excess $[K^+]$ has also been tested on BetP WT solubilized in detergent DDM. The results are different from that of the BetP WT in 2D crystals. Figure 3.34 shows the difference spectra of BetP WT in detergent in H_2O-buffer as a function of increasing $[K^+]$ indicated on the figure. The first difference between the two forms of the protein is that the activation is achieved at 220 mM $[K^+]$ for detergent environment, which is much lower than the value determined with 2D crystals. Further increase in salt concentration did not induce any further effect on the protein structure. If the excess K^+ is removed so that the buffer is free of salt, the structural differences are reversed, which is the proof that the changes are indeed induced when there is excess K^+. As the previous studies

have also suggested, the protein should have a specific kind of interaction with the surrounding lipid molecules in order to have such a difference in activation concentration. Although the protein in detergent is enriched with POPG, these lipids could either be bound to positions not accessible for an activating interaction or prevent just dilapidation during purification. In that case, the lipid species bound to BetP would be those of its expression host *E. coli.* Anyway, it is highly probable that a number of amino acids at different points of the C-terminus are interacting with the lipid molecules.

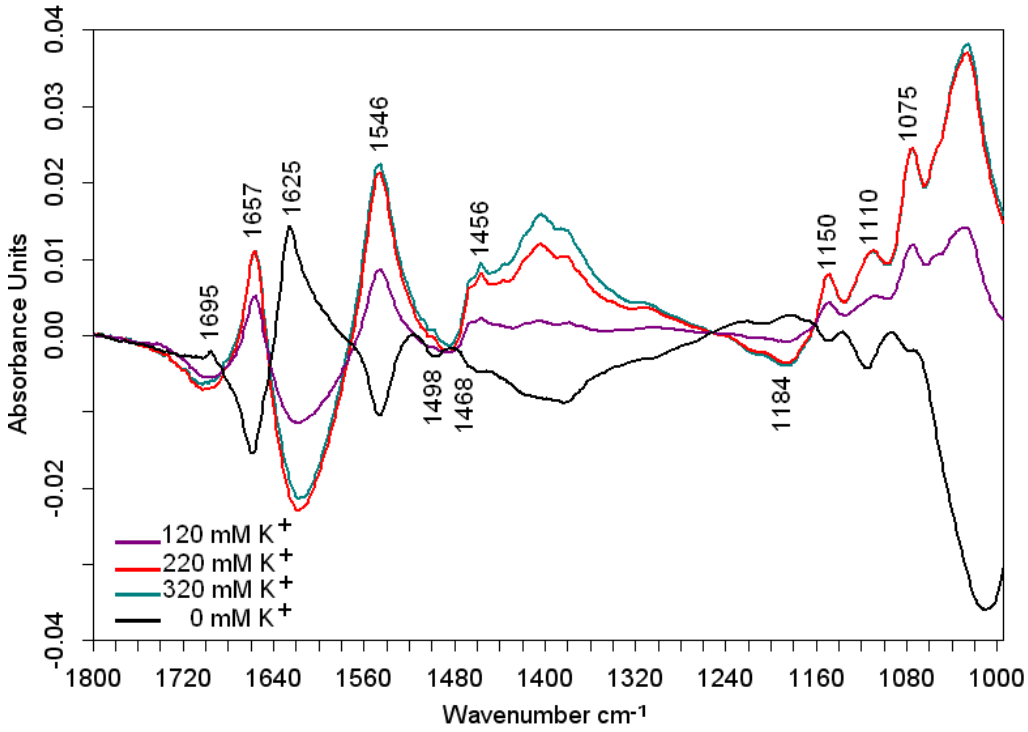

Figure 3. 34 Difference spectra of activation of BetP WT in detergent DDM. Protein is incubated in 10mM KPi-H_2O buffer and 100mM KCl is added in stepwise. After the full activation, the protein is suspended in 10mM NaPi-H_2O buffer in order to remove all K^+ ions.

Activation of BetP is mainly reflected by positive peaks at 1657 and 1546 cm^{-1} and negative peaks at 1695 and 1625 cm^{-1} in the amide I and II region, respectively. Although the peak positions are in good agreement between the two forms of the protein, the signals are reverse in two cases. While the 1657 cm^{-1} signal is positive for the protein in detergent solution, it is negative for BetP in 2D crystals. Considering that the buffers are the same for the two forms, the only difference is the environment surrounding the protein. However, it is hard to explain the opposite signals simply by the changing environment. The 1657 cm^{-1}

signal might originate from different parts of the protein in the two forms reflecting the changing environment. Nevertheless, there is still a positive correlation between the bands at 1657 and 1545 cm^{-1}, possibly representing changes in α-helical moiety. The peaks at 1695 and 1625 cm^{-1} indicate changes in intermolecular β-sheet. This could represent changes in protein-protein contacts among monomers or changes in the orientation of helices with activation. Therefore, BetP in 2D crystals and in detergent differ in their activation profile most likely due to the differences in the environment surrounding BetP. The changes are induced by the excess K^+ based on the reversing signal when the K^+ is removed; however, this does not necessarily mean that the protein is activated since we can not monitore betaine uptake rates while measuring the structural changes by IR spectroscopy. These changes could merely be due to an electrostatic effect induced by the increased number of positive charges.

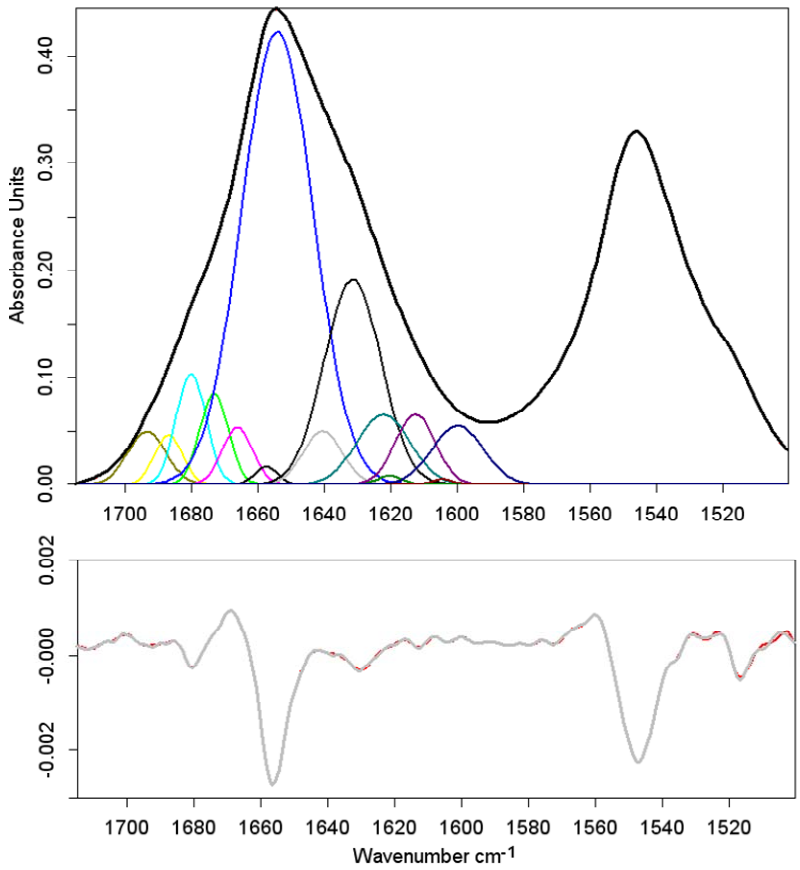

Figure 3. 35 Curve fit analysis of BetP WT in inactive state for amide I region. The envelope band formed by the fitted bands is shown by red and the original spectrum is shown with black in the upper box, with grey in the lower box. Second derivatives of the original spectrum and the fitted envelope are compared in the lower box as a measure of the curve fit success.

In order to have a better idea about the structural changes upon BetP activation, the secondary structure of the protein is analyzed using the amide I region of IR absorption spectra. We have performed curve fit analysis for active and inactive states of the WT protein in H_2O and D_2O buffers. Table 3.3 shows the component bands and percentage fraction of their area integrals relative to the total amide I area. Before curve fitting, corresponding buffers were subtracted and a straight line, generated between the wavenumbers 1715 and 1590 cm^{-1}, was subtracted to minimize the side chain contribution to amide I (Dousseau and Pezolet, 1990). Spectra were deconvolved using the Fourier self deconvolution built-in macro, available with the OPUS software[5]. Fourier self deconvolution considerably reduces the time for fitting and helps better determining the component band contours. Fit results were then used as the initial set for the fitting of the original spectrum. The number and position of components were determined from the second derivative and the resulting fit envelope was compared with the original spectrum from second derivative profiles to judge the overall success of the fit procedure (Fig 3.35, lower box).

Table 3. 3 Percentage fractions of fitted bands for detergent solubilized BetP WT in active and inactive state and in 100mM KPi pH7.5 buffer in H_2O and D_2O. 500mM KCl is added for activation of the protein.

WT in H_2O Buffer				**WT in D_2O Buffer**			
Inactive		**Active**		**Inactive**		**Active**	
position	% area	position	% area	position	% area	position	% area
1622	6.1	1622	6.6	1621	12.7	1623	9.1
1631	19	1630	7	1631	18.7	1633	16.3
-	-	1636	9.8	-	-	-	-
1640	3.4	1643	10.7	1643	17.2	1641	11.5
-	-	1649	5.4	-	-	1648	9.8
1655	53.3	1656	29	1656	45.5	1655	4.4
1666	2.9	1666	6.5	-	-	1659	40.3
1673	4.3	1671	8	1676	5.2	1674	4.6
1680	5.4	1679	8	-	-	1681	2.3
1687	2.3	1688	6.2			1689	1.7
1693	3.3	1698	2.2	1693	0.7		

The activation of BetP was assured by adding 500 mM KCl to 100 mM KPi buffer. The inactive state of the protein in H_2O buffer has the biggest fraction of secondary structure

[5] Fourier self deconvolution was performed with Lorentzian band shape of 29 cm^{-1} half width and noise reduction of 0.2 factors.

located at 1655 cm^{-1}. The corresponding state in D_2O buffer however suggests a lesser contribution in the same region. This position is occupied both by α-helices and unordered structures in H_2O buffer; however the unordered structure shifts by about 10 cm^{-1} to lower wavenumbers upon incubation in D_2O. This can be seen by the significant increase in the fraction of 1643 cm^{-1} when the protein is in D_2O. Accordingly, the 1656 cm^{-1} component decreases from 53% to 45% under the same conditions. Therefore the data suggests that the protein actually has 45% α-helix structure in inactive state. The components at 1622 and 1693 cm^{-1} can be attributed to intermolecular β-sheet rather than side chain absorbance, since their position does not change upon H_2O to D_2O exchange. However there is significant difference in the percentage fraction of these components in different buffer media. While their sum is ~9% in H_2O buffer, it increases to ~13% in D_2O buffer. This extra 4% can be due to some side chains absorbing around 1620 cm^{-1} upon incubation in D_2O. On the other hand, protein-protein contacts could have been affected from the buffer environment as well. Another component band unaffected from deuteration in terms of signal position and percentage fraction is centered at 1631 cm^{-1}. In previous IR spectroscopy studies, 1630 cm^{-1} is mainly attributed to β-sheet and also in some cases to extended chain (Arrondo and Goni, 1999; Arrondo et al., 1988; Susi, 1969). It was explained to be the hydrogen bonding pattern formed by peptide residues with other molecular structures, e.g. intermolecular hydrogen bonding in monomer-monomer interaction or a β-sheet structure hydrogen-bonded to α-helix (Alvarez et al., 1987; Castresana et al., 1988). The fact that it occupies a fraction of ~20% makes this signal a less likely candidate for a β-sheet signal. Therefore we prefer to assign this band to intermolecular β-sheet, which originates from a different molecular group than the one giving rise to the signals at 1622 and 1693 cm^{-1}. The two different intermolecular β-sheet signals may reflect two different clusters of helix bundles or one representing helix interactions and the other monomer-monomer interactions. The fact that the percentage fraction of the signal at 1630 cm^{-1} is not affected from buffer conditions implies that the hydrogen bonding is in the hydrophobic region of the protein. The percentage fraction of

these signals correspond to 80 a.a. for the signal at 1630 cm^{-1} and 110 a.a. for the signals at 1622 and 1693 cm^{-1}. BetP has 12 transmembrane helices in the hydrophobic region, the shortest being 16 a.a. and the longest being 31 a.a. long. Therefore 4 or more helices are in close contact with one another in the WT protein either due to the close packing in one monomer unit or due to the monomer-monomer interactions.

Between the active and inactive states of the protein in D_2O, the most prominent difference is at 1656 cm^{-1} band mainly shifting to 1660 cm^{-1}, which can be assigned to loosely interacting α-helices. Therefore the presented data so far argues that the activation causes changes in α-helical parts of the protein. According to the secondary structure assignments to the IR signals, WT protein has 67% α-helix, 25% loops and 8% restricted loops/turns in inactive state and 62% α-helix, 28% loops and 9% restricted loops/turns in the active state.

The secondary structure analysis with curve fitting method has also been applied to the three mutants of this protein. The type of mutations has been explained in the Materials and Methods chapter of this study. Each mutant has been suspended in KPi-D_2O buffer without any salt and hence results represent the inactive forms of each protein. Band assignments listed in the figure caption are as described for BetP WT. The percentage fraction of each secondary structure type is color coded in Figure 3.36. Although the curve fitting method is a rough calculation of the secondary structure of a protein when compared to the methods like X-ray or NMR, here we can use the method to compare the structures of mutants with the WT protein. All mutants and the WT have around 60% α-helix structure. The structure prediction of WT protein based on the amino acid polarity yields that around 55% of the amino acids are hydrophobic and hence buried in the membrane (Peter et al., 1998). According to our calculations, all the membrane-buried parts should then be in α-helical form and an additional 5% helix should be in the hydrophilic region. The remaining parts are turns/restricted loops (~10%) and random coil structure (~25%). The intermolecular β-sheet fraction is not included in the secondary structure composition determination since the three signals identified above represent additional hydrogen bonding among secondary structures.

The BetA mutant has 29 a.a. truncation from its N-terminus. Although the truncation constitutes 5% of the protein, the α-helical part is decreased by 8% and both the coil and turns are increased by 3% and 5%, respectively. Therefore it can be assumed that the N-terminus has α-helix structure and thus, deleting almost half of this chain could have disturbed the folding motif of the remaining chain. WT protein has 60 a.a.'s in the N-terminus, corresponding to 10% of the protein. 8% loss in α-helical structure would then lead to the conclusion that the 29 a.a. truncation eliminated the α-helical structure and the remaining part of the N-terminus, having 30 a.a.'s left (corresponding to 5% of the protein), has the partially restricted random coil property based on the increase in turn structure fraction. The secondary structure composition BetA shows a good correlation with the active state of the WT protein.

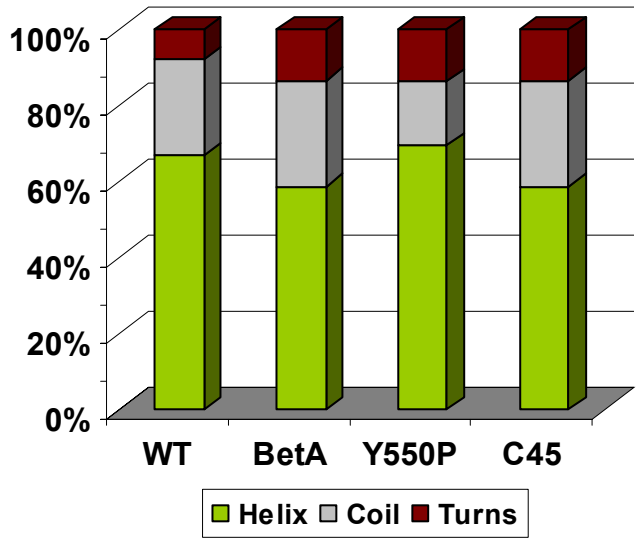

Figure 3. 36 Secondary structure analysis of BetP WT and mutants in detergent solution in inactive state in 100mM KPi-D_2O buffer. Band assignments are as follows: 1630-1648 cm^{-1} random coil; 1648-1662 cm^{-1} to α-helix; 1662-1686 cm^{-1} to turns/restricted loops.

The mutant, called Y550P, has only one amino acid replacement, i.e. the tyrosine at position 550 is replaced with proline, in order to immobilize the last 45 a.a.'s in the C-terminus. Present data suggests that while the α-helical content remains to be the same, there is an increase in turn structure and a decrease in random coil content by ~6%. Functional data confirm that Y550P mutant has the same properties as BetPΔC45, being always active

independent from the external osmolarity or internal [K^+] changes. K^+ activation of the WT protein requires a high flexibility of the C-terminus starting from the Tyr550 residue. Replacing the tyrosine with proline should abolish this flexibility and leave the protein in either active or inactive form permanently. In terms of the secondary structure composition, the mutant shows similar α-helical content to the inactive state of the WT protein, however the fraction of turns and loops are changed. This could be due to the proline replacement, where the immediate up and downstream of Pro550 are restricted, or it could also be that a possible interaction of C-terminus with a loop is also abolished due to the mutation.

The BetPΔC45 mutant lacks the last 45 a.a. from the C-terminal domain. In terms of the secondary structure composition, this mutant has 13% less α-helix structure as compared to the WT protein in inactive state. Instead, it has more turns (6%). The deleted part corresponds to ~7% in terms of the number of amino acids. The great decrease in α-helical structure leads to the idea that the deleted part has α-helix structure, similar to the results of computer calculations for structure prediction (Schiller et al., 2006); however, the increase in turn structure suggest that some loops are more restricted when the C-terminus is truncated. The C-terminus is predicted to interact with the head group of lipid molecules in the inactive state. Assuming that this is the case for activation, loosing such an interaction with membrane surface may have led to the packing differences and altered the conformation of loops.

3.3.1 Temperature Dependent Structure Stability

We have investigated the thermal stability of BetP WT both in 2D crystals and in detergent solution in order to study the structural differences between the active and inactive state of BetP. Figure 3.37 shows the amide I and II regions of the WT protein in inactive state in 2D crystals with respect to increasing temperature. Black lines represent the spectral profile of the protein from 10 °C to 40 °C, where some structural changes are seen indicated by the band shifts. From 40 °C to 105 °C, spectra are shown in red. In order to see whether the changes are reversible, we cool down the protein back to room temperature, and the

corresponding spectra are shown with blue in the figure. Amide I peak position is located at 1654 cm^{-1} at room temperature; however, as the temperature is increased, it shifts down to 1623 cm^{-1}, which is indicative of the dominating intermolecular β-sheet taken together with the band appearing at 1686 cm^{-1}. Similarly the amide II band is located at 1544 cm^{-1} at room temperature (RT) but it shifts to 1565 cm^{-1} with increasing temperature, indicating the loss of tertiary structure and as the blue spectra indicate, these changes are not reversible.

BetP has mostly α-helical structure as discussed in the previous section of this study. In order to determine the transition temperature of the protein, we have first extrapolated the amide I peak position with respect to increasing temperature. Although the amide I band is a superposition of all the secondary structure types in the protein, it mainly reflects changes in α-helical moiety. Figure 3.38 shows two graphs, each representing two different forms of the protein. Active state condition for the protein is induced by adding 800 mM KCl to BetP in 2D crystals and 400 mM KCl in the detergent solution. Active state conditions are represented by pink squares in both graphs.

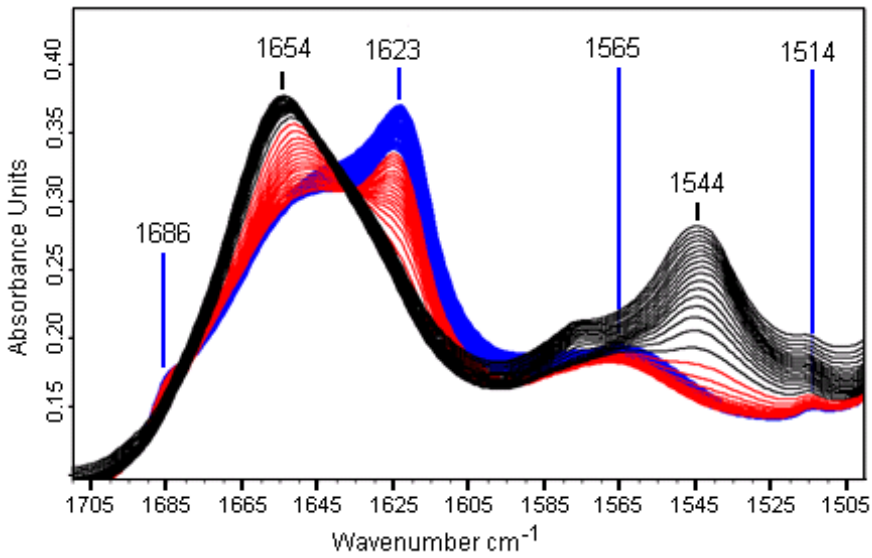

Figure 3. 37 IR absorbance spectra collected at increasing temperatures for BetP WT in detergent DDM in inactive state. Spectra are shown in black for the temperature range between RT and 40 °C; in red between 40 and 105 °C; and in blue while decreasing the temperature. from 105 °C back to RT.

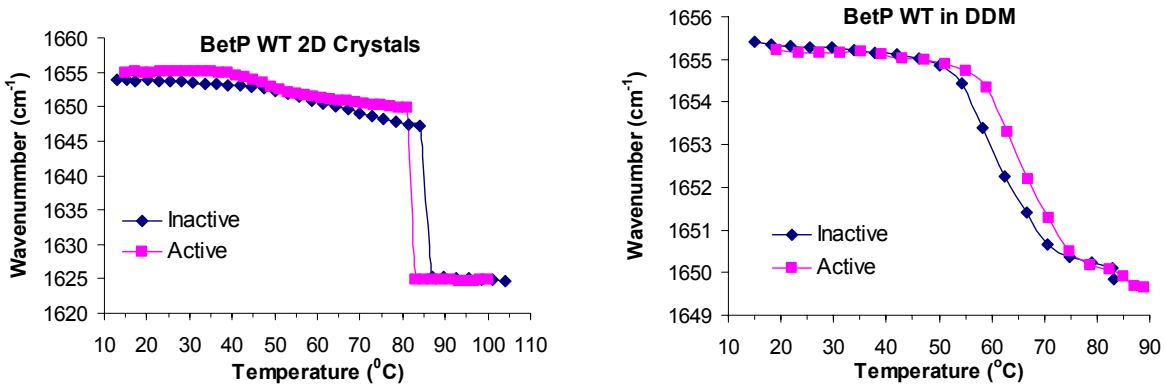

Figure 3. 38 Amide I peak position with respect to increasing temperature for BetP WT in detergent DDM and in 2D crystals for active (pink squares) and inactive (blue diamonds) states.

It is expected for almost every membrane protein to be more stable in lipid environment than in detergent micelles. BetP WT in detergent micelles has the transition temperature of 62 °C for inactive and 66 °C for the active state, respectively. In 2D crystals, these values are elevated to 85 °C and 82 °C, respectively. Lipid environment has increased the transition temperature values by around 20 °C for both states of the protein. The amide I band position for the 2D crystals stays unaffected from increasing temperature between RT and ~50 °C, above which it shows a slight and smooth downshift until the main, sharp transition (Fig. 3.38, left panel). For the same temperature range between RT and 50 °C, the protein in detergent micelles shows gradual but small shifts in peak position. After 50 °C, the main transition starts; however, the transitions are not sharp for both states for the detergent solubilized protein as compared to the protein in 2D crystals. The main transitions are completed in a temperature range of 2 °C for 2D crystals but they are distributed to almost 30 °C range for the detergent solubilized form. From the presented data we argue that the temperature induced transition of the protein starts above 50 °C for both states and forms of the protein; however since the lipid molecules provide a more protecting environment, structural changes affect firstly the hydrophilic regions and the transition can be completed only when the lipid packing is disrupted because of higher thermal energy. Although the main transition appears to be around ~80 °C in lipid environment, it starts at the same temperature value as the detergent-solubilized form of the protein. On the other hand, the initial decrease

in the amide I peak position between RT and 50 °C can be due to the dissociation of oligomeric assembly of the protein and the sharp transition at ~80 °C can be attributed to the transition of monomers. Therefore, although the monomerization starts at the same temperature values for both forms of the protein, it requires higher thermal energy for the globular structural breakdown in 2D crystals. Based on this conclusion, we argue that the oligomeric assembly of the protein is stabilized by the interaction of hydrophilic regions of each monomer. Since the cytoplasmic region of the protein is populated more by polar amino acids, an interaction of loops and termini among the monomers is more probable.

Between the active and inactive state of the protein there is only a slight difference in terms of the transition temperature values. While the inactive state is more stable in the case of 2D crystals, the active form is more stable in detergent-solubilized form. This reverse effect was also encountered when the difference spectra of activation was discussed in the previous section. In this respect the T-ramp experiments are in accordance with the activation experiments but it is still unclear why the K^+ activation causes reverse effects on different forms of the protein. It could only be that the correct conformational transition from the inactive state to the active state is undergone with a certain role of membrane surface, which can not be fulfilled by detergent micelles an therefore WT protein in detergent solution might have a different activation mechanism.

Temperature-induced structural transition of the protein can also be detected using the second derivative profie of the IR spectrum. This method allows following the changes in different secondary structure elements with respect to increasing temperature and to understand the timeline of event. We have extrapolated the negative peak positions from second derivative profile with respect to temperature from BetP WT in DDM and in 2D crystals. Figure 3.39 shows the temperature-induced changes of the signals at positions 1660 and 1680 cm^{-1}, which are attributed to helices and turns, respectively. In the case of detergent-solubilized BetP, helices show two transitions; the first is between RT and 40 °C and the second is between 60 and 75 °C. As already discussed above, BetP WT in detergent solution has the main transition between 60 and 70 °C. Hence the second transition from the

helices is indicative of the main transition of the protein. In this respect the changes in α-helical environment at rather low temperatures can be attributed to the reorganization of helices. While the signal is initially located at 1660 cm^{-1} at RT, it shifts down to 1657 cm^{-1}. Both signal positions are indicative of α-helices with different H-bond strengths (Dousseau and Pezolet, 1990). Therefore we assume that the α-helical segments undergo an organizational change. We know from our secondary structure analysis that the long C- and N-termini of the protein are in α-helical conformation. Since these parts are the first to be affected upon increasing temperature, this first transition could show the changes in the H-bond properties of α-helices in the terminals, which, in this case, can be the strengthening of the bonds based on the downshifting signal. This first transition can also be evaluated as the rearrangement of helices from the membrane-buried parts of the protein. In this respect it could be indicative of a change in oligomeric assembly of the protein.

On the other hand, the signal at 1680 cm^{-1} shows a stable profile up to 55 °C. While the signal disappears at 55 °C, another signal at ~1690 cm^{-1} replaces it, which is indicative of the structural breakdown of the protein. The temperature induced transition for turns is completed within approximately 5 °C. This sharp transition is a few degrees at lower temperature than the main transition determined from the amide I peak position. Therefore the transition starts from the turns, which are located outside the membrane. The transition of helices is seen when the temperature is further increased. This result is expected given the fact that most α-helical segments in BetP are buried in the membrane bilayer, and thus are more protected.

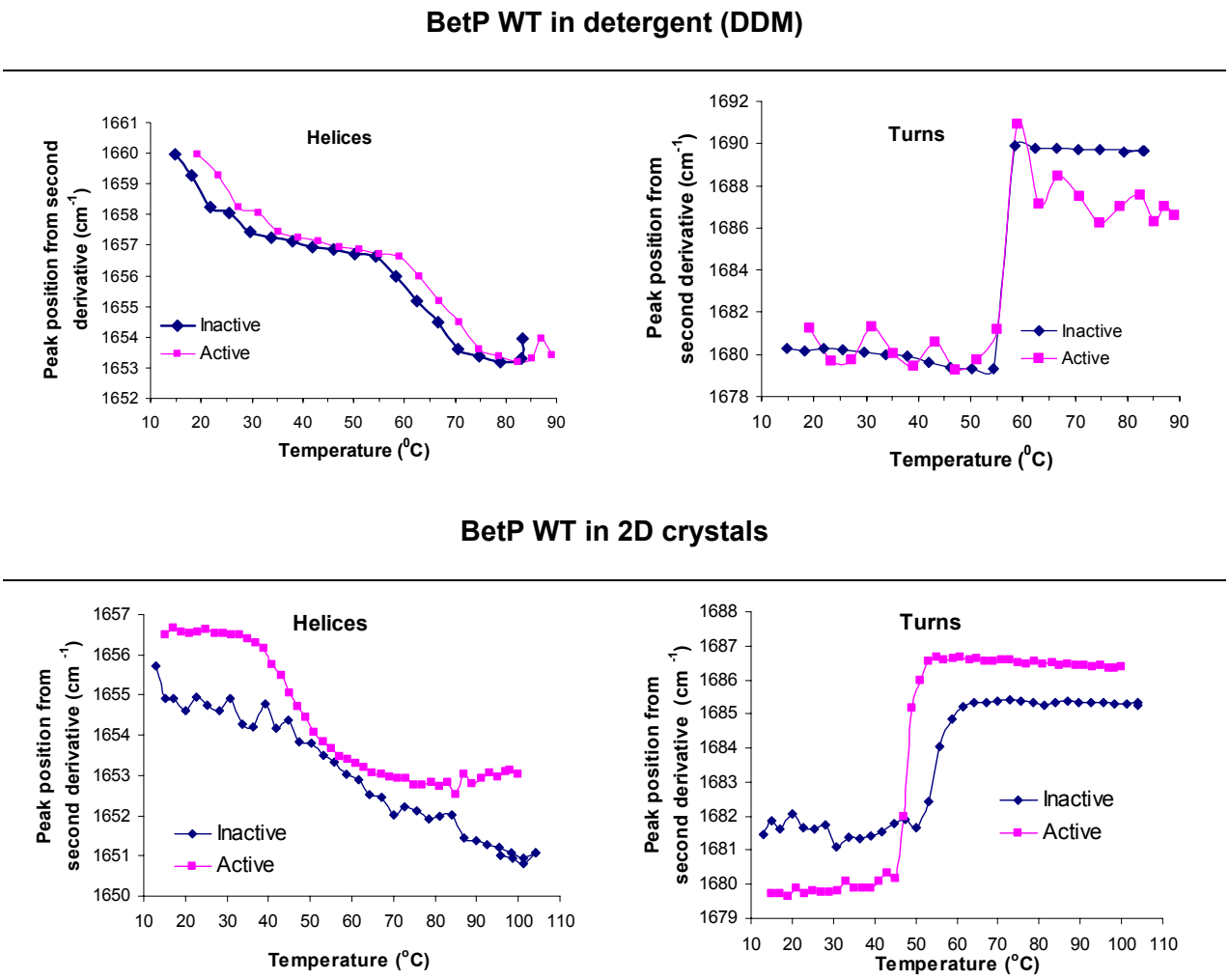

Figure 3. 39 Temperature dependent positions of the secondary sructure components at 1660 and 1680 cm^{-1} from the second derivative profiles of BetP WT in detergent solution and in 2D-crystals. 1660 cm^{-1} is assigned to helices and 1680 cm^{-1} to turns.

Although BetP in 2D crystals show very sharp transitions at around 85 °C, some small shifts in position are seen starting from 40 °C. When the 1657 cm^{-1} signal from the second derivative is plotted against the increasing temperature, both states of the protein are observed to show changes starting from 40 °C. Instead of two well-defined transitions, like in the case of detergent solubilized protein, here we see a gradual, steady shift of the signal. Since the changes start at lower temperatures as compared to the main transition, we assume that the protein is undergoing similar structural rearrangements before the main transition. However, these changes occur at higher temperature values when compared to the protein in detergent. This is also the reason for one broad transition instead of two separated ones. Since the lipid environment has elevated the first transition temperature

value, these rearrangements should involve membrane buried helices rather than the terminals. Therefore the first transition is attributed to the changes in oligomeric assembly properties of the protein, which is potentially a temperature induced-monomerization.

The transition of 1680 cm^{-1} signal occurs almost at the same temperature value for detergent-solubilized protein. Turns are located outside the membrane and hence, they are not affected by the changing lipid/detergent environment. There is, on the other hand, a slight difference between the transition temperatures of active and inactive forms. This can be an indication of different interaction of turns at the two states of the protein in 2D crystals.

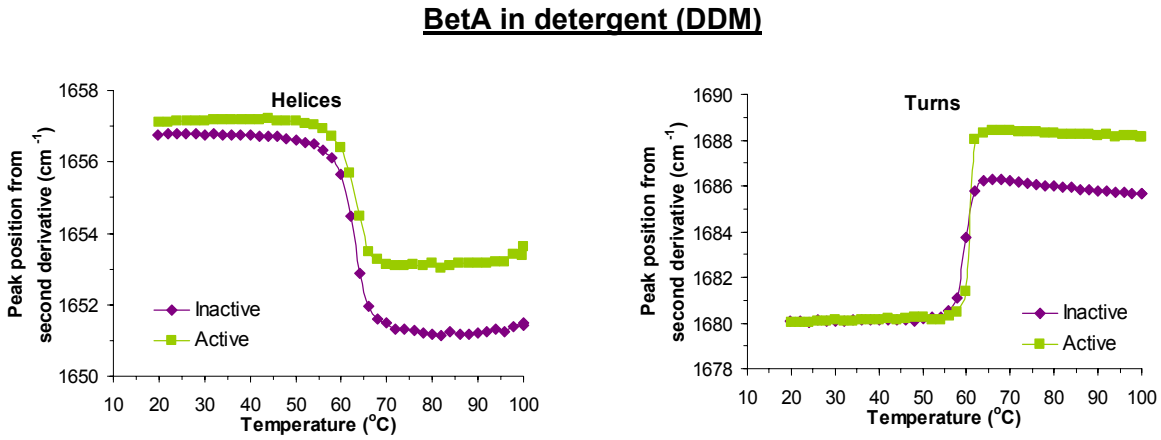

Figure 3. 40 Temperature dependent peak positions of 1657 and 1680 cm^{-1}, assigned to helices and turns, from the second derivative profile of BetA in active (green) and inactive (purple) state conditions.

The same series of experiments were also applied to the BetA mutant, which lacks the last 29 a.a. from the N-terminal domain. The detergent-solubilized protein shows the transition temperature of 62 °C for both active and inactive state conditions of the protein. The transition profile of helices is the same as the amide I profile of the protein, therefore only the second derivative readings are given in Figure 3.40. Unlike the WT protein in detergent solution, BetA shows only one transition. Therefore it is likely that the helices in BetA do not undergo the same type of changes with increasing temperature compared to the WT protein. It is also likely that the first transition in WT protein, which is due to the dissociation of

trimeric assembly, is related with the N-terminal of the protein, which is missing in this mutant.

On the other hand, although there is a slight difference between the transition temperatures of the active and inactive states of the WT protein, they are almost the same for BetA and this common transition temperature value is closer to the inactive state of the WT protein. The N-terminal domain of the BetP is involved in activation of the protein but its role in a K^+-induced activation was never tested up to now. Therefore, the slight difference between the two states of the WT protein can be attributed to the role of the N-terminal domain in thermal stability.

The transition of turns is completed just before the transition of helices for BetA for reasons explained previously for the WT protein. However, while there is ~10 °C difference between the transition values of turns and helices for WT, it is 2 °C for BetA because the transition temperature of turns is elevated by ~5 °C for BetA compared to the WT protein. BetP WT has 11 loops in hydrophilic regions. Among them are three loops that are relatively shorter, i.e. loop 6, 8 and 11 and the loops 6 and 8 are located in the intracellular region. The signal at 1680 cm^{-1} could be originating from these short loops or restricted loops due to some interactions. Our band assignment is based on the following arguments; (i) the peak position remains the same in H_2O and D_2O buffers and (ii) the transition temperature value of this signal is lower than the value of helices. The fact that turns show greater temperature stability leads to the idea that some short/restricted loops are interacting with another unit of the BetA mutant. It has been suggested for WT protein that the C-terminus interacts with the membrane surface in inactive state and shift to interact with either N-terminus or loop 8 in the active state (Ott et al., 2008). The interaction partner is either only the N-terminus or it is a simultaneous interaction with both N-terminus and loop 8 in the WT protein. Therefore the missing N-terminus could have changed the interaction of C-terminus with the loop 8. Since BetA can still be regulated, its activation mechanism is assumed to be the same as the WT protein. Therefore, although the protein still undergoes a similar cascade of electrostatic interactions during the activation, the number of bonds is limited to the amino acids of loop 8

and the C-terminus for BetA. However, it is still unclear why the turns have lower transition temperature value for active state of the WT protein, since according to the working model, it is supposed to be the interaction partner of C-terminus. We are also unable to explain why the BetA mutant in the inactive state condition is as stable as the WT protein despite of having more unordered structure according to the secondary structure analysis and thus similar to the active state of the WT protein in terms of the secondary structure composition.

3.3.2 H/D Exchange Profile of BetP

H/D exchange is a powerful method to determine the solvent-accessible regions of a protein. Using the exchange dynamics, fast exchanging protons of the protein surface, slower exchanging protons of the flexible regions buried in the protein and slowly exchanging protons from the protein core can be discriminated (Goormaghtigh et al., 1999). The advantage of the ATR perfusion microcell is that we can perform the H/D exchange for one state of the protein (e.g. inactive state) and switch to another state (e.g. the active state) in order to see the structural components revealed only in the second state.

BetP WT in detergent solution has been incubated first in the inactive state in H_2O buffer. Then the perfusion system is changed to the same buffer prepared in D_2O. The corresponding spectra in H_2O and D_2O are shown in Figure 3.41, with blue and black lines respectively. It is expected that the hydrophilic regions of the protein will exchange with D_2O rather rapidly while the remaining parts either will exchange at a much slower rate or will not be affected from the changing buffer conditions. Under the amide I region, an overall band shift is clearly visible due to the exchanging secondary structure components and side chains. The amide II region is the main area used to determine the degree of exchange. It is also evident from the figure that the intensity of the band at 1547 cm^{-1} decreases and the band at 1455 cm^{-1} increases upon exchange. However, when 500 mM KCl is added to the buffer for activation, there is no further significant exchange, as seen by the red line representing the active state of the protein.

In order to observe the changes during the H/D exchange for the first 3 hours, each spectrum taken within this time interval was subtracted from the protein spectrum incubated in H_2O.

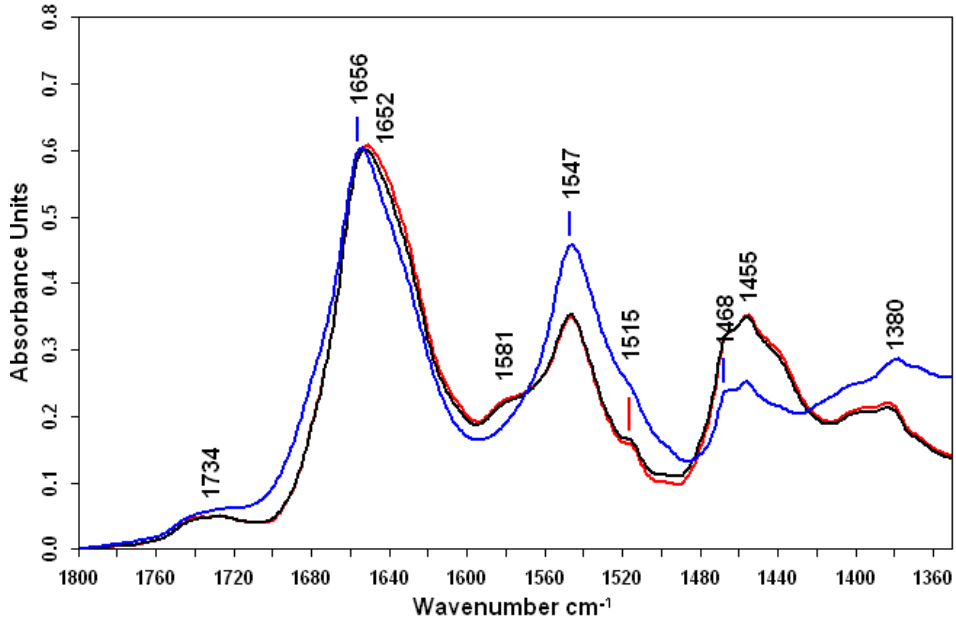

Figure 3. 41 IR absorption spectrum of BetP WT in detergent DDM, in 100 mM KPi pH 7.5-H_2O buffer (blue line); in D_2O buffer pD 7.5 (black line); in D_2O buffer pD 7.5 with 500 mM KCl (red line).

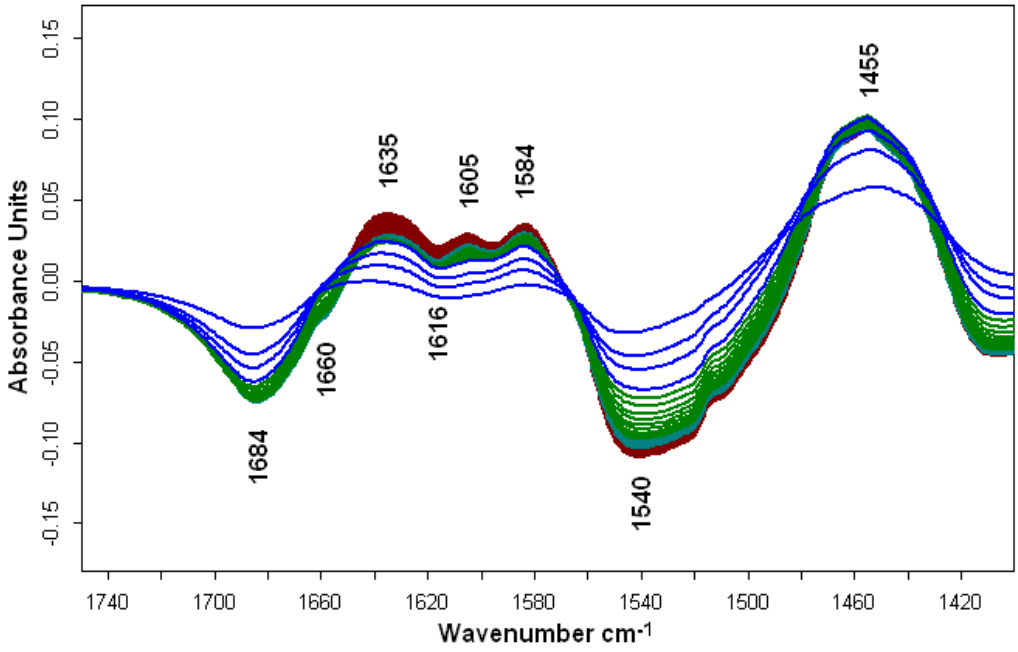

Figure 3. 42 Difference spectra of H/D exchange in inactive state of BetP WT in detergent DDM. The spectrum in H_2O buffer is taken as the reference for the difference spectra shown. Blue lines represent the first 10 min of the experiment. Time evolution of the exchange is represented by green, turquoise and red lines. Positive peaks represent the signal appearing after the exchange.

The resultant difference spectra are shown in Figure 3.42, where the negative peaks indicate the disappearing components and the positive peaks indicate the components appearing with D_2O. The main difference in the figure is the shift of 1540 cm^{-1} band to 1455 cm^{-1} due to the exchanging NH bending mode from the protein backbone. On the other hand, the bands located at 1684 cm^{-1} and 1660 cm^{-1} decrease in absorbance and 1635, 1605 and 1584 cm^{-1} arise during the exchange. Based on our secondary structure analysis, the 1680 cm^{-1} region has been attributed to turns and the 1660 cm^{-1} region to α-helix and random coil in H_2O. It is known from many previous studies that α-helix only shifts by a few wavenumbers in absorption frequency upon H/D exchange; however, random coil shifts down by about 10-15 cm^{-1} (Goormaghtigh et al., 1994b). Therefore the negative peak at 1660 cm^{-1} in the difference spectra represents the random coil structure located at the exterior regions of the protein.

Similarly, the turns absorb in the same wavenumber region, ~1680 cm^{-1}, of the amide I band in both H_2O and D_2O buffers. Thus, the negative peak at 1684 cm^{-1} is attributed to the asymmetric stretching mode of arginine, which is expected to shift down to ~1608 cm^{-1} in heavy water (Chirgadze et al., 1975). Thus, the positive peak at 1605 cm^{-1} corresponds to the exchanged arginine. The symmetric stretching mode of this residue is located at ~1635 cm^{-1} in H_2O and at ~1586 cm^{-1} in D_2O. In our difference spectra, due to the coil structure shifting from 1660 cm^{-1} down to ~1640 cm^{-1}, such a negative peak due to exchanging arginine residues is not observed but the positive peak at 1584 cm^{-1} is clearly distinguished. BetP has 23 a.a. in the exterior part of the membrane and 22 of them are located in the intracellular region. Hence it is reasonable to see the shift of this residue upon exchange.

In order to see the differences between the active and inactive states, 500 mM KCl is added to the D_2O buffer. The difference of these two states is shown in Figure 3.43, where the positive peaks represent the structural elements appearing in the active state. A slight further exchange is seen from the overall negativity in the amide II region. Thus, it is reasonable to argue that the membrane-buried parts are still shielded in the active state of the WT protein.

There are also random coil structures exchanged with activation of the protein, shifting from 1661 cm^{-1} down to 1638 cm^{-1}. The positive peak at 1632 cm^{-1} has been attributed to extended chain previously in the secondary structure analysis. This signal is due to the interacting helix bundles either in a single monomer or among the monomers. Therefore, the changes in the band intensity/position can be used to probe changes in protein packing differences. Thus, a positive signal with activation reflects a change in protein packing upon activation.

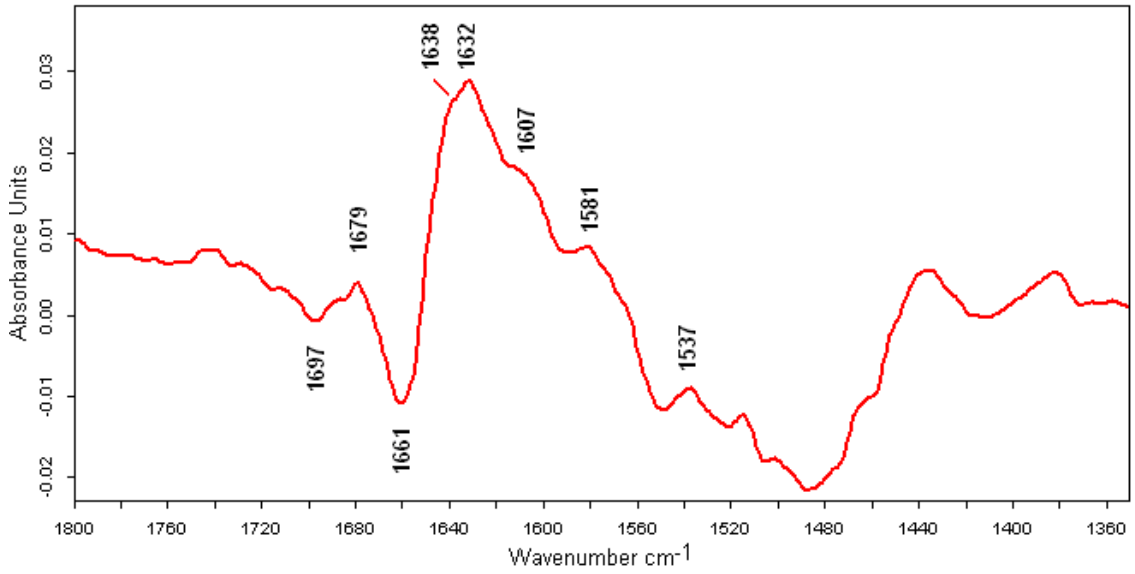

Figure 3. 43 Difference spectra of BetP WT activation in detergent solution in D_2O buffer, calculated as active *minus* inactive.

In order to resolve the overlapping bands, the spectra of active and inactive states have been deconvoluted using the Fourier self deconvolution. Deconvoluted absorbance spectra and the difference of the two states are shown in Figure 3.44. Although the deconvoluted absorbance spectra show the same secondary structure components in both states, difference spectra show differences especially in α-helix moiety as shown by the negative peak at 1657 cm^{-1}, which was not evident from the raw spectra. As a general rule, a sharp inclined line in a difference spectrum indicates the shift of components to nearby wavenumbers, as for the case of 1657 cm^{-1} band shifting down to 1650 cm^{-1}. These two positions can be evaluated as the different conformational properties of the helices upon activation of the protein. It has been suggested previously that helices having different

positions or lengths within the membrane absorb at slightly different wavenumbers (Dousseau and Pezolet, 1990; Mukherjee et al., 2007; Turner and Kubelka, 2007; Van Wart and Scheraga, 1978). Helices located at lower wavenumber regions have been attributed to the short and/or hydrated helices having stronger backbone hydrogen bonding properties. Although the helices in BetP are mostly within the membrane, it is predicted that N- and C-termini are also in α-helical conformation and directly accessible by solution (Schiller et al., 2006). Therefore such a band shift from 1657 cm^{-1} to 1650 cm^{-1} represents helical regions exposed to buffer solution upon activation. Although the termini domains are in the cytoplasmic region and hence exposed to solution, they are predicted to interact with other units of the protein in the inactive state. Upon activation, these domains could be forming hydrogen bonds with water molecules. It could also be that some membrane buried parts are exposed to solution by a conformational change.

The negative peak at 1685 cm^{-1} is shifted down to 1678 cm^{-1} upon activation. In the H/D exchange kinetics of the protein in the inactive state, 1684 cm^{-1} has been attributed to the exchanging arginine residues. However, as the deconvolved difference spectra suggests, this signal shifts by 7 cm^{-1}, which makes it a more likely candidate for turns, having different conformations or binding properties at different states of the protein. On the other hand, the negative signal at 1673 cm^{-1} can be attributed to the arginine residues that are exposed to D_2O only in the active state of the protein, since the positive peaks at 1607 and 1581 cm^{-1} indicate the exchanged asymmetric and symmetric stretching mode of arginine, respectively. The band position difference between the arginine modes in the active and inactive states could be evaluated as the different status of the residues. They give rise to a band at 1684 cm^{-1} in inactive state and 1673 cm^{-1} in the active state. It might be that the differences in binding properties of the $-N^+H_2$ group cause different vibrational frequencies. Until now, there is no study that shows the spectral differences between bound and free modes of arginine. On the other hand, it is known that arginine mode shows variances in peak position among different proteins (Berendzen and Braunstein, 1990; Chirgadze et al., 1975; Ortiz et al., 2005). We argue that the exchanging arginine residues in the inactive state are the

noninteracting ones and hence are located in the higher wavenumber values. Therefore the lower wavenumber value corresponds to the interacting residues in the inactive state and deuterated in switching to the active state.

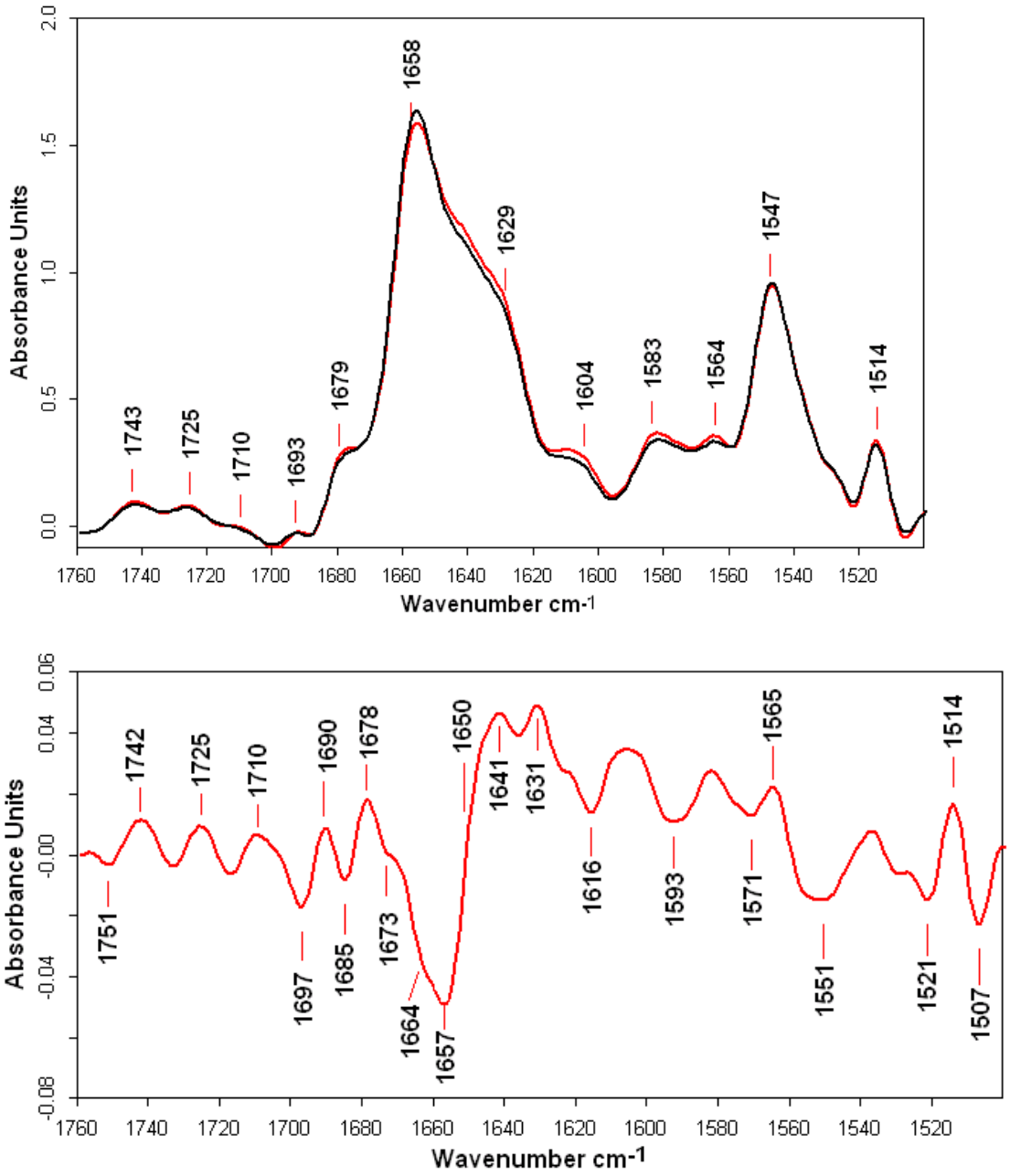

Figure 3. 44 Fourier self deconvolution applied to the active (red) and inactive (black) states of detergent solubilized BetP WT with Lorentzian band shape with 0.2 noise reduction factor and 25 cm^{-1} bandwidth. The difference spectrum in the lower box is calculated as active *minus* inactive from the deconvoluted spectra.

The negative peak at 1697 cm^{-1} and 1624 cm^{-1}, which appears only as a shoulder on 1616 cm^{-1} signal, and the positive peak at 1631 cm^{-1} are attributed to intermolecular β-sheet that can be used to extract information about the helix-helix contacts. The shift of the signal to a higher wavenumber could imply the loosening of such contacts upon activation of the protein.

Signals at 1616 and 1515 cm^{-1} in general can be due to the tyrosines; C=C stretching from the aromatic ring ending with an OH group (Venyaminov and Kalnin, 1990a). Hydrogen bonding of the hydroxyl group leads to the frequency shifts of the C=C stretching from 1616 to ~1603 cm^{-1} and 1518 to ~1500 cm^{-1}. BetP WT deconvoluted difference spectrum shows a negative peak at 1616 cm^{-1} shifting down to 1605 cm^{-1} and at 1521 cm^{-1} shifting down to 1514 cm^{-1} indicating changes around tyrosine environment. The positive 1605 cm^{-1} peak has also been attributed to the arginine mode. This peak is quite broad even after deconvolution and since the 1616 cm^{-1} can only shift by ~15 cm^{-1}, we assume that 1605 cm^{-1} band is the superposition of tyrosine and arginine modes in the active state. However, the new peak positions for tyrosine do not match with the position of hydrogen bonded tyrosine mode. Therefore these signals still represent the hydroxyl group attached to the aromatic ring but due to the changing environment they show small shifts due to different bond lengths. Downshifting of this signal represents a shorter bond length between C=C from the C-ring and O from the hydroxyl group. This could be due to an orientation change of the residue upon activation. There are 9 tyrosines in total and 4 of them are located in the transmembrane region of the protein, in helix-3, -4, and -8. The remaining five residues are at positions 171 (loop 3), 304 (loop 6), 340 (loop 7), 550 and 553 (C-terminus). The absorption intensity of the 1605 cm^{-1} peak is 0.02 in the difference spectrum presented in Fig. 3.43. As discussed previously, it roughly corresponds to 1 residue. Thus, it is possible to argue that activation causes an orientational change in one of the tyrosine residues. In previous studies, the role of C-terminus was found to depend on the correct folding and flexibility of the chain starting from Tyr550. Therefore the spectral change we observe could

be due to the Tyr550, having different side chain orientations in different states of the WT protein.

Deconvoluted difference spectra also enable us to see the differences in the C=O groups between the 1750 and 1700 cm^{-1} region. These reflect either the changes in the lipid interfacial region of the membrane or they belong to the C=O groups of aspartic or glutamic acid, or a combination of both. A series of positive and negative peaks indicate that upon activation, C=O groups are changing their hydrogen bonding properties. It is quite reasonable that negatively charged amino acids are involved in the activation process since BetP has 41 negatively charged a.a. on the exterior region of the membrane and 29 of them are located in the intracellular region. The N-terminus sequence contains 15 Asp and Glu residues, and as discussed in the previous section, N-terminus and/or loops bind to the C-terminus via these residues. This interaction is satisfied by the positive and negatively charged residues among the interaction partners. It has also been proposed as the working model for BetP that a positively charged C-terminus interacts with the negatively charged head group of surrounding lipid molecules in the inactive state. This binding property of the lipid head groups may change the hydration status of the interfacial region of the lipid molecules, which would also indirectly be an indicator for BetP activation of the protein. In either of the states, the C-terminus causes changes in the hydration status of C=O groups from different hosts. Therefore at this point, we are not able to distinguish between different interaction partners.

We have also performed the H/D exchange experiments and activation in D_2O buffer on BetA. Protein spectra in the inactive state in H_2O buffer and in D_2O buffer are shown with blue and purple lines in Figure 3.45, respectively. The activation conditions are satisfied by adding 700 mM KCl to the D_2O buffer and the corresponding spectrum is shown with the pink line. Between the active and inactive state conditions, there is only a slight further exchange with D_2O, as seen from the amide II absorbance value. The band at 1582 cm^{-1} is, however, increased in absorbance, which we attributed to arginine residues. The difference of the active and inactive states is shown in Figure 3.46, where the positive peaks correspond to

the mutant in the active state condition. BetA and BetP WT undergoes similar changes when the buffer is switched to D_2O (Fig. 3.43 & 3.46). Random coil structure shifts down from 1660 cm^{-1} to 1640 cm^{-1} and it is also possible to see the shift of arginine signals at almost the same positions as compared to the WT protein. This is quite expected since the truncation from the N-terminal domain did not affect the number of arginine residues.

Comparison of BetP WT with BetA from the difference of deconvoluted spectra shows that both proteins undergo similar structural changes upon activation (Fig. 3.47 & 3.44). Deconvoluted WT difference spectra allow discriminating between the α-helical structure and random coil by resolving the broad band at 1660 cm^{-1}. Instead for BetA, there is only one single negative peak at 1660 cm^{-1} even after the deconvolution. However, the positive peaks at 1670, 1649 and 1644 cm^{-1} are better distinguished. Interestingly the absorbance value of the band at 1639 cm^{-1} is twice the same band in the corresponding spectra of WT, which means that BetA has more random coil in its structure. The same conclusion was drawn from the secondary structure analysis for BetA in inactive state and it has been discussed that the truncation could have affected the structure of the remaining N-terminus. Activation of BetA in D_2O buffer confirms that this mutant has more random coil.

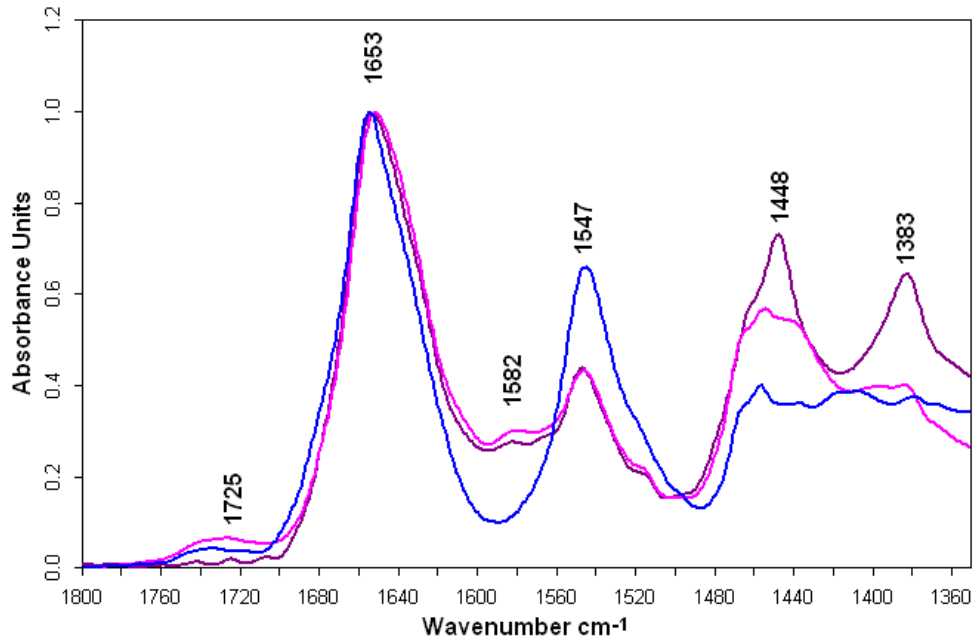

Figure 3. 45 BetA in detergent DDM in 100 mM KPi pH7.5 H_2O buffer (blue); in D_2O buffer (purple); and in D_2O buffer with 700 mM KCl (pink).

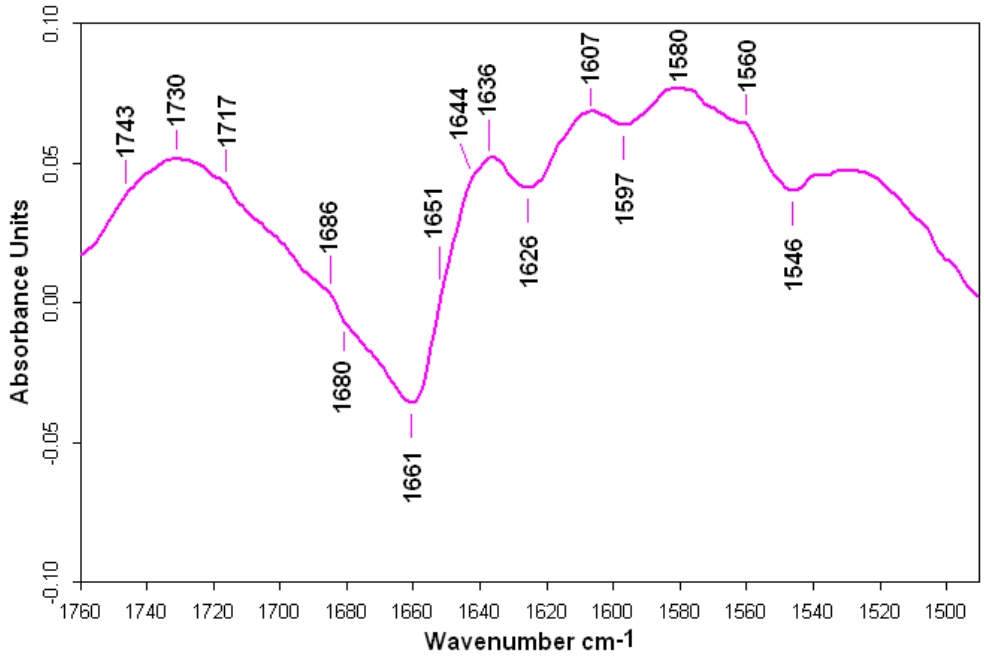

Figure 3. 46 Difference spectrum of BetA in D_2O buffer calculated as active state *minus* inactive state.

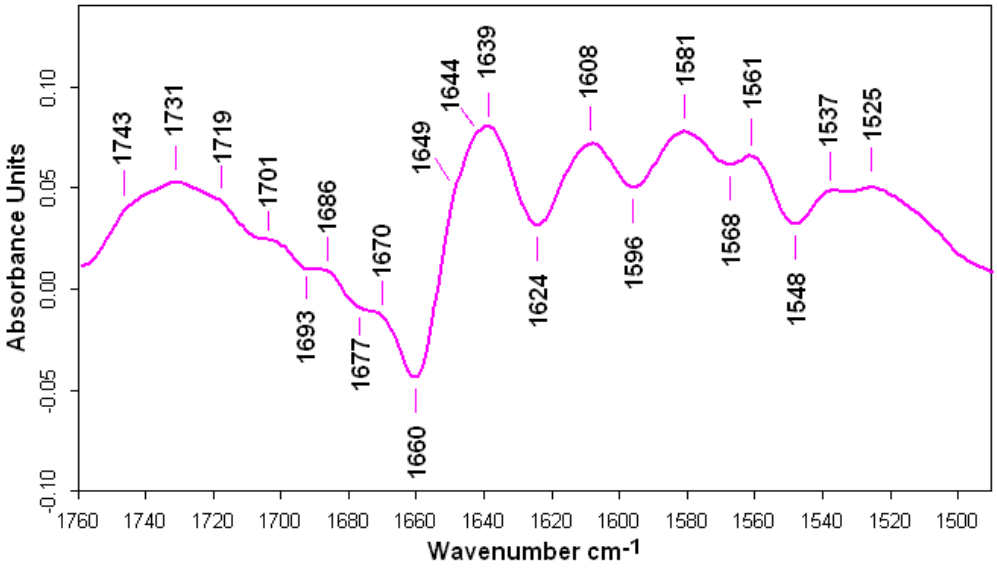

Figure 3. 47 Difference spectrum of deconvoluted absorbance spectra. Deconvolution is performed with Lorentzian band shape with 25 cm^{-1} bandwidth and 0.2 noise reduction factor.

The negative peak at 1673 cm^{-1} is attributed to the arginine signal in H_2O buffer in the analysis of the WT protein. The position of this signal is slightly different for BetA; being at 1677 cm^{-1}. However, the positive peaks at 1608 and 1581 cm^{-1} are the positions for deuterated arginine. Hence, there are some arginine residues that are shielded in the inactive state and only accessible by solution in the active state, which is also the conclusion

for the WT protein. The negative peak at 1624 cm^{-1}, however, is broader in the case of BetA as compared to WT protein. In the same spectral region, WT protein has also the negative 1616 cm^{-1} band due to the changing tyrosine aromatic ring C=C mode differences in the two states of the protein, overlapping with 1624 cm^{-1} signal. Signals at 1693 and 1624 cm^{-1} are attributed to the extended chain for WT. The negative peaks would then correspond to the changing hydrogen bonding properties among helices or monomers upon activation. However, the tyrosine signal, which is supposed to appear at 1616 cm^{-1}, is not well resolved in the deconvoluted difference spectrum of BetA as compared to the WT protein. On the other hand the broad positive peak at 1608 cm^{-1} enables us to conclude that it is actually a superposition of tyrosine and arginine modes and that the negative tyrosine signal actually overlaps with the broad 1624 cm^{-1} signal and thus, the activation leads to similar changes around tyrosine for BetA with the WT protein. However, the intensity of the 1608 cm^{-1} signal is three times higher than the corresponding signal for the WT protein. Since the signal is a superposition of the two residues, either the number of arginines or the tyrosine is increased that are deuterated in the active state.

Another interesting point is the missing signals for the turns for BetA. Fig. 3.44 for WT protein revealed changes in turns upon activation indicated by the shift of the band at 1685 cm^{-1} down to 1678 cm^{-1}; however BetA does not show such a change. It could be concluded that the changes in turns are related with the N-terminus, since the truncation has abolished the corresponding signal.

There are also changes in the C=O environment either from lipid interfacial region or from negatively charged amino acids. Signal positions are slightly different for BetA as compared to the WT protein. During the perfusion cell experiment of the inactive state of BetA, a higher amount of lipid molecules were washed away with the circulating buffer and may cause a broad band in the spectral region 1750-1700 cm^{-1}. However, the peaks are still well distinguished from the difference spectrum. The signal at 1743 cm^{-1} is common for both WT and BetA. However, the bands at 1725 and 1710 cm^{-1} in the WT protein are shifted to 1731 and 1719 cm^{-1} for BetA. Since BetA lacks 5 negatively charged amino acids due to the N-

terminus truncation, it would be expected to see differences in the peak positions. Therefore, it confirms that the changing signals represent the contribution of these negatively charged amino acids. Overall, there are still two possibilities for the source of these peaks; either from the negatively charged amino acids in mainly the intracellular region of the protein or from the surrounding lipid molecules.

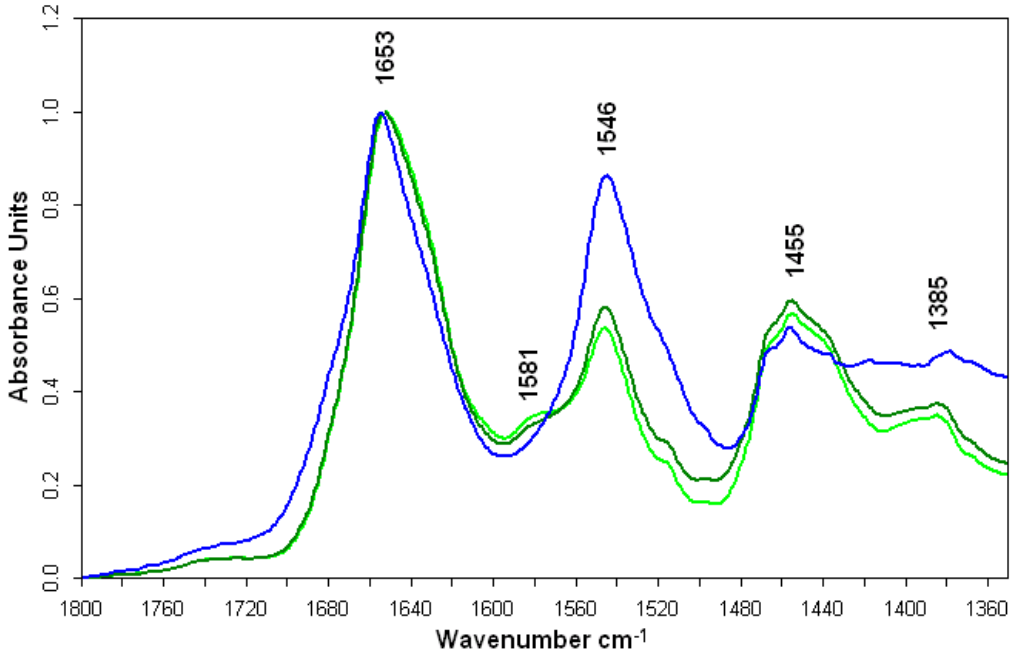

Figure 3. 48 IR absorbance spectra of BetPΔC45 mutant in 100 mM Kpi pH7.5 buffer in H_2O (blue); in D_2O (dark green); in D_2O with 500 mM KCl (light green).

The H/D exchange experiment was performed on BetPΔC45 in the inactive state condition, where both H_2O and D_2O buffers were free of excess K^+. The active state condition was, then, satisfied by adding 500mM KCl in the perfusing D_2O buffer. The comparison of absorbance spectra, corresponding to the active and inactive state conditions, revealed fewer differences as compared to both the WT protein and BetA. As shown in Figure 3.48, the active and inactive states almost exactly match in the amide I region, however the H/D exchange rates slightly differ between them.

The difference spectrum between the active and inactive states, nevertheless, shows the same characteristic differences with the WT protein as shown in Figure 3.49. The shift of the band at 1661 cm^{-1} to 1639 cm^{-1} is due to the random coil structure accessed by D_2O buffer when the active state condition is induced. The positive peak at 1582 cm^{-1} is due to the

deuterated arginine residues; however the absorbance is less than half of the absorbances in WT and BetA. The last 45 amino acids that are truncated rom the C-terminus include 14 Arg residues, which is two-third of the total number in the intracellular region. Therefore the signal should be originating from the residues located in the cytoplasmic region of the protein.

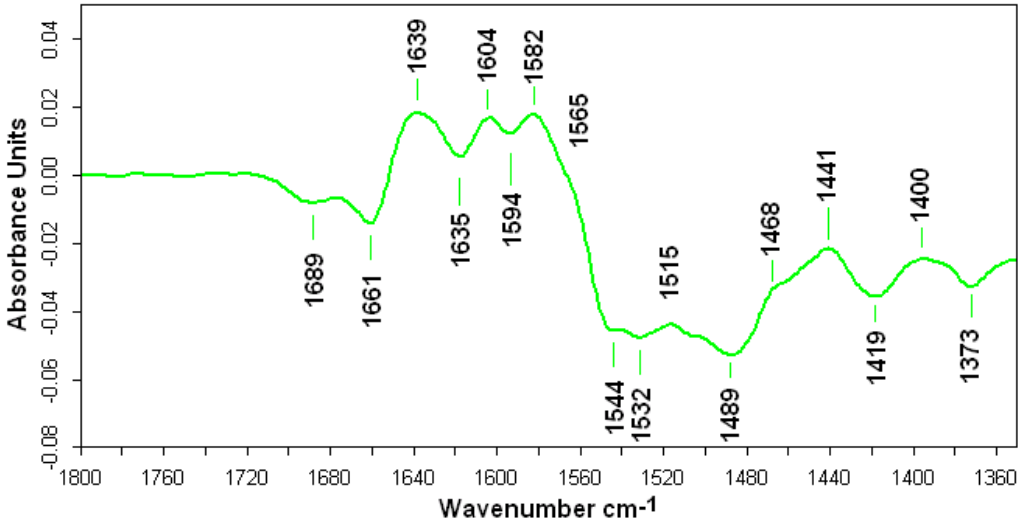

Figure 3. 49 Difference spectrum of BetPΔC45 in 100 mM KPi in D_2O buffer. Absorbance spectra corresponding to active and inactive states are normalized in the amide I range and that the inactive state is one-to-one subtracted from the active state.

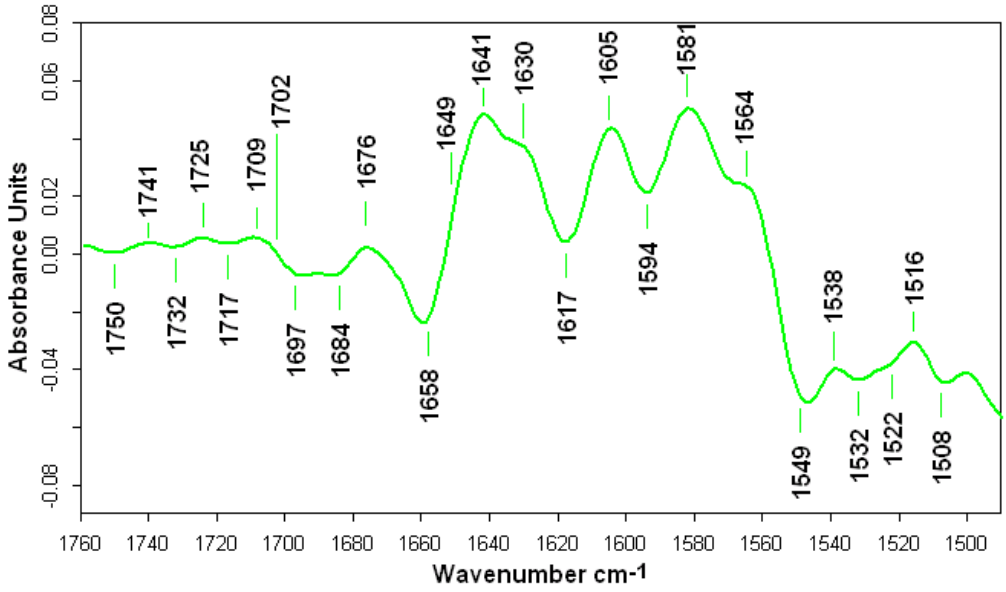

Figure 3. 50 Difference spectrum of deconvoluted active and inactive spectra. Absorbance spectra are deconvoluted as described in Materials and Methods. The spectrum corresponding to the inactive state is one-to-one subtracted from the spectrum of the active state.

In order to resolve the broad bands, the spectra corresponding to the active and inactive state are deconvoluted and the difference is calculated as active-*minus*-inactive and the result is shown in Figure 3.50. The signal at 1624 cm^{-1} has been attributed to extended chain in the corresponding spectra of WT and BetA, which gives a negative signal during the activation of protein. For the BetP∆C45 mutant, this signal is only a slight shoulder on the negative 1617 cm^{-1} peak. Apparently a certain change in intermolecular hydrogen bonding properties is required in order to become active for the protein. A shift to higher wavenumbers is observed for WT and the two mutants; indicating relatively poorly interacting helices upon activation. According to the working model of BetP activation, the C-terminus is detached from the lipid headgroups in the vicinity of excess K^+ resulting in a conformational change of the C-terminus, which could affect some individual or a group of membrane-buried helices. However this model is not valid for BetP∆C45 mutant since it is no longer sensitive to changes in K^+ concentration. Therefore the conformational changes should be triggered by another stimulus like the N-terminus or the electrostatic interactions due to increased polarity in the buffer. On the other hand, there are also changes in the tyrosine environment, represented by the shift of 1617 to 1605 cm^{-1} and 1522 to 1516 cm^{-1}. This has also been evaluated as the orientational change of one tyrosine residue, based on the absorption intensity, probably due to the Tyr550 in the C-terminus.

The negative band at 1684 cm^{-1} shifting down to 1676 cm^{-1} indicates changes in the turns in the vicinity of excess K^+. In the case of WT protein, the signals are located at 1685 and 1678 cm^{-1}. This signal is missing in the case of BetA, therefore we can conclude that excess K+ causes changes in the interaction of N-terminus with the turns. In the 1750-1700 cm^{-1} region, the signal positions are exactly the same as for the WT protein signals. However the absorbance values of all the signals are relatively smaller compared to the WT protein. Since the number of arginine residues is the main difference with this mutant, the signals originate from hydrogen bonding among arginines and C=O group of the negatively charged amino acids. When the 45 amino acids are truncated from the C-terminal domain, there are no other arginine residues left to interact with the membrane surface. Therefore the present data

suggest that the remaining 8 residues scattered in the loops located at the intracellular region of the protein are also taking part in the activation by interacting with Asp or Glu in the N-terminus (Fig. 3.51). This conclusion may, however, be only valid for the case of C-terminus truncated mutants to compensate for the missing arginines.

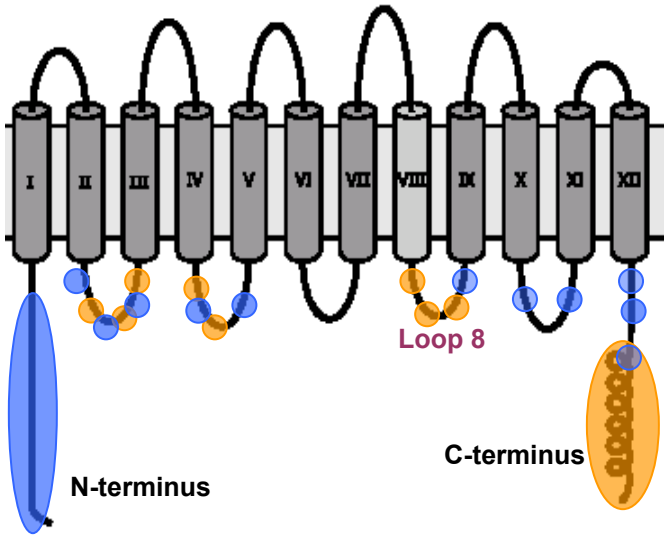

Figure 3. 51 Schematics of BetP WT (reproduced from Morbach and Kramer, 2005). Negatively charged amino acids (Asp and Glu) are shown with blue circles and arginines are shown with orange circles. N-terminus has an overall negative charge due to 12 Asp/Glu and does not include any Arg residues. C-terminus has 14 Arg and 8 Asp/Glu. Loop 8 has 3 Arg and 1 Glu.

H/D Exchange Rates

The rate of exchange with D_2O-buffer has been calculated as described in Materials and Methods chapter. All proteins are initially incubated in 100 mM KPi-H_2O buffer in the inactive state. The external parameters such as the pump speed, buffer volume, diameter of tubings and temperature of sample compartment were kept constant for all the experiments (see Materials and Methods). The graph on the left in Figure 3.53 shows the time rate of exchange with D_2O-buffer for the first three hours. All proteins were subject to D_2O-buffer for 24 hours to ensure the maximal exchange. The beginning of the experiment was set to zero time where the protein is in H_2O-buffer. After the D_2O-buffer is introduced to the protein, the amide II mode in the spectrum shifts down by ~100 cm^{-1} as explained previously and thus, the amide II/I ratio decreases as the exchange rate with D_2O increases. We then calculate the percentage of exchange in order to observe the kinetics with respect to time.

BetP WT has a total exchange rate of 43% in inactive state, i.e. 43% of the amino acids are readily accessible by D_2O buffer. From the 595 amino acids, 279 of them are in the hydrophilic regions of the protein, which corresponds to ~47% of the total number. Therefore almost all the amino acids in this region are accessed by the buffer solution. It is interesting to note that the maximal exchange is almost complete within the first hour of the experiment and BetPΔC45 has the same kinetics and exchange rate with WT protein although 7% of the protein is truncated. A possible explanation could be that the truncation has led some of the membrane buried parts to be exposed to solution or the truncated region does not exchange. It is also seen from the chart in Figure 3.52 that the active state of BetPΔC45 exchanges 5% more as compared to the WT protein in active state. In the vicinity of excess K^+, electrostatic interactions may have caused a further exchange since we know that the C-terminus truncated mutant is not able to sense the presence of K^+. BetA, on the other hand, exhibits

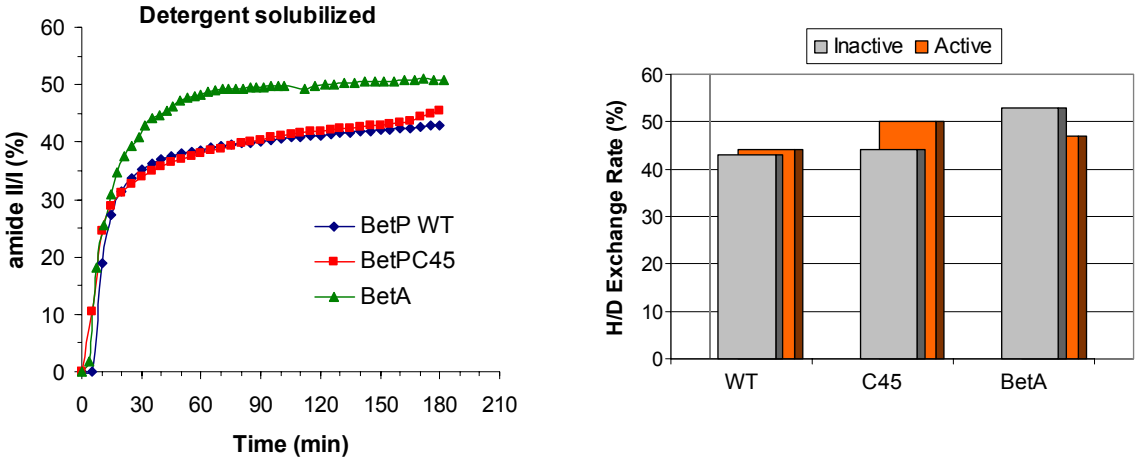

Figure 3. 52 H/D exchange kinetics of BetP WT, BetA and BetPΔC45 in the inactive state condition for the first three hours (left panel). Total exchange rates are shown on the right by grey and orange blocks, representing the inactive and active state conditions, respectively.

the highest exchange rate as compared to the others in inactive state. The exchange kinetics is very similar to the others. This fact is also in accordance with our previous conclusions that BetA has more random coil structure that are accessible to buffer. When we started with the inactive state of BetA and added KCl to the perfusing buffer in order to activate the protein, we did not see further exchange with D_2O buffer. In a separate experiment, the protein is first

incubated in H_2O-buffer with active state condition and then the buffer is changed to D_2O. The result is shown in the chart in Figure 3.52, right panel. Surprisingly, BetA in the active state condition is less accessible by the buffer and the degree of exchange is in the order of the active state of the WT protein. When we performed the same reverse-order experiment, i.e. switching from the active to inactive state conditions, for WT and BetPΔC45, we found the same exchange rate between the active and inactive states. Therefore, based on the present data, the active state of WT protein and BetPΔC45 mutant is more open to solution with respect to their inactive states; however the opposite is true for BetA. BetA can retain the fully active form although the 29 a.a. are truncated from the N-terminus in proteoliposomes but in the inactive state the protein is more unordered in structure due to the missing amino acids. The secondary structure analysis revealed that BetA has 8% less α-helical structure as compared to the WT protein in the inactive state conditions and H/D exchange experiments show 10% higher accesbility for BetA. Therefore the higher exchange rate is due to the unordered structure induced by the N-terminus truncation. The decreased exchange rate in the active state conditions suggests that BetA forms hydrogen bonds in the hydrophilic regions, so that there are fewer protons accessible by the buffer solution in the active state conditions. A possible interaction would be among the loops and the C-terminus; however it is not known whether BetA can be activated by excess K^+ in detergent solution. Nevertheless we argue that BetA attains different conformations in the presence and absence of K^+ ions.

It could be that the N-terminus interacts with loops either from its own monomer or from another monomer in the inactive state for BetP WT (Fig. 3.53). This argument is supported by the deconvoluted difference spectra of the WT protein and the two mutans discussed in the previous section. Data showed that there are changes in the hydrogen bonding properties of turns in the vicinity of excess K^+ for the WT protein and BetPΔC45 mutant but not for BetA. Thus, when 29 a.a. are truncated from the N-terminus, the interaction partner loop is left free in the inactive state, which in turn provides more protons to be exchanged in D_2O-buffer. Since BetA exchanges less in the active state conditions, there is less number of

protons available for deuteration, which would imply an interaction in the hydrophilic region in the active state conditions, which is probably among the C-terminus and the loops as suggested by previous studies (Ott et al., 2008). Although the presented data can be explained by such a scenario, it may not necessarily be the case for the WT protein.

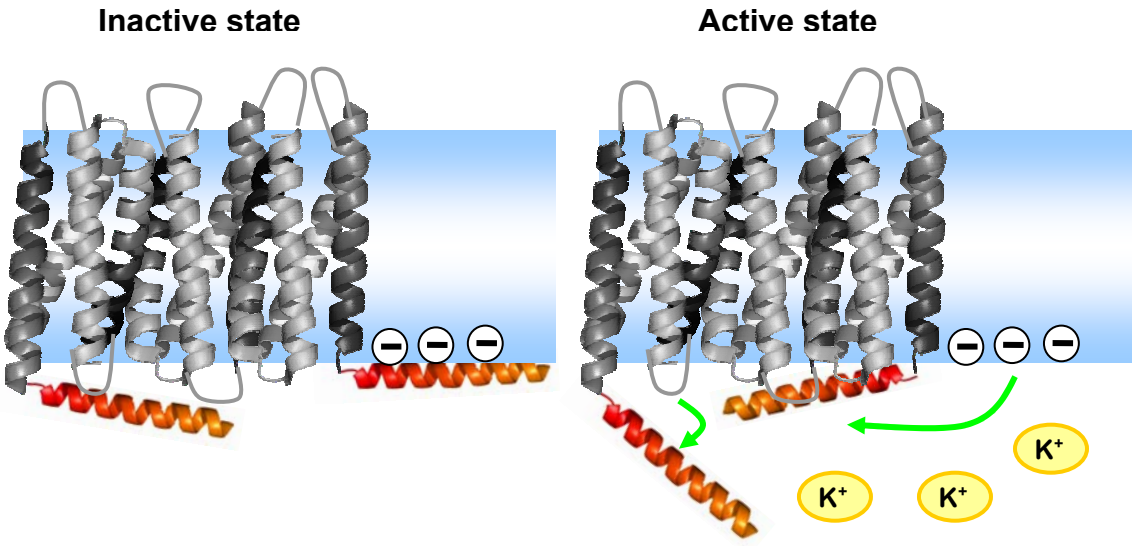

Figure 3. 53 Schematics of the proposed activation mechanism for BetP WT. In the inactive state, the C-terminus interacts with the negativelycharged headgroups of lipid molecules and the N-terminus interacts with the loops. In the vicinity of excess K+, both termini are detached and the C-terminus forms hydrogen bonds with cytoplasmic loops.

4. CONCLUSION

This study addresses the structure-function relationships of three essential membrane proteins: Porin from *Paracoccus denitrificans*, Porin OmpG from *Eschericia coli* and BetP from *Corynobacterium glutamicum* using Fourier transform infrared (FT-IR) spectroscopy and Attenuated Total Reflection (ATR) techniques.

The structure of porin from *P. denitrificans* is known for more than a decade; however, the mechanism for loss of functionality together with the monomerization was not clear. In this study we have addressed the role of lipids for the functionality of porin using FT-IR. OmpF porin was found to interact with the lipid molecules via the aromatic girdles surrounding the protein for functionality. In this study, molecular bonds and groups of the lipids were established as reporter groups probing at different depths of the bilayer in order to understand the interaction partner of the aromatic girdles of porins. Monomerization of the trimeric assembly of OmpF porin reconstituted in lipids is induced by increasing the temperature. Porin (OmpF) was found to be extremely stable: The secondary structure of the protein was unaltered up to the temperature-induced main transition, around 80-90 °C, above which it is denatured. However, the interaction of the aromatic girdle with the lipid molecules exhibited distinct changes at much lower temperature values (40 - 50°) where, according to the previous functional studies, monomerization and the loss of function occurs. The results are compared with OmpG porin from *E.coli*, for which the functional unit is a monomer. The aromatic girdle-lipid interaction was monitored by the tyrosine aromatic ring C=C vibrational mode, a universal marker for the protein stability and interaction. We have also found that the aromatic girdles of porins are interacting with the interfacial region of the lipid bilayer instead of lipid headgroups. Lipid-protein interaction was found to be not only essential for the structural stability, but also for the functionality of OmpF porin.

We have also studied the structural properties of OmpG from *E.coli.* The structure of OmpG at two pH values has been resolved using X-ray crystallography and the channel has been proposed to attain different states at different pH values as closed (pH < 5.5) and open

(pH >7.5). This study, using IR spectroscopy, revealed that the pH-induced opening and closing of the channel is reflected by the frequency shifts of the β-sheet structure. OmpG has more rigid β-barrel properties upon opening of the channel. IR spectral analysis revealed multiple β-sheet signals with different hydrogen bond strengths. This enabled us to monitor the formation of hydrogen bridges between the extracellular loops upon opening of the channel. The conclusion that OmpG porin having two states at different pH values was also confirmed by the three mutants where the role of the histidine pair (H231 & H261) and loop 6 has been addressed. Temperature-profiling of the wild type (WT) protein and the mutants did not show pH-dependent structural stability differences in detergent solution. However, the WT protein was found to be more stable in the open form in 2D crystals than the closed form. Reconstitution into lipids has increased the transition temperature value by ~20 °C in the closed state and ~25 °C in the open state. Therefore we conclude that the open and closed state of OmpG has structural stability differences that are only revealed in the lipid environment.

A comparison of the transition temperature values of OmpG WT and the mutants suggested that the hydrogen bond network among S218-H231-H261-D267, together with the formation of 12 residue-long β-sheet contributes to the structural stability of the open channel. In the process of closing and opening of the channel, the globular structure of the protein remains mainly unchanged, while there are changes in the side chain moieties. In addition to the role of the histidine pair and the loop L6, *in situ* opening/closing experiments showed that the negatively charged amino acids, i.e. Asp and Glu, and Arg residues also play an active role; possibly by interacting with each other inside the pore lumen. Therefore it could be concluded that the closure of the channel at acidic pH values is not only via closing the channel entrance by loop 6, but also via changing the electric potential inside the lumen due to the different states of charged amino acids in order to effectively block the gateway.

BetP from *C.glutamicum* attains an active and inactive state in order to adjust its glycine betaine uptake rate to the osmotic conditions that the cell encounters. The structure of BetP

is not yet available. The WT protein exhibited structural differences in the presence of excess K^+, which is one of the activation conditions. In 2D crystals, increasing the ionic strength to 700 mM K^+ was shown to induce changes in the α-helical moiety with contributions from the ester groups and one Tyr residue using ATR-FTIR. An increase in ionic strength to 220 mM K^+ was found to be the threshold value of potassium concentration ($[K^+]$) where the protein exhibits structural alterations in detergent solution. The determined $[K^+]$ values are in good agreement with the previous functional studies. However, there are differences in the activation profile of BetP in 2D crystals and in detergent solution, which points out that the lipids are involved in the conformational transition from the inactive to the active state and their absence can lead to different structural properties.

BetP WT was found to have ~65% α-helix, ~25% random coil and ~10% turn structure in detergent solution. In the presence of excess K^+, the WT protein is found to adapt more unordered structure. Secondary structure analysis of the mutants revealed that both the N- and C-terminus are in α-helical conformation. Reconstitution of WT protein in 2D crystals increased the main transition (denaturation) temperature value from ~62 °C to ~85 °C, a clear indication that the protein is more stable in lipid environment. Temperature-profiling of the two forms of the WT protein revealed that the structural breakdown is preceeded by monomerization of the trimeric assembly. Comparing the two forms of the WT protein and the mutant BetA, we conclude that the oligomeric status is stabilized via the interactions among hydrophilic regions involving the N-terminus.

H/D exchange and activation with excess K^+ in D_2O-buffer revealed that activation of the protein involves the interaction of Arg and Asp/Glu residues in the cytoplasmic region of the protein. BetP WT and the two mutants tested, i.e. BetA and BetPΔC45, showed differences in protein packing upon activation. The WT protein and BetPΔC45 mutant also show changes in the hydrogen bonding properties of turns. Since BetA does not show such a property in activation, we conclude that the N-terminus interacts with the loops in the inactive state via the interaction of charged amino acids for the WT protein and that this interaction is

altered during the activation. It could be argued that the protein packing is affected via the changes in turns upon activation. We also have found experimental evidence that one Tyr residue has different orientations in the active and inactive state of BetP. Based on the previous functional studies, it could be one of the five Tyr residues in the cytoplasmic region of the protein (in loop 3, 6, 7 or C-terminus). The mutant BetPΔC45, on the other hand, showed fewer differences between the active and inactive state conditions and based on the H/D exchange rates, the mutant shows the properties of an active WT protein, proving that the C-terminal truncation impairs the conformational transition between the active and inactive states.

5. ZUSAMMENFASSUNG

In der vorliegenden Arbeit werden Struktur-Funktions-Beziehungen von drei verschiedenen Membranproteinen mittels Fourier-Transformations-IR-Spektroskopie (FT-IR) und abgeschwächter Totalreflexion (ATR) untersucht. Die analysierten Membranproteine umfassen die Außenmembranproteine OmpG aus *Escherichia coli* und OmpF aus *Paracoccus denitrificans,* sowie der osmoregulierte Sekundärtransporter BetP aus *Corynebacterium glutamicum*.

Obwohl die Struktur des *P. denitrificans* Porins schon seit mehr als einem Jahrzehnt bekannt ist, sind die der Monomerisierung und des Funktionsverlustes zugrundeliegenden Mechanismen unbekannt. In dieser Arbeit wurde daher die Rolle der Lipide für die Funktionalität von OmpF unter Verwendung von FT-IR untersucht. Es konnte gezeigt werden, dass OmpF mit Lipidmolekülen über den sogenannten aromatischen Gürtel interagiert, welcher das Molekül an der Außenseite umgibt. Die Bindungen und Lipidgruppen, die in unterschiedlicher Tiefe der Membran lokalisiert sind, wurden damit als Reportergruppen für die Interaktion der Lipide mit dem aromatischen Gürtel identifiziert. Die Monomerisierung des in Lipiden rekonstituierten trimeren OmpF Porins wurde durch Erhöhung der Temperatur induziert. Dabei wurde festgestellt, dass OmpF extrem stabil ist: Die Sekundärstruktur des Proteins blieb bis zu der Übergangstemperatur von 80-90°C unverändert und denaturierte bei weiterer Temperaturerhöhung. Dagegen wies die Interaktion des aromatischen Gürtels mit den Lipidmolekülen bereits deutliche Änderungen bei niedrigeren Temperaturen (40-50°C) auf, wo gemäß bisheriger funktioneller Studien die Monomerisierung und der Funktionsverlust stattfindet.

Die Ergebnisse der Studie am OmpF Porin aus *P. denitrificans* wurden mit denen vom OmpG Porin aus *E. coli* verglichen, bei dem die funktionelle Einheit ein Monomer ist. Die Interaktion der Lipide mit dem aromatischen Gürtel wurde mittels des C=C Vibrationsmodus des aromatischen Tyrosins, einem universellen Marker für Proteinstabilität und Interaktion, untersucht. Dabei stellte sich heraus, dass der aromatische Gürtel der Porine mit der Region

zwischen den Lipidkopfgruppen interagiert und nicht direkt mit ihnen. Darüber hinaus konnte für das OmpF Porin gezeigt werden, dass die Lipid-Protein-Interaktion nicht nur essentiell für die strukturelle Stabilität, sondern auch für die Funktionalität ist.

Als weiteres Projekt wurden die strukturellen Eigenschaften von OmpG aus *E. coli* untersucht. Die dreidimensionale Struktur von OmpG wurde mittels Röntgenstrukturanalyse bei zwei pH-Werten gelöst (Yildiz et al.). Es war bekannt, dass der Kanal verschiedene Zustände bei unterschiedlichen pH-Werten einnimmt, nämlich einen geschlossenen (pH < 5,5) und einen offenen (>pH 7,5). In der vorliegenden Arbeit wurde mittels IR-Spektroskopie gezeigt, dass das pH-induzierte Öffnen und Schließen durch Frequenzverschiebung der β-Faltblatt Struktur wiedergegeben wird. OmpG besitzt rigidere β-Fass Eigenschaften wenn der Kanal geöffnet ist. Die Auswertung der IR-Spektren ergab, dass mehrere β-Faltblattsignale mit unterschiedlichen Wasserstoffbindungsstärken vorliegen. Diese Beobachtung ermöglichte uns, die Ausbildung der Wasserstoffbrücken zwischen den extrazellulären Schleifen bei der Öffnung des Kanals zu verfolgen. Den pH-abhängigen Kanalzustand des OmpG Porins konnte auch durch drei Mutanten bestätigt werden, bei denen die Rolle des Histidin-Paares (H231 und H261) und der Schleife L6 untersucht wurde. Das Temperaturprofil des Wildtyp-Proteins (WT) und der Mutanten zeigte keine pH-abhängigen strukturellen Stabilitätsunterschiede, wenn das Protein in Detergenzlösung vorlag. War das WT Protein jedoch in 2D Kristallen eingebettet, stellte sich heraus, dass es im offenen Zustand stabiler war als im geschlossenen. Die Rekonstitution in Lipide hat dabei die Übergangstemperatur um ~20°C für den geschlossenen und ~25°C für den offenen Kanalzustand erhöht. Es konnte geschlussfolgert werden, dass der offene und geschlossene Zustand von OmpG strukturelle Stabilitätsunterschiede besitzt, die jedoch nur in der Lipidumgebung nachweisbar waren. Ein Vergleich der gemessenen Übergangstemperaturwerte von OmpG-WT mit denen der Mutanten deutet an, dass das Wasserstoffbrücken-Netzwerk zwischen S218-H231-H261-D267, zusammen mit der Ausbildung von einem zwölf Reste umfassenden Faltblatt zur strukturellen Stabilität des offenen Kanals beiträgt. Im Prozess des Schließens und Öffnens bleibt die Gesamtstructure

des Proteins unverändert, während Änderungen der Seitenkettenpositionen vorliegen. Zusätzlich zu der Rolle des Histidin-Paares und der Schleife L6 haben *in situ* Experimente gezeigt, dass die negativ geladenen Aminosäuren Asp und Glu sowie Arg Reste auch eine aktive Rolle spielen, möglicherweise durch Interaktionen miteinander im Porenlumen. Daher kann angenommen werden, dass das Schließen bei saurem pH-Wert nicht allein am Kanaleingang durch Schleife L6 stattfindet, sondern auch über eine Änderung des elektrischen Potentials im Lumen, was zu unterschiedlichen Zuständen von geladenen Aminosäuren und schließlich zu einem effizienten Kanalverschluss führt.

BetP aus *C. glutamicum* kann in einem aktiven und inaktiven Zustand vorliegen und dient dem Schutz der Zelle, indem es Änderungen von osmotischen Bedingungen durch einen Transport von Glycin-Betain kompensiert. Die dreidimensionale Struktur von BetP (ist zwar bislang noch nicht verfügbar) jedoch ist bekannt, dass die Zugabe eines Überschusses an K^+-Ionen strukturelle Unterschiede zur Folge hat. Damit ist K^+ bei der Aktivierung des Transports beteiligt. In der vorliegenden Arbeit konnte mittels ATR-FTIR gezeigt werden, dass die Erhöhung der Ionenstärke auf 700 mM in 2D Kristallen Änderungen des α-helikalen Anteils induziert, wobei Estergruppen und ein Tyr Rest beteiligt sind. Die Erhöhung der Ionenstärke auf 220 mM K^+ wurde als Grenzwert der Kaliumkonzentration ($[K^+]$) bestimmt, bei der das Protein strukturelle Änderungen in Detergenzlösung aufwies. Die definierten $[K^+]$ Werte stehen in guter Übereinstimmung mit vorhergehenden funktionalen Studien. Dennnoch gibt es Unterschiede im Aktivitätsprofil von BetP in 2D Kristallen und in Detergenzlösung. Diese Unterschiede weisen darauf hin, dass Lipide beim Konformationsübergang vom inaktiven zum aktiven Zustand involviert sind und dass ihre Abwesenheit andere strukturelle Eigenschaften zur Folge hat.

In Detergenzlösung wurde der α-helikale Anteil von BetP WT mit ~65% bestimmt, ~25% liegen als random coil vor und ~10% als Turns. In Anwesenheit eines K^+-Überschusses nimmt das WT-Protein eine ungeordnetere Struktur an. Sekundärstrukturanalysen von mutiertem BetP zeigten, dass sowohl N- als auch C-Terminus in einer α-helikalen Konformation vorliegen. Rekonstitution des WT Proteins in 2D Kristalle erhöhte die

Temperatur des Hauptübergangszustandes (Denaturierung) von etwa 62°C auf 85°C, ein klarer Indikator dass das Protein stabiler in Lipidumgebung vorliegt. Die Temperaturprofile der zwei Formen des WT Proteins zeigt, dass die Monomerisation der trimeren Anordnung dem strukturellen Zusammenbruch vorausgeht. Der Vergleich der beiden Formen des WT Proteins und der Mutante BetA ließ die Schlussfolgerung zu, dass der oligomere Zustand über die Interaktionen entlang der hydrophilen Regionen stattfindet, einschließlich dem N-Terminus. H/D Austausch-Experimente mit einer einhergehenden Proteinaktivierung durch K^+ Überschuss im D_2O Puffer zeigt, dass die Interaktionen von Arg und Asp/Glu Resten auf der cytoplasmatischen Region involviert sind. BetP WT und die beiden getesteten Mutanten, d.h. BetA und BetΔC45, zeigten Unterschiede in der Proteinpackung nach Aktivierung. Das WT Protein und die BetPΔC45 Mutante zeigten zudem Unterschiede in den Eigenschaften der Wasserstoffbrücken Eigenschaften in den Turns. Da BetA solch eine Eigenschaft nach Aktivierung nicht zeigt, konnte geschlussfolgert werden, dass der N-Terminus beim WT Protein mit den Schleifen im inaktiven Zustand über die Interaktion der geladenen Aminosäuren interagiert und dass sich diese Interaktion während der Aktivierung verändert.

Es kann angenommen werden, dass die Proteinpackung über Änderungen in den Turn-Bereichen nach Aktivierung beeinflusst ist. Wir fanden experimentelle Beweise, dass ein Tyr Rest unterschiedliche Orientierung im aktiven und inaktiven Zustand von BetP besitzt. Basierend auf vorhergehende funktionale Studien könnte es einer der fünf Tyr Reste in der cytoplasmatischen Region des Proteins sein (in Schleife drei, sechs, sieben oder dem C-Terminus).

Die Mutante BetPΔC45 hingegen zeigte weniger Unterschiede zwischen dem aktiven und inaktiven Zustand sowie basierend auf den H/D Austauschraten, zeigt diese Mutante Eigenschaften eines aktiven WT Proteins, was beweist, dass die C-terminale Verkürzung den Konformationsübergang zwischen dem aktiven und inaktivem Zustand beeinflusst.

6. REFERENCES

Alcaraz, A., Nestorovich, E.M., Aguilella-Arzo, M., Aguilella, V.M. and Bezrukov, S.M. (2004) Salting out the ionic selectivity of a wide channel: the asymmetry of OmpF. *Biophys J*, **87**, 943-957.

Alvarez, J., Haris, P.I., Lee, D.C. and Chapman, D. (1987) Conformational changes in concanavalin A associated with demetallization and alpha-methylmannose binding studied by Fourier transform infrared spectroscopy. *Biochim Biophys Acta*, **916**, 5-12.

Anbazhagan, V., Qu, J., Kleinschmidt, J.H. and Marsh, D. (2008) Incorporation of outer membrane protein OmpG in lipid membranes: Protein-lipid interactions and beta-barrel orientation. *Biochemistry*, **47**, 6189-6198.

Arrondo, J.L., Blanco, F.J., Serrano, L. and Goni, F.M. (1996) Infrared evidence of a beta-hairpin peptide structure in solution. *FEBS Lett*, **384**, 35-37.

Arrondo, J.L. and Goni, F.M. (1999) Structure and dynamics of membrane proteins as studied by infrared spectroscopy. *Prog Biophys Mol Biol*, **72**, 367-405.

Arrondo, J.L., Young, N.M. and Mantsch, H.H. (1988) The solution structure of concanavalin A probed by FT-IR spectroscopy. *Biochim Biophys Acta*, **952**, 261-268.

Arrondo, J.L.R., Goni, F.M. and Macarulla, J.M. (1984) Infrared-Spectroscopy of Phosphatidylcholines in Aqueous Suspension - a Study of the Phosphate Group Vibrations. *Biochimica Et Biophysica Acta*, **794**, 165-168.

Bandekar, J. (1992) Amide modes and protein conformation. *Biochim Biophys Acta*, **1120**, 123-143.

Barth, A. (2000) The infrared absorption of amino acid side chains. *Progress in Biophysics & Molecular Biology*, **74**, 141-173.

Barth, A. and Zscherp, C. (2002) What vibrations tell us about proteins. *Q Rev Biophys*, **35**, 369-430.

Beck, M., Siebert, F. and Sakmar, T.P. (1998) Evidence for the specific interaction of a lipid molecule with rhodopsin which is altered in the transition to the active state metarhodopsin II. *FEBS Lett*, **436**, 304-308.

Becker, J.W., Reeke, G.N., Jr., Wang, J.L., Cunningham, B.A. and Edelman, G.M. (1975) The covalent and three-dimensional structure of concanavalin A. III. Structure of the monomer and its interactions with metals and saccharides. *J Biol Chem*, **250**, 1513-1524.

Behlau, M., Mills, D.J., Quader, H., Kuhlbrandt, W. and Vonck, J. (2001) Projection structure of the monomeric porin OmpG at 6 A resolution. *J Mol Biol*, **305**, 71-77.

Berendzen, J. and Braunstein, D. (1990) Temperature-derivative spectroscopy: a tool for protein dynamics. *Proc Natl Acad Sci U S A*, **87**, 1-5.

Blume, A., Hubner, W. and Messner, G. (1988) Fourier-Transform Infrared-Spectroscopy of C-13=O-Labeled Phospholipids Hydrogen-Bonding to Carbonyl Groups. *Biochemistry*, **27**, 8239-8249.

Butz, S., Benz, R., Wacker, T., Welte, W., Lustig, A., Plapp, R. and Weckesser, J. (1993) Biochemical-Characterization and Crystallization of Porin from Rhodopseudomonas-Blastica. *Archives of Microbiology*, **159**, 301-307.

Cameron, D.G., Casal, H.L. and Mantsch, H.H. (1980) Characterization of the Pretransition in 1,2-Dipalmitoyl-Sn-Glycero-3-Phosphocholine by Fourier-Transform Infrared-Spectroscopy. *Biochemistry*, **19**, 3665-3672.

Castresana, J., Muga, A. and Arrondo, J.L. (1988) The structure of proteins in aqueous solutions: an assessment of triose phosphate isomerase structure by Fourier-transform infrared spectroscopy. *Biochem Biophys Res Commun*, **152**, 69-75.

Chehin, R., Iloro, I., Marcos, M.J., Villar, E., Shnyrov, V.L. and Arrondo, J.L.R. (1999) Thermal and pH-induced conformational changes of a beta-sheet protein monitored by infrared spectroscopy. *Biochemistry*, **38**, 1525-1530.

Chirgadze, Y.N., Fedorov, O.V. and Trushina, N.P. (1975) Estimation of amino acid residue side-chain absorption in the infrared spectra of protein solutions in heavy water. *Biopolymers*, **14**, 679-694.

Chirgadze, Y.N. and Nevskaya, N.A. (1976) Infrared spectra and resonance interaction of amide-I vibration of the paraellel-chain pleated sheets. *Biopolymers*, **15**, 627-636.

Conlan, S. and Bayley, H. (2003) Folding of a monomeric porin, OmpG, in detergent solution. *Biochemistry*, **42**, 9453-9465.

de Planque, M.R.R., Bonev, B.B., Demmers, J.A.A., Greathouse, D.V., Koeppe, R.E., Separovic, F., Watts, A. and Killian, J.A. (2003) Interfacial anchor properties of tryptophan residues in transmembrane peptides can dominate over hydrophobic matching effects in peptide-lipid interactions. *Biochemistry*, **42**, 5341-5348.

Dousseau, F. and Pezolet, M. (1990) Determination of the secondary structure content of proteins in aqueous solutions from their amide I and amide II infrared bands. Comparison between classical and partial least-squares methods. *Biochemistry*, **29**, 8771-8779.

Dutzler, R., Wang, Y.F., Rizkallah, P., Rosenbusch, J.P. and Schirmer, T. (1996) Crystal structures of various maltooligosaccharides bound to maltoporin reveal a specific sugar translocation pathway. *Structure*, **4**, 127-134.

Dzafic, E., Klein, O., Screpanti, E., Hunte, C. and Mantele, W. (2009) Flexibility and dynamics of NhaA Na(+)/H(+)-antiporter of Escherichia coli studied by Fourier transform infrared spectroscopy. *Spectrochim Acta A Mol Biomol Spectrosc*, **72**, 102-109.

Fabian, H. and Mäntele, W. (2002) *Infrared spectroscopy of proteins*. John WIley & Sons Ltd., Chichester.

Fajardo, D.A., Cheung, J., Ito, C., Sugawara, E., Nikaido, H. and Misra, R. (1998) Biochemistry and regulation of a novel Escherichia coli K-12 porin protein, OmpG, which produces unusually large channels. *J Bacteriol*, **180**, 4452-4459.

Forst, D., Welte, W., Wacker, T. and Diederichs, K. (1998) Structure of the sucrose-specific porin ScrY from Salmonella typhimurium and its complex with sucrose. *Nat Struct Biol*, **5**, 37-46.

Fringeli, U.P. and Gunthard, H.H. (1976) Hydration Sites of Egg Phosphatidylcholine Determined by Means of Modulated Excitation Infrared Spectroscopy. *Biochimica Et Biophysica Acta*, **450**, 101-106.

Glasoe, P.K. and Long, F.A. (1960) Use of Glass Electrodes to Measure Acidities in Deuterium Oxide. *Journal of Physical Chemistry*, **64**, 188-190.

Goormaghtigh, E., Cabiaux, V. and Ruysschaert, J.M. (1994a) Determination of soluble and membrane protein structure by Fourier transform infrared spectroscopy. II. Experimental aspects, side chain structure, and H/D exchange. *Subcell Biochem*, **23**, 363-403.

Goormaghtigh, E., Cabiaux, V. and Ruysschaert, J.M. (1994b) Determination of soluble and membrane protein structure by Fourier transform infrared spectroscopy. III. Secondary structures. *Subcell Biochem*, **23**, 405-450.

Goormaghtigh, E., Raussens, V. and Ruysschaert, J.M. (1999) Attenuated total reflection infrared spectroscopy of proteins and lipids in biological membranes. *Biochim Biophys Acta*, **1422**, 105-185.

Goormaghtigh, E., Ruysschaert, J.M. and Raussens, V. (2006) Evaluation of the information content in infrared spectra for protein secondary structure determination. *Biophys J*, **90**, 2946-2957.

Griffiths, P.R., and de Haseth, J. A. (1986) *Fourier Transform Infrared Spectroscopy*. John Wiley and Sons, NY.

Gronholz, J., and Herres, W. (1985) Understanding FTIR data processing. In. I&C (Bruker Co), Vol. 3, pp. 1-23.

Haltia, T. and Freire, E. (1995) Forces and Factors That Contribute to the Structural Stability of Membrane-Proteins. *Biochimica Et Biophysica Acta-Bioenergetics*, **1228**, 1-27.

Haris, P.I. and Chapman, D. (1995) The Conformational-Analysis of Peptides Using Fourier-Transform Ir Spectroscopy. *Biopolymers*, **37**, 251-263.

Heinz, C., Engelhardt, H. and Niederweis, M. (2003) The core of the tetrameric mycobacterial porin MspA is an extremely stable beta-sheet domain. *J Biol Chem*, **278**, 8678-8685.

Hirsch, A., Breed, J., Saxena, K., Richter, O.M., Ludwig, B., Diederichs, K. and Welte, W. (1997) The structure of porin from Paracoccus denitrificans at 3.1 A resolution. *FEBS Lett*, **404**, 208-210.

Hoischen, C. and Kramer, R. (1990) Membrane alteration is necessary but not sufficient for effective glutamate secretion in Corynebacterium glutamicum. *J Bacteriol*, **172**, 3409-3416.

Hubner, W., Mantsch, H.H. and Casal, H.L. (1990) Beware of Frequency-Shifts. *Applied Spectroscopy*, **44**, 732-734.

Iwaki, M., Yakovlev, G., Hirst, J., Osyczka, A., Dutton, P.L., Marshall, D. and Rich, P.R. (2005) Direct observation of redox-linked histidine protonation changes in the iron-sulfur protein of the cytochrome bc1 complex by ATR-FTIR spectroscopy. *Biochemistry*, **44**, 4230-4237.

Korkmaz, F., Koster, S., Yildiz, O. and Mantele, W. (2008) The role of lipids for the functional integrity of porin: an FTIR study using lipid and protein reporter groups. *Biochemistry*, **47**, 12126-12134.

Korkmaz, F. and Severcan, F. (2005) Effect of progesterone on DPPC membrane: Evidence for lateral phase separation and inverse action in lipid dynamics. *Archives of Biochemistry and Biophysics*, **440**, 141-147.

Kramer, R. and Morbach, S. (2004) BetP of Corynebacterium glutamicum, a transporter with three different functions: betaine transport, osmosensing, and osmoregulation. *Biochim Biophys Acta*, **1658**, 31-36.

Krimm, S. and Bandekar, J. (1986) Vibrational spectroscopy and conformation of peptides, polypeptides, and proteins. *Adv Protein Chem*, **38**, 181-364.

Laemmli, U.K. (1970) Cleavage of structural proteins during the assembly of the head of bacteriophage T4. *Nature*, **227**, 680-685.

Lee, A.G. (2003) Lipid-protein interactions in biological membranes: a structural perspective. *Biochimica Et Biophysica Acta-Biomembranes*, **1612**, 1-40.

Lewis, R.N. and McElhaney, R.N. (2000) Calorimetric and spectroscopic studies of the thermotropic phase behavior of lipid bilayer model membranes composed of a homologous series of linear saturated phosphatidylserines. *Biophys J*, **79**, 2043-2055.

Lopez-Garcia, F., Micol, V., Villalain, J. and Gomez-Fernandez, J.C. (1993) Infrared spectroscopic study of the interaction of diacylglycerol with phosphatidylserine in the presence of calcium. *Biochim Biophys Acta*, **1169**, 264-272.

Mantele, W. (1993) Reaction-induced infrared difference spectroscopy for the study of protein function and reaction mechanisms. *Trends Biochem Sci*, **18**, 197-202.

Mantsch, H.H. and Mcelhaney, R.N. (1991) Phospholipid Phase-Transitions in Model and Biological-Membranes as Studied by Infrared-Spectroscopy. *Chemistry and Physics of Lipids*, **57**, 213-226.

Meyer, J.E., Hofnung, M. and Schulz, G.E. (1997) Structure of maltoporin from Salmonella typhimurium ligated with a nitrophenyl-maltotrioside. *J Mol Biol*, **266**, 761-775.

Misra, R., Benson, S.A. (1989) A novel mutation, cog, which reslts in production of a new protein (OmpG) of *Eschericia coli* K-12. *Journal of Bacteriology*, **171**, 4105-4111.

Morbach, S. and Kramer, R. (2005) Structure and function of the betaine uptake system BetP of Corynebacterium glutamicum: strategies to sense osmotic and chill stress. *J Mol Microbiol Biotechnol*, **10**, 143-153.

Mukherjee, S., Chowdhury, P. and Gai, F. (2007) Infrared study of the effect of hydration on the amide I band and aggregation properties of helical peptides. *J Phys Chem B*, **111**, 4596-4602.

Nabedryk, E., Garavito, R.M. and Breton, J. (1988) The Orientation of Beta-Sheets in Porin - a Polarized Fourier-Transform Infrared Spectroscopic Investigation. *Biophysical Journal*, **53**, 671-676.

Naumann, D., Schultz, C., Gorne-Tschelnokow, U. and Hucho, F. (1993) Secondary structure and temperature behavior of the acetylcholine receptor by Fourier transform infrared spectroscopy. *Biochemistry*, **32**, 3162-3168.

Ortiz, M., Sanoguet, Z., Hu, H., Chazin, W.J., McMurray, C.T., Salisbury, J.L. and Pastrana-Rios, B. (2005) Dynamics of hydrogen-deuterium exchange in Chlamydomonas centrin. *Biochemistry*, **44**, 2409-2418.

Ott, V., Koch, J., Spate, K., Morbach, S. and Kramer, R. (2008) Regulatory properties and interaction of the C- and N-terminal domains of BetP, an osmoregulated betaine transporter from Corynebacterium glutamicum. *Biochemistry*, **47**, 12208-12218.

Peter, H., Burkovski, A. and Kramer, R. (1998) Osmo-sensing by N- and C-terminal extensions of the glycine betaine uptake system BetP of Corynebacterium glutamicum. *Journal of Biological Chemistry*, **273**, 2567-2574.

Phale, P.S., Philippsen, A., Widmer, C., Phale, V.P., Rosenbusch, J.P. and Schirmer, T. (2001) Role of charged residues at the OmpF porin channel constriction probed by mutagenesis and simulation. *Biochemistry*, **40**, 6319-6325.

Prasad, R. (1996) *Manual of membrane lipids*. Springer-Verlag Berlin and Heidelberg GmbH & Co. K., Heidelberg, Germany.

Rubenhagen, R., Morbach, S. and Kramer, R. (2001) The osmoreactive betaine carrier BetP from Corynebacterium glutamicum is a sensor for cytoplasmic K+. *Embo Journal*, **20**, 5412-5420.

Rubenhagen, R., Ronsch, H., Jung, H., Kramer, R. and Morbach, S. (2000) Osmosensor and osmoregulator properties of the betaine carrier BetP from Corynebacterium glutamicum in proteoliposomes. *Journal of Biological Chemistry*, **275**, 735-741.

Saxena, K., Richter, O.M., Ludwig, B. and Benz, R. (1997) Molecular cloning and functional characterization of the Paracoccus denitrificans porin. *Eur J Biochem*, **245**, 300-306.

Schiller, D., Kramer, R. and Morbach, S. (2004) Cation specificity of osmosensing by the betaine carrier BetP of Corynebacterium glutamicum. *Febs Letters*, **563**, 108-112.

Schiller, D., Ott, V., Kramer, R. and Morbach, S. (2006) Influence of membrane composition on osmosensing by the betaine carrier BetP from Corynebacterium glutamicum. *J Biol Chem*, **281**, 7737-7746.

Severcan, F., Sahin, I. and Kazanci, N. (2005) Melatonin strongly interacts with zwitterionic model membranes--evidence from Fourier transform infrared spectroscopy and differential scanning calorimetry. *Biochim Biophys Acta*, **1668**, 215-222.

Siebert, F., Hildebrandt, P. (2008) *Vibrational Spectroscopy in Life Science*. Wiley-VCH Verlag GmbH & Co. KGaA, Germany.

Studier, F.W. (2005) Protein production by auto-induction in high-density shaking cultures. *Protein Expression and Purification*, **41**, 207-234.

Sukumaran, S., Hauser, K., Maier, E., Benz, R. and Mantele, W. (2006a) Structure-function correlation of outer membrane protein porin from Paracoccus denitrificans. *Biopolymers*, **82**, 344-348.

Sukumaran, S., Hauser, K., Maier, E., Benz, R. and Mantele, W. (2006b) Tracking the unfolding and refolding pathways of outer membrane protein porin from Paracoccus denitrificans. *Biochemistry*, **45**, 3972-3980.

Sukumaran, S., Hauser, K., Rauscher, A. and Mantele, W. (2005) Thermal stability of outer membrane protein porin from Paracoccus denitrificans: FT-IR as a spectroscopic tool to study lipid-protein interaction. *FEBS Lett*, **579**, 2546-2550.

Sukumaran, S., Zscherp, C. and Mantele, W. (2004) Investigation of the thermal stability of porin from Paracoccus denitrificans by site-directed mutagenesis and Fourier transform infrared spectroscopy. *Biopolymers*, **74**, 82-86.

Susi, H. (1969) *Infrared spectra of biological macromolecules and related systems*. Dekker, New York.

Susi, H. and Byler, D.M. (1987) Fourier-Transform Infrared Study of Proteins with Parallel Beta-Chains. *Archives of Biochemistry and Biophysics*, **258**, 465-469.

Toyran, N., Turan, B. and Severcan, F. (2007) Selenium alters the lipid content and protein profile of rat heart: an FTIR microspectroscopic study. *Arch Biochem Biophys*, **458**, 184-193.

Turner, D.R. and Kubelka, J. (2007) Infrared and vibrational CD spectra of partially solvated alpha-helices: DFT-based simulations with explicit solvent. *J Phys Chem B*, **111**, 1834-1845.

Van Wart, H.E. and Scheraga, H.A. (1978) Raman and resonance raman spectroscopy. *Methods Enzymol*, **49**, 67-149.

Venyaminov, S.Y. and Kalnin, N.N. (1990a) Quantitative Ir Spectrophotometry of Peptide Compounds in Water (H2o) Solutions .1. Spectral Parameters of Amino-Acid Residue Absorption-Bands. *Biopolymers*, **30**, 1243-1257.

Venyaminov, S.Y. and Kalnin, N.N. (1990b) Quantitative Ir Spectrophotometry of Peptide Compounds in Water (H2o) Solutions .2. Amide Absorption-Bands of Polypeptides and Fibrous Proteins in Alpha-Coil, Beta-Coil, and Random Coil Conformations. *Biopolymers*, **30**, 1259-1271.

Yau, W.M., Wimley, W.C., Gawrisch, K. and White, S.H. (1998) The preference of tryptophan for membrane interfaces. *Biochemistry*, **37**, 14713-14718.

Yildiz, O., Vinothkumar, K.R., Goswami, P. and Kuhlbrandt, W. (2006) Structure of the monomeric outer-membrane porin OmpG in the open and closed conformation. *Embo J*, Vol. 25, pp. 3702-3713.

Zandomeneghi, G., Krebs, M.R.H., Mccammon, M.G. and Fandrich, M. (2004) FTIR reveals structural differences between native beta-sheet proteins and amyloid fibrils. *Protein Science*, **13**, 3314-3321.

Zhang, Y.P., Lewis, R.N.A.H., Hodges, R.S. and Mcelhaney, R.N. (1992a) Ftir Spectroscopic Studies of the Conformation and Amide Hydrogen-Exchange of a Peptide Model of the Hydrophobic Transmembrane Alpha-Helices of Membrane-Proteins. *Biochemistry*, **31**, 11572-11578.

Zhang, Y.P., Lewis, R.N.A.H., Hodges, R.S. and Mcelhaney, R.N. (1992b) Interaction of a Peptide Model of a Hydrophobic Transmembrane Alpha-Helical Segment of a Membrane-Protein with Phosphatidylcholine Bilayers - Differential Scanning Calorimetric and Ftir Spectroscopic Studies. *Biochemistry*, **31**, 11579-11588.

Ziegler, C., Morbach, S., Schiller, D., Kramer, R., Tziatzios, C., Schubert, D. and Kuhlbrandt, W. (2004) Projection structure and oligomeric state of the osmoregulated sodium/glycine betaine symporter BetP of Corynebacterium glutamicum. *Journal of Molecular Biology*, **337**, 1137-1147.

Zscherp, C., Aygun, H., Engels, J.W. and Mantele, W. (2003) Effect of proline to alanine mutation on the thermal stability of the all-beta-sheet protein tendamistat. *Biochimica Et Biophysica Acta-Proteins and Proteomics*, **1651**, 139-145.

8. ACKNOWLEDGMENTS

I would like to express my sincere graditude to **Prof. Dr. W. Mäntele**, Institute for Biophysics, Frankfurt am Main, for his constant guidance, support, patience, understanding, and thus being the perfect mentor to me throughout my PhD. Thank you for giving me the opportunity to work in your laboratory.

I would like to thank **Dr. Christine Ziegler**, Max Planck Institute for Biophysics, Frankfurt am Main for providing me the protein BetP and the support she gave me. BetP is definitely not the easiest protein to work with but the enthusiasm in her eyes during our discussions gave me the courage at times I lost hope.

I would like to thank **Dr. Özkan Yildiz**, Max Planck Institute for Biophysics for providing me the channel protein OmpG in vast amounts unhesitantly. I also want to thank you for your support, for the long discussions we had and the German translation. I am so grateful to you!

I would like to extend my thanks to **Stefan Köster** and **Susanne Ressl**, Max Planck Institute for Biophysics for their contribution in this study in many ways like expressing the proteins (OmpG and BetA, respectively), discussions in beer-hours and even in retreat vacations. Thank you very much.

Dr. Enela Džafić, Institute for Biophysics, Frankfurt am Main is specially thanked for her constant scientific and daily-life support. If this PhD period has been a little bit of fun, it is thanks to you. Thank you very much.

I want to thank to **Dr. Carsten Krejtschi** for being always ready to help. I may not have learned a fluent German but I will always remember the words "*Gutentag*", "*Servus*", "*Zylinderkopfdichtung*" und natürlich "*Glühwein*"!

I want to thank to all members of **Institute for Biophysics** for the moments we shared together. Many thanks to **Dr. Georg Wille** and **Monique van Straaten** for helping me out with the bacterias, to **Gabriela Schäfer** for ice cream supplience, to **Dr. Vitali Vogel** for being a very kind office-mate.

My sincere thanks to my cousins **Semir, Ramazan** and **Faik** for their support and to **Nursel** for delicious meals and all-night-long chats.

I want to express my graditude to my landlady **Barbara Hoffman** for Sunday afternoon coffee chats and for sharing her house with me. You were more than a landlady for me, thank you for everything.

My sincere graditude to my brother **Yasin** and his wife **Nese** for always being there for me. We had so much fun together and thank you for the trips to Europapark, which I always refer to in freshmen Physics lectures. I will always remember the day you travelled for 500 km just because I was not feeling so good. Thank you so much!

My sincere graditude to **my family**. You learned to use a computer just to be able to hear from me. Thank you for the unending and unconditional love and support.

My sincere thanks to my friends **Dilem** and **Fuat** for all the joyful moments we had together.

FİLİZ KORKMAZ

Alt-heddernheim 80, 60439,
Frankfurt am Main, Germany
Email: korkmaz@biophysik.org

ACADEMIC QUALIFICATIONS

PhD Degree — Johann Wolfgang Goethe University, Institute for Biophysics, Frankfurt am Main, Germany. Since 2005

MSc Degree — Middle East Technical University (METU), Department of Physics, Ankara, Turkey. 2001-2003

"Biophysical studies of progesterone-model membrane interactions"

Supervisor: Prof.Dr. Halil Kırbıyık, METU, Department of Physics, Ankara, Turkey

Co-advisor: Prof.Dr. Feride Severcan, METU, Department of Biology, Ankara, Turkey

BSc Degree — Middle East Technical University, Department of Physics Education, Ankara, Turkey. 1997-2001

"*Pulsating stars*"

Supervisor: Prof.Dr. Rikkat Civelek, METU, Department of Physics, Ankara, Turkey

High School — Teachers Training Anatolian High School, Afyon, Turkey. 1993-1997

EXPERIENCE

University Lecturer — Atılım University, Faculty of Engineering, Physics Group, Ankara, Turkey. 2004-2005

"Mechanics, Electricity & Magnetism for freshman engineers"

Teaching Assistant — Atılım University, Faculty of Engineering, Physics Group, Ankara, Turkey. 2001-2004

"Mechanics, Electricity & Magnetism Laboratory"

PUBLICATIONS

Korkmaz, F. and Severcan, F. Effect of progesterone on DPPC membrane: Evidence for lateral phase separation and inverse action in lipid dynamics. *Archives of Biochemistry and Biophysics*, 440 (2005) 141-147.

Korkmaz, F., Kirbiyik H. and Severcan, F. Concentration dependent different action of progesterone on the order, dynamics and hydration states of the headgroup of dipalmitoyl-phosphatidycholine. *Spectroscopy-An International Journal*, 19 (2005) 213-219.

Erkoc, S., **Korkmaz, F**. Structural and electronic properties of the DPPC molecule. *Int. J. Mod. Phys. C*, 17 (2006) 967-974.

Korkmaz, F., Köster, S., Yildiz, Ö. and Mäntele, W. The role of lipids for the functional integrity of porin: an FTIR study using lipid and protein reporter groups. *Biochemistry*, 47 (2008) 12126-12134.

Korkmaz, F., Köster, S., Yildiz, Ö., W. Kühlbrandt and Mäntele, W. Contribution of the histidine-trigger H231/H261 and loop L6 on gating of OmpG. *Manuscript in preparation.*

CONFERENCES ATTENDED

Korkmaz, F. Köster, S., Yildiz, Ö. and Mäntele, W. (February, 2008) The role of lipids for the functional integrity of OmpF and OmpG porins: An analysis by FTIR spectroscopy. The Joint Biophysical Society 52nd Annual Meeting, Long Beach, California, USA. Poster # 2064.

Korkmaz, F. (January, 2008) Structure properties and lipid-protein interaction in monomeric & trimeric pores. Kolloquium SFB-472 seminar talk, Frankfurt am Main, Germany.

Köster, S., Yildiz, Ö., Hizlan, D., **Korkmaz, F**. and Kühlbrandt, W. (March, 2008) Structure of the monomeric outer-membrane protein OmpG in the open and closed conformation. Gordon Conference: Ligand Recognition & Molecular Gating, Ventura, CA, USA.

Korkmaz, F. (December, 2007) BetP & OmpG: Different Proteins, Different Structures and Different Functions. Institute for Biophysics, Johann Wolfgang Goethe-Universität, seminar talk, Frankfurt am Main, Germany.

Korkmaz, F. and Mäntele, W. (September, 2007) The role of lipids for the functional integrity of porin: An analysis by FTIR spectroscopy. 12th European Conference on the Spectroscopy of Biological Molecules, Bobigny, France. Poster # 194.

Korkmaz, F. and Mäntele, W. (September, 2006) Detecting markers for functional integrity of a protein by FTIR. Deutche Gesellschaft für Biophysik, Mainz, Germany. Poster # 56.

Korkmaz, F and Severcan, F. (September, 2005) Effect of progesterone of DPPC membrane. 11th European Conference on the Spectroscopy of Biological Molecules, Aschaffenburg, Germany. Poster # 281FK. *Poster has been awarded a Mension Prize.*

PERSONAL DETAILS

Date of Birth 23.02.1979
Place of Birth Amsterdam, The Netherlands
Nationality Turkish

Erklärung

Ich versichere hiermit, dass ich die vorliegende Arbeit selbstständig verfasst, keine anderen, als die angegebenen Hilfsmittel verwendet und sämtliche Stellen, die aus benutzten Werken im Wortlaut oder dem Sinne nach entnommen sind, mit Quellen- bzw. Herkunftsangaben kenntlich gemacht habe.

Frankfurt am Main, den.....

.....